Origin and dynamics of volcanic debris avalanches : surface structure analysis of Tutupaca volcano (Peru)

Patricio Valderrama Murillo

N° d'Ordre : D.U : 2731

UNIVERSITÉ BLAISE PASCAL-CLERMONT II

U.F. R. Sciences et Technologies

ÉCOLE DOCTORALE DES SCIENCES FONDAMENTALES
N° 877

THÈSE

présentée par

PATRICIO VALDERRAMA MURILLO
Titulaire d'un Master

pour obtenir le grade de

DOCTEUR D'UNIVERSITÉ

Spécialité : Volcanologie

ORIGINE ET DYNAMIQUE DES AVALANCHES DES DÉBRIS VOLCANIQUES : ANALYSE DES STRUCTURES DE SURFACE AU VOLCAN TUTUPACA (PÉROU)

Soutenue publiquement le 30 septembre 2016 devant le jury :

M. Georges BOUDON	Rapporteur
Mme Lucia CAPRA	Rapporteur
Mme Irene MANZELLA	Examinateur
M. Karim KELFOUN	Examinateur invité
M. Olivier ROCHE	Directeur de thèse
M. Benjamin VAN WYK DE VRIES	Co-directeur de thèse
M. Pablo SAMANIEGO	Co-encadrant de thèse

Résumé

Les glissements de terrain se produisent dans toutes les chaînes des montagnes où la résistance des massifs rocheux est insuffisante pour contrer l'action de la gravité. Les terrains volcaniques sont particulièrement susceptibles de s'effondrer car les édifices sont composés des lithologies diverses et variées qui peuvent être fortement fracturées. En plus, la croissance rapide des édifices volcaniques favorise leur instabilité et leur effondrement. L'activité magmatique est un facteur additionnel responsable de la déformation des édifices, tandis que l'activité hydrothermale réduit la résistance des roches volcaniques. Pour ces raisons, l'évaluation des aléas liés à l'effondrement des édifices et à la formation des avalanches des débris volcaniques mérite une attention particulière. Les caractéristiques physiques des composants des avalanches des débris ont une influence directe sur la dynamique de ce type d´écoulement. Les dépôts des avalanches de débris présentent une morphologie de surface composée des nombreuses collines (hummocks), qui montrent fréquemment les séquences volcaniques initiales, ce qui suggère un mécanisme de mise en place proche de celui des glissements de terrain. Cependant, d'autres dépôts présentent des crêtes allongées (rides) dont le mécanisme de formation est encore méconnu.

Le volcan Tutucapa (sud du Pérou) a été affecté récemment par deux avalanches de débris. La plus ancienne, « Azufre », est d'âge Holocène et résulte de l'effondrement d'un complexe des dômes et d'une séquence volcanique altérée (hydrothermalisée) sous-jacente. La deuxième avalanche, « Paipatja », a eu lieu il y a seulement 200-230 ans BP et est associée à une grande éruption explosive du Tutupaca. Les dépôts de cette avalanche présentent notamment de nombreuses rides. Les deux dépôts d'avalanche montrent deux unités différentes : une unité inferieure, caractérisée par la présence des blocs altérés (hydrothermalisés) provenant de l'édifice basal, tandis que l'unité supérieure est constituée par des blocs du complexe de dômes actifs.

Le travail de terrain montre que les rides de l'avalanche « Paipatja » présentent une forte variation de granulométrie entre leur partie centrale (enrichie en blocs grossiers) et leurs parties latérales, ce qui suggère un processus de ségrégation granulaire. Des expériences analogiques montrent que des écoulements de mélanges de particules des différentes tailles subissent un processus de ségrégation et de digitation granulaire qui engendre des rides par jonction de levées statiques qui délimitent un chenal d'écoulement. Le processus de formation des rides est facilité par de faibles différence de taille des particules dans des mélanges bidisperses. Ces résultats suggèrent que les rides observées au Tutupaca résultent d'un écoulement granulaire. Les principales caractéristiques morphologiques des structures formées lors de ces expériences de laboratoire ont été comparées qualitativement avec les structures observées dans les dépôts du Tutupaca.

Les structures observées au Tutupaca montrent que deux mécanismes de mise en place peuvent coexister dans les avalanches de débris volcaniques : le glissement de blocs plus ou moins cohérents, et l'écoulement semblable à celui d'un matériau granulaire. Cela dépend probablement de la nature des différents matériaux à la source des avalanches. Cette information doit être prise en compte pour l'évaluation des aléas liés aux avalanches des débris car des mécanismes d'écoulement différents peuvent induire des fortes variations de la distance parcourue par ces avalanches.

Mots-clefs: Avalanche des débris, glissements de terrain, digitation granulaire, modelés analogiques, Tutupaca

Abstract

Landslides occur in all mountainous terrain, where the rock strength is unable to support topographic loading. Volcanic rocks are particularly landslide prone, as they mix strong and weak lithologies and are highly pre-fractured. Also, volcanoes themselves, are peculiar mountains, as they grow, thus creating their own topographic instability. Magmatic activity also deforms the edifice, and hydrothermal activity reduces strength. For all these reasons, volcanoes need close consideration for hazards, especially for the landslide-derived rock avalanches. The characteristics and properties of different debris avalanche components influence their behavior during motion. Deposits are generally hummocky, preserving original layering, which indicates a slide-type emplacement. However, some deposits have ridged morphology for which the formation mechanisms are not well understood.

Two recent debris avalanches occurred at the Tutupaca volcano (S Peru). The first one, “Azufre” is Holocene and involved the collapse of active domes and underlying older hydrothermally altered rocks. The second debris avalanche, “Paipatja” occurred 200-230 y BP and is associated with a large explosive event and this deposit is ridged. The excellent conservation state of the deposits and surface structures allows a comprehensive analysis of the ridges. Both deposits have two contrasting units: a lower basal edifice-derived hydrothermally-rich subunit and an upper dome-derived block-rich unit.

Detailed fieldwork has shown that Paipatja ridges have coarser core material and are finer in troughs, suggesting grain size segregation. Using analog experiments, the process that allow ridge formation are explored. We find that the mixtures undergo granular segregation and differential flow that create fingering that forms ridges by junction of static léeves defining a channel flow. Granular segregation and fingering are favored by small particle size contrast during bi-dispersed flow. The results suggest that the ridges observed at Tutupaca are product of a granular flow We extract the morphological characteristics of the deposits of granular flows generated in the laboratory and make a qualitative comparison with the Tutupaca deposits.

The description of the different landslide and debris avalanche features at Tutupaca shows that two types of debris avalanche motion can occur in volcanic debris avalanches: the sliding of blocks more or less coherent and a flow similar to a granular material. This probably depends on source materials and the conditions of different parts of the initial landslide. Such information should be taken into account when estimating hazards at other volcanic landslide sites, as the different behaviors may result in different run outs.

Keywords: Debris avalanches – Volcanic Landslides - Granular fingering – – Analog experiments – Tutupaca

Resumen:

Los deslizamientos ocurren en todo terreno montañoso, cuando la resistencia de las rocas no es capaz de contra restar el efecto de la gravedad. Las rocas volcánicas son particularmente propensas a generar deslizamientos, ya que los macizos volcánicos están constituidos de secuencias heterogéneas constituidas de diferentes litologías altamente fracturadas. Además, los volcanes son montañas peculiares, ya que a medida que crecen, van creando su propia inestabilidad topográfica. Adicionalmente, la actividad magmática deforma el edificio, y la actividad hidrotermal reduce su resistencia. Por todas estas razones, los volcanes la evaluación de la estabilidad de dichos macizos rocosos debe ser considerada con mucha cuidado. Las características y propiedades de los diferentes componentes de una avalancha de escombros pueden influir en su comportamiento durante el movimiento. Los depósitos de dichas avalanchas muestran generalmente una superficie ondulada con colinas (hummocks), las cuales frecuentemente preservan la estratigrafía original, lo que indica un modo de emplazamiento rotacional. Sin embargo, algunos depósitos presentan morfologías caracterizadas por numerosas crestas alargadas (ridges), para los cuales sus mecanismos de formación no se conocen muy bien.

El volcán Tutupaca (Sur de Perú) fue afectado recientemente por al menos dos avalanchas de escombros. La primera de ellas, denominada "Azufre" es de edad Holocena e implicó el colapso de un complejo de domos y de una secuencia volcánica subyacente que muestra una alta alteración hidrotermal. La segunda avalancha, denominada "Paipatja" se produjo hace solamente 200-230 aAP y se asocia con un gran evento explosivo. El depósito de dicha avalancha presenta numerosas ridges. El excelente estado de conservación de estos depósitos permite un análisis exhaustivo de los ridges. Ambos depósitos tienen dos unidades diferentes: una subunidad basal, caracterizada por la presencia de abundante material alterado hidrotermalmente, proveniente del edificio inferior y una subunidad superior, caracterizada por abundantes bloques de los domos recientes.

Gracias al trabajo de campo detallado se demostró que los ridges de la avalancha “Paipatja” están compuestos por material más grueso en la parte central y por material más fino en los bordes, lo que sugiere un proceso de segregación granular. Los resultados de los experimentos analógicos muestran que las mezclas de partículas de diferentes tamaños sufren un proceso de segregación y de digitación granular que produce los ridges por la unión de las crestas de los léeves estáticos que delimitan un canal de flujo. La segregación granular y la digitación están favorecidas por un contraste leve entre los tamaños de grano de las partículas durante un flujo bi-disperso. Estos resultados sugieren que los ridges observados en el Tutupaca son producto de un proceso de segregación en un flujo granular. Las principales características morfológicas de las estructuras formadas en los experimentos fueron comparadas cualitativamente con las estructuras observadas en los depósitos Tutupaca.

Las estructuras observadas en el Tutupaca muestran que dos mecanismos de emplazamiento pueden coexistir en una avalancha de escombros volcánica: el deslizamiento rotacional de los bloques más o menos coherentes y un flujo de tipo granular. Estas condiciones probablemente dependen de los materiales de origen y de las condiciones en las zona fuente de la avalancha. Esta información debe de tomada en cuenta cuando se estima el peligro por avalancha de escombros en otros terrenos volcánicos, ya que estos diferentes mecanismos pueden dar lugar a grandes variaciones de la distancia recorrida por una avalancha.

Palabras clave: Avalancha de detritos, deslizamientos, digitación granular, experimentos analógicos, Tutupaca

Acknowledgements

My sincere thanks to *Institut de Recherche pour le Développemnt* (IRD) financed this thesis thanks to scholarship *Allocations de recherché pour une thèse au Sud* (ARTS) bourse, under the cooperation between the Instituto Geológico Minero y Metalúrgico (INGEMMET) and IRD, without this support would have been impossible for the finish of this thesis. Likewise, my sincere appreciation to the directives of INGEMMET who gave me the facilities and necessary permissions for my stays in France.

A very special thanks to The University Blaise Pascal and Laboratorie Magma et Volcans (LMV) that was like my second home in France and gave me all the facilities to make analog experiments and writing the thesis. In this four years I have the opportunity to meet and interact with world-kind scientists, from all branches of volcanology.

To the jury for my thesis, Lucia Capra and Georges Boudon for accepting to be part of my thesis jury as rapporteurs. To Irene Manzella as examiner, their recommendations helped to significantly improve the original manuscript.

To my dear thesis advisors: Olivier Roche, Benjamin Van Wyk de Vries and Pablo Samaniego for the friendship, the patience, for the great willingness to help and teaching me so much about the world of volcanology, debris avalanches and analog experiments, meeting and working with them was an experience I will never forget.

It would be unfair not thank separately to Pablo Samaniego for all his support, for those 200+ days spent in the field over 5000 m asl, for the innumerable number of revisions to this and other manuscripts, and especially for teaching me how to be a good scientist and a better person.

A very special thanks to Ing. Lionel Fidel, Director of Environmental Geology and Geological Hazard INGEMMET for having trusted me from the beginning and always given me the support I needed, without their support this achievement would not have been possible. Chief, thank you very much!

To my friends and colleagues of the Volcanological Observatory of INGEMMET (OVI), especially to Jersy Mariño and Marco Rivera for their friendship, support in the field work and for teaching me so patiently.

To the wonderful group of doctoral students of the LMV, especially for Silvia, Alejandra, Anne, Swetha, Corantin, Gio, Marie-Anne, Giacomo and everyone! Thank you all for your friendship, I'm going to miss you! To my friends Nelida, Diego, Damien, Laura, Luis, Ademir, Daniel and McVicius.

To my mother Beatriz Murillo, I dedicate this achievement only to you, thanks for everything mom! To the best sister in the world Beatriz Garcia, who always make me feel so proud. To my uncles Helard, Dante and Herbert and for my dear cousins. To my loved dad Helard C. Murillo, I am just following your path. To my mammy Beatriz.

To the woman who filled with love, happiness and joy my life Estephani Callirgos, thank you for having come into my life at the right time, and give me a new reason to continue, thanks for everything my love, *As always it should be*. And for her lovely family, thanks so much to all of you!

To the Landslide Research Team of INGEMMET: To Gael for her invaluable help, to Christian for his great help. To Edú, Rafael and Jonathan for doing a perfect job.

Finally, to Christopher E., David T., Matt S. and Peter C. for all the company during the hard times.

Agradecimientos

Mis más sinceros agradecimientos al *Institut de Recherché pour le Développemnt* (IRD) que financia esta tesis gracias con el fondo *Allocations de recherche pour une thèse au Sud* (ARTS), en el marco del convenio de cooperación entre el Instituto Geológico Minero y Metalúrgico (INGEMMET) e IRD, sin este apoyo hubiera sido imposible la culminación de esta tesis. De igual manera mis sinceros reconocimientos a los directivos de INGEMMET quienes me dieron las facilidades y permisos necesarios para mis estadías en Francia.

Un agradecimiento muy especial para La Universidad Blaise Pascal y al Laboratorie Magma et Volcans (LMV) que fue como mi segundo hogar en Francia y me brindó todas sus instalaciones para realizar los experimentos analógicos y la redacción de la tesis, además que me permitió conocer e interactuar con científicos de nivel mundial, de todas las ramas de la volcanología.

Para los miembros del jurado de mi tesis, Lucia Capra y Georges Boudon por aceptar ser parte de mi jurado en calidad de rapporteurs y a Irene Manzella y Karim Kelfoun como examinadores, sus recomendaciones ayudaron a mejorar notablemente el manuscrito original.

A mis queridos asesores de tesis: Olivier Roche, Benjamin Van Wyk de Vries y Pablo Samaniego por su gran amistad, su paciencia, su siempre gran disposición a ayudarme y por enseñarme tanto sobre el mundo de la volcanología y los experimentos analógicos, conocerlos y trabajar con ellos a sido una experiencia que nunca olvidaré.

Sería injusto no agradecer separadamente a Pablo Samaniego por toda su ayuda, por esos 200+ días que pasamos en el campo a más de 5000 msnm, por la innumerable cantidad de revisiones a este y otros manuscritos y especialmente por enseñarme a ser un buen científico y una mejor persona.

Un muy especial agradecimiento al Ing. Lionel Fidel, Director del Geología Ambiental y Riesgo Geológico de INGEMMET, por haber confiado en mí desde un inicio y haberme siempre dado el apoyo que necesité, sin su apoyo este logro no hubiera sido posible. Muchas gracias, Jefe!

A mis amigos y colegas del Observatorio Vulcanológico del INGEMMET (OVI), en especial para Jersy Mariño y Marco Rivera por su gran amistad, apoyo en los trabajos de campo y por enseñarme con tanta paciencia.

Para el maravilloso grupo de doctorates del LMV, especialmente para Silvia, Alejandra, Anne, Swetha, Corantin, Gio, Marie-Anne, Giacomo y a todos! Gracias por su amistad, los voy a extrañarlos. A mis amigos Nelida, Diego, Damien, Laura, Luis, Ademir, Daniel and McVicius.

Para mi madre, Beatriz Murillo, a ti te dedico este logro Gracias por todo mamita!. A la mejor hermana del mundo, Beatriz Garcia, quien siempre me hace sentir tan orgulloso. Para mis tíos Helard, Dante y Herbert y mis queridos primos. Para que adorado padre Helard C. Murillo, solo estoy siguiendo tus enseñanzas. A mi mamá Beatriz.

Para la mujer que llenó mi vida de amor, alegría felicidad, Estephani Callirgos, gracias por llegar a mi vida en el momento justo, y por darme un nuevo motivo para seguir adelante, gracias amor mío… Como siempre debió ser… A su hermosa familia, gracias a todos ustedes!

Al Equipo de Investigación de Deslizamientos de INGEMMET: a Gael por su invaluable ayuda, a Christian por todo su apoyo. A Edú, Rafael y Jonathan por hacer un trabajo perfecto.

Finalmente, para Christopher E., David T., Matt S. and Peter C. por su compañía durante los tiempos difíciles.

INDEX

CHAPTER 6: SUMMARY AND CONCLUSIONS

Chapter 1:

INTRODUCTION

1. Volcanic collapses and related debris avalanches

Debris avalanches are huge mass-movements that occur in all mountainous terrain, and are commonly found in association with volcanic rocks, and especially with collapse of volcanic edifices themselves. These events may occur several times during the lifetime of a volcanic edifice. Such avalanches are characterized by a large deposit at the base of the volcano and a horseshoe-shaped scar in the source are on the edifice (van Wyk de Vries and Davis 2015). Such events and their non-volcanic equivalents are able to travel a long distance (L) with respect to the total height loss (H). The H/L ratio is commonly about 0.6 for small valley slope landslides, but can be very low (0.1) for the larger events with volumes over 0.1 km^3 (van Wyk de Vries and Davis 2015). The volcanic landslides in particular are high-volume events, commonly with volumes greater than 0.1 km^3 (Siebert et al. 1987) that can cover hundreds of square kilometers. A volcanic debris avalanche forms when a volcanic landslide accelerates due to a rapid loss of resistance at the base of the rock mass, with velocities that can be greater than 100 m/s and have run-outs of up to 70 km (Siebert, 2002).

Debris avalanches caused by sector or flank collapses are caused by a number of factors: tectonic activity (Lagmay et al., 2000; Vidal and Merle, 2000), internal growth by magmatic intrusion (Hoblitt et al., 1981; Donnadieu and Merle, 1998; Tibaldi, 2001), weakening of the edifice by hydrothermal alteration (Reid et al., 2001; van Wyk de Vries and Francis, 2001) and gravitational spreading (Borgia et al., 1992; van Wyk de Vries et al., 2000). One or a combination of many triggering mechanisms like earthquakes (Montaldo et al., 1996), magmatic intrusions (Elsworth and Voight, 1996; Voight et al., 1983), atmospheric events (van Wyk de Vries et al., 2000) and extreme weather conditions or even climate change (Capra, 2006) can trigger collapses. Avalanches can reshape mountains by leaving collapse scars on the edifice and depositing voluminous debris avalanche deposits (DAD) on the lower slopes and even further beyond. The scar may be rapidly refilled and completely concealed.

On the basis of trigger and the depth of the fault plane, different types of avalanche deposit have been defined:

Volcano landslides involving substrata, is when the initial instability occurs under the volcano edifice, and the deposit includes a large portion of substrata as well as cone material. This kind of event frequently forms the largest-volume volcanic deposits. The Socompa volcano debris avalanche is one of the best examples, where up to 60 vol.% of the deposit comes from the substrate (van Wyk de Vries et al., 2001). Volcanic domes often grow on a hydrothermally-altered volcanic rock which also may provide the substrate for similar collapses that while being of lower volume may also have a high proportion of substrate. This is the case of Soufrière Hills volcano on Montserrat (Sparks et al., 2002) or both volcanic debris avalanches described at Tutupaca volcano (Southern Peru, Samaniego et al., 2015, this thesis).

Sector collapse at oceanic volcanoes may trigger very large debris avalanches, frequently of tens of km^3 in volume, because these volcanoes are usually the largest in terms of volume and they are constructed on weak sedimentary basement. Examples of these high volume events are described at La Reunion Island (Bachèlery et al., 1996) and the Hawaiian volcanoes (Iverson, 1995). Oceanic arc volcanoes also have large collapses, such as the 1888 collapse of Mount Ritter (Papua New Guinea, Ward and Day, 2003) and the volcanoes of the Lesser Antilles arc (Guadalupe, Martinique, etc. Bourdier et al. 1989, Deplus et al., 2001).

Other factor that can trigger a volcanic debris avalanche is when the hydrothermally-altered core is affected by a magmatic intrusion at very shallow levels, frequently involving the volcanic edifice (van Wyk de Vries and Francis, 1997). This fact is a conditional factor for the volume of the subsequent debris avalanche, that usually is limited by the available portions of the edifice affected by the localized deformation.

Superficial volcanic landslides are also very common and it develops near the surface of the volcano, without involving the volcanoes core. This kind of debris avalanche deposit (DAD) are associated with small-to-moderate flank collapse (in comparison with the previous types that associated with sector collapses). These events display small volumes reaching up to several million cubic meters such Mount Meager (Canada, Guthrie et al., 2012) where a deep glaciar incision and glacial retreat have eroded an edifice already weakened by

hydrothermal alteration, leaving steep slopes that are prone to frequent landslides. Also, this type of volcanic landslide is very common in some monogenetic volcanoes.

2. Debris avalanches deposits: facies and distribution

Deposits of debris avalanches are characterized by having two distinct facies with a possible facies transition between them. The internal framework of debris avalanche deposits comprises debris avalanche blocks facies and a debris avalanche matrix facies (Figure 1a). Usually, debris avalanche block facies are surrounded by a debris avalanche matrix facies (Ui et al., 2000). In general, the facies of debris avalanches are characterized by breccias and textures Jigsaw-crack (see below), clasts tend to be angular, but their shape and size depend on the type of rock that they are made of.

Block facies is made of parts of the original volcanic structure, can be almost intact but partially rotated (like torevas) or highly fractured (Figure 1b). The classic texture is that of jigsaw cracks, or jigsaw fit, where the original position of the elements is maintained but the mass is shattered (van Wyk de Vries and Davis 2015). Block facies can be highly brecciated into a fine sand to silt-sized material and there can be a complete gradation between block facies and matrix facies. The size of such debris-avalanche blocks is generally not as big as the blocks derived from the source volcano (Ui et al., 2000). The size of the blocks can vary from up to 200 m to less than 1 m of diameter.

The most remarkable characteristic is the fracture patterns called jigsaw cracks. These joint planes usually remain closed, but some of them open widely due to deformation during transport of the debris avalanche (Ui et al., 2000). The frequency and size of the jigsaw cracks depends of the rock type and the traveled distance of the block.

The matrix of a debris avalanche deposit consists of a mixture of smaller volcanic fragments derived from various parts of the source volcano (Figure 1c). It is composed of sand-to-silt-size fragments and isolated blocks (of up to a few meters in diameter). The matrix can be highly polylithologic. The type of the components may vary according to the rock-type of the source or if there is or no substrate incorporation (Capra et al., 2002). Fluidal textures are

often found at the boundaries of different units of this facies. Injection features of matrix suggest that the mixed facies can behave as a granular fluidized mass.

The general distribution of the facies of the debris avalanche deposit is that the block facies are surrounded by the matrix facies in both the proximal and medial parts.

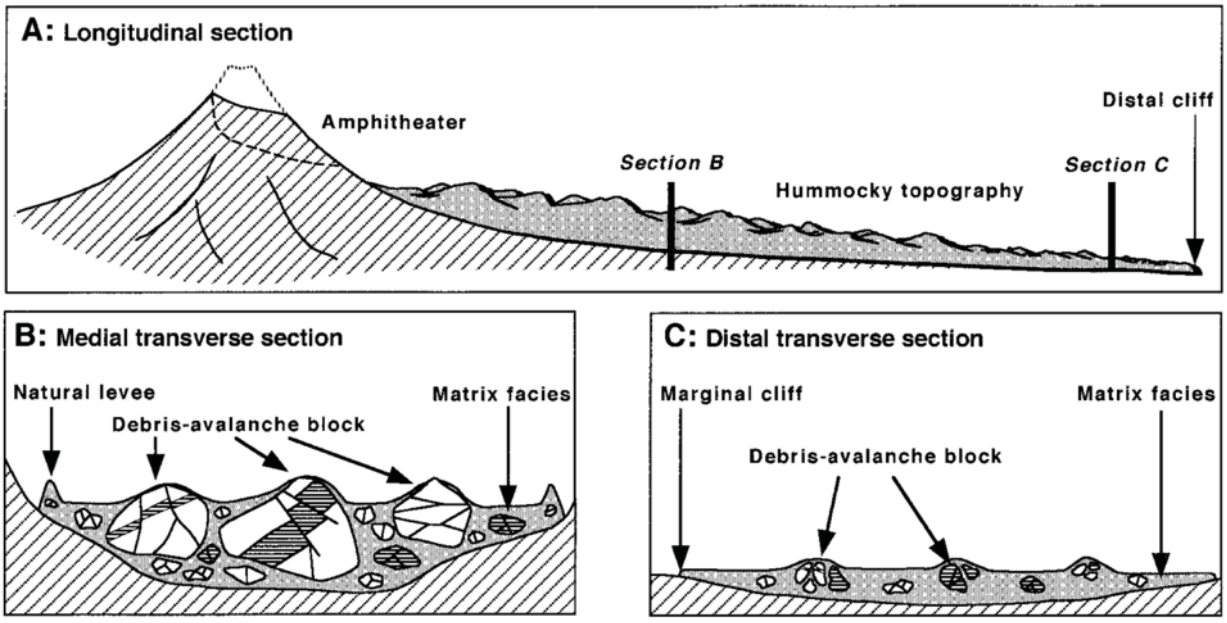

Figure 1: Schematic representation of a debris avalanche deposit (DAD): (A) longitudinal section of a volcano from the edifice source (amphitheater) to the distal end; (B) a transverse section of the medial part of the deposit when the DAD block facies is more notorious; (C) a transverse section for the distal region of the deposit. Size of hummocks gradually decreases. Debris-avalanche blocks are smaller and scarce at the distal area when the DAD-matrix facies is predominant. (From Ui et al., 2000).

3. Surface structures associated to debris avalanche deposits

One of the most important characteristics of a debris avalanche are the structures and morphology that are left on the surface of the deposit and at the source area. In the source area of a debris avalanche or a volcanic landslide a scar is commonly found. This scar has a horseshoe or U shape (Figure 2) or is in some cases triangular, it may cut only the partial affected edifice or can extend out into the piedmont and reach into the substrate (van Wyk de Vries and Davis 2015).

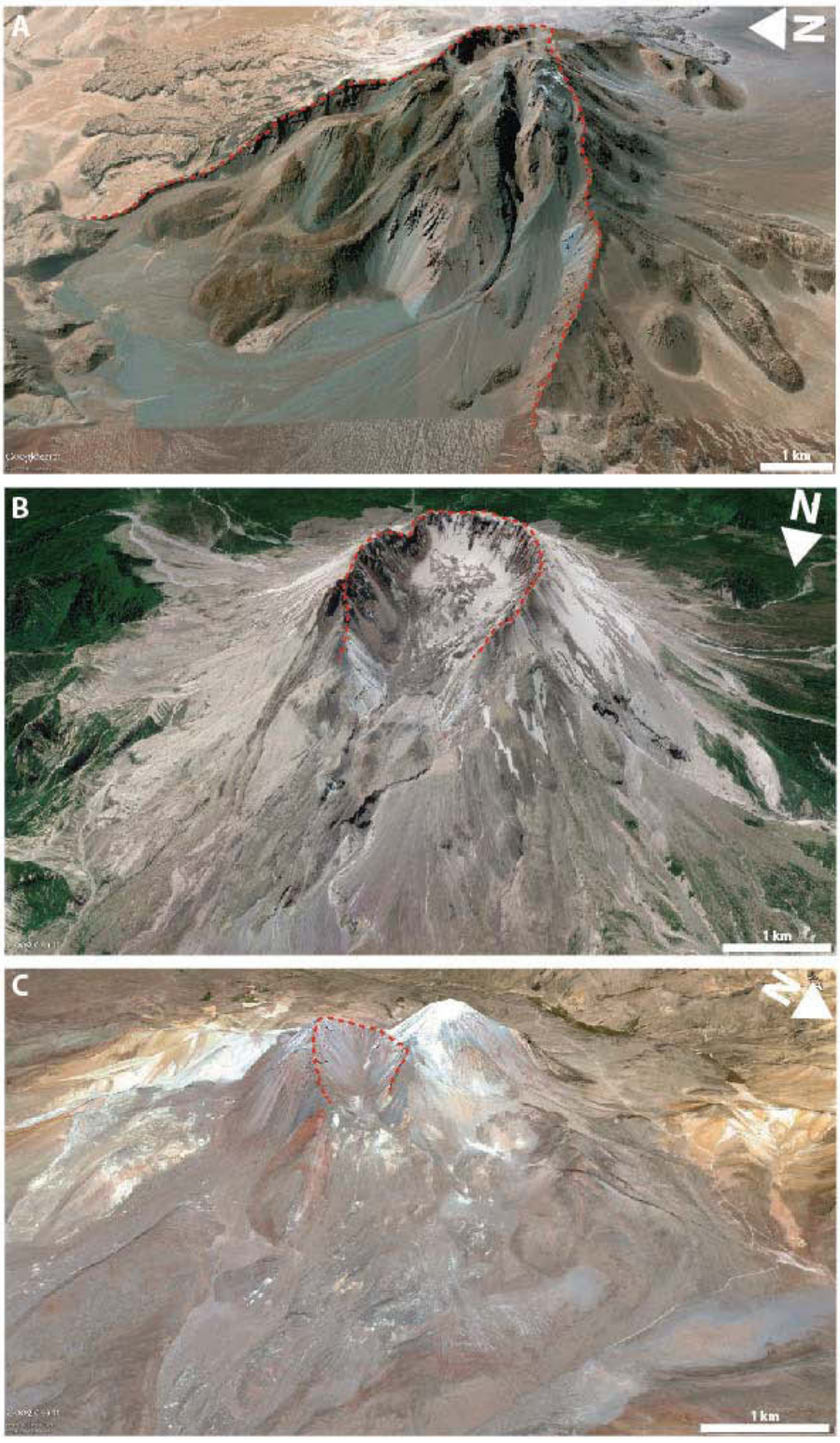

Figure 2: Examples of debris avalanches scarps. (A) Socompa volcano - Chile (B) Mount Saint Helens – USA. (C) Tutupaca volcano – Peru.

Two major surface features are commonly found in the deposit: hummocks / Torevas (e.g. Paguican et al., 2014) and ridges (or longitudinal ridges, e.g. Belousov et al., 1999; Dufresne and Davies 2009).

Hummocks and Torevas

Hummocks are morphological features seen as small mounds that are characteristic of major landslides and debris avalanches (Capra et al., 2002). They are seen on most sub-aerial and sub-marine mass movement deposits on the Earth and also on other planets (Paguican et al., 2014). Hummocks and torevas are commonly preserved in the largest volume avalanches that cut deep into the volcano and substrata, but they are not preserved where topography drops steeply away from the flank of the volcano (van Wyk de Vries and Davis 2015). Hummock size generally decreases with increasing distance from source. The hummocks most probably originate from a horst and graben structure, through brittle deformation of the avalanche core. There are also smaller ones formed by boudinage, where individual blocks of a layer, such as a lava flow, are pulled apart (van Wyk de Vries and Davis 2015). The size of these hummocks depends on the spreading and are generally less than meters in height and 10's of meters in width.

Hummocks are formed initially by extensional forces acting on the landslide (or avalanche) mass when it begins to move (Figure 3). During the motion, the mass develops individual large blocks that spread, creating small hummocks at the landslide mass front and larger ones at the back (that could be torevas). As the mass spreads as result of the movement, hummocks can become wider but may decrease in height, break up, or merge to form bigger and long anticlinal hummocks when confined. In areas of transverse movement within a landslide, elongate hummocks develop between strike–slip flower structures.

The mechanism for hummock formation is brittle (faulting), as shown by Paguican et al (2014), and Shea and van Wyk de Vries (2008).

Absence of hummocks and fault-like features in the deposit may imply a more fluidal flow of emplacement (like 1963 and 1970 Huascaran – Peru avalanches, Evans et al., 2009) or very low cohesion of lithologies (Paguican et al., 2014). In the case of Tutupaca, both hummocky and smoother, ridged deposits are found. This allows the different mechanisms of formation to be explored by comparison.

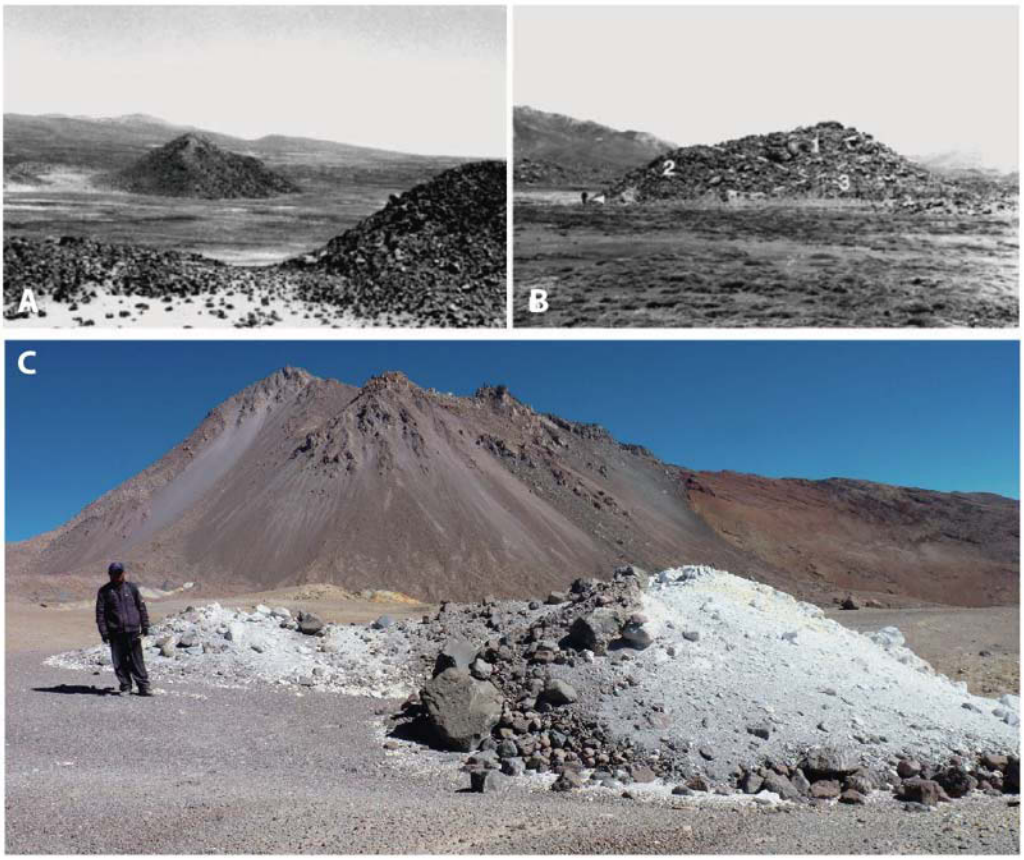

Figure 3: (A, B) Hummocks from Parinacota debris avalanche deposit (from Clavero et al., 2002). Hummock on picture (A) is approximately 25m high and in (B) is 7 m high. (C) Hummock of Azufre debris avalanche (Tutupaca volcano).

A Toreva is a large back-tilted and rotated block left within or at the foot of the failure scar (Figure 4). Torevas can reach up to several kilometers in size and can disaggregate during the motion into smaller hummocks (Lucchitta, 1979; Francis et al., 1985; Wadge et al., 1995). Often steep-sided in the downslope direction, the proximal sides of torevas are often filled in by post-collapse material (Glicken, 1991; Palmer et al., 1991).

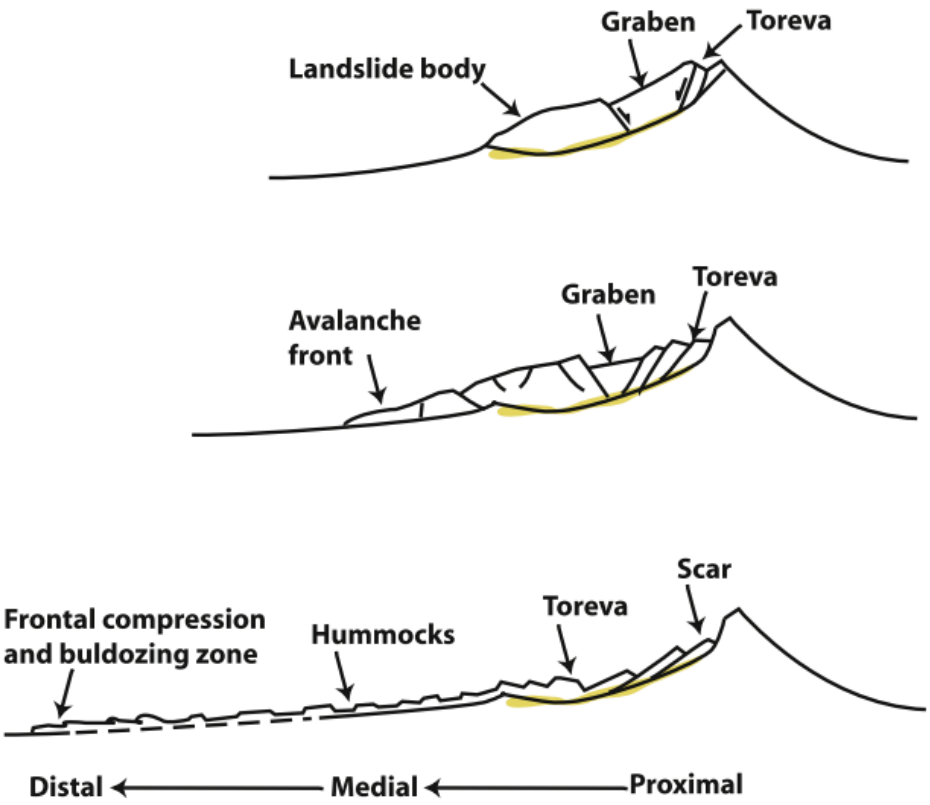

Figure 4: Schematic representation of a flank collapse showing the spreading of the motion mass and the formation of the Toreva and Hummocks. From van Wyk de Vries and Davis (2015).

Ridges

Hummocks have been analyzed comprehensively in the literature (Clavero et al., 2002; Paguican et al., 2014, Yoshida et al., 2012) but the ridges (or longitunal ridges, or flowbands according of Dufresne and Davies 2009, Figure 5) have not been studied in detail in the field in relation to structure and sedimentology (Valderrama et al., 2016). The ridges may be related to differential granular sorting during high-velocity motion and have been described at the debris avalanche deposits of Shiveluch (Belousov et al., 1999) as well as some other volcanic debris avalanche deposits like Socompa (Kelfoun et al., 2008; van Wyk de Vries et al., 2001), Llullaillaco (Richards and Villeneuve, 2001) and others.

The ridges develop in strong, competent, high friction material, sometimes with involvement of a mechanically weak substrate such as loose saturated material (Dufresne, 2009). Such ridges may indicate an emplacement mechanism different than that of

hummocks. While the latter are indicators of brittle movement and deformation localized in shear zones, the ridges indicate a more homogeneous type of deformation where the whole body deforms, like in granular flows. Because parts of a debris avalanche may behave like a granular flowing mass the fundamental mechanisms of granular flows relevant for the present work are presented below.

4. Mechanisms of granular flows

Granular flows consist of a mass of solid grains, possibly with an intergranular fluid, set in motion because of gravity: Iverson (2001) gives the following definition for natural granular flows: "Granular mass flows include rock avalanches, debris flows, pyroclastic flows, and other phenomena in which gravity drives rapid downslope motion of grains and intergranular fluid. The word ''granular'' highlights the importance of momentum transport by large (>0.06 mm) solid grains, mixed with less- dense intergranular liquid or gas. The word ''mass'' implies that a finite, contiguous body of solid and fluid moves almost in unison, and the word ''flow'' indicates that the grain-fluid body deforms irreversibly as it moves downslope. High volumetric grain concentrations distinguish granular mass flows from phenomena such as density currents and water floods, in which fluid forces dominate momentum transport and weak interactions of suspended solids influence effective fluid properties (cf. Bagnold, 1956; Lowe, 1976; Middleton, 1993)."

Particle segregation occurs when granular materials containing particles of different sizes are sheared or vibrated. In such conditions, mixtures of large and small particles unmix (Pouliquen, 1999). Pouliquen and Vallance (1999) describe that segregation occurs when cohesionless mixtures of small and large particles flow down roughened inclined planes. Large particles rise rapidly to the free surface owing to kinetic sieving and then move toward the propagating flow front. The kinetic sieving mechanism is a combination of percolation and squeeze expulsion. Gravitational attraction causes both large and small particles to percolate downward through the granular medium whenever a sufficiently large void opens beneath them (Savage et al., 1988). The small particles percolate more often than large ones because they more often encounter sufficiently large voids below. Large particles that segregate to the free surface migrate toward the flow margins because velocities at the surface are greater

than the average flow velocity. In consequence, large particles gradually collect at the front of the flow as it moves down slope (Pouliquen and Vallance, 1999).

The particle-size segregation process can have a significant feedback on the bulk motion of granular mass flows if the larger grains experience greater resistance to motion than the fine grains (Woodhouse, 2012). When such segregation-mobility feedback effects occur the flow may form digitate lobate fingers at the front or spontaneously self-channelize to form lateral levees that enhance run-out distance (Woodhouse, 2012; Kokelaar et al., 2014; Valderrama et al., 2016). This is particularly important in granular mass flows, such as pyroclastic currents, snow avalanches and debris flows, where run-out distance is of crucial importance in hazards assessment (Woodhouse, 2012).

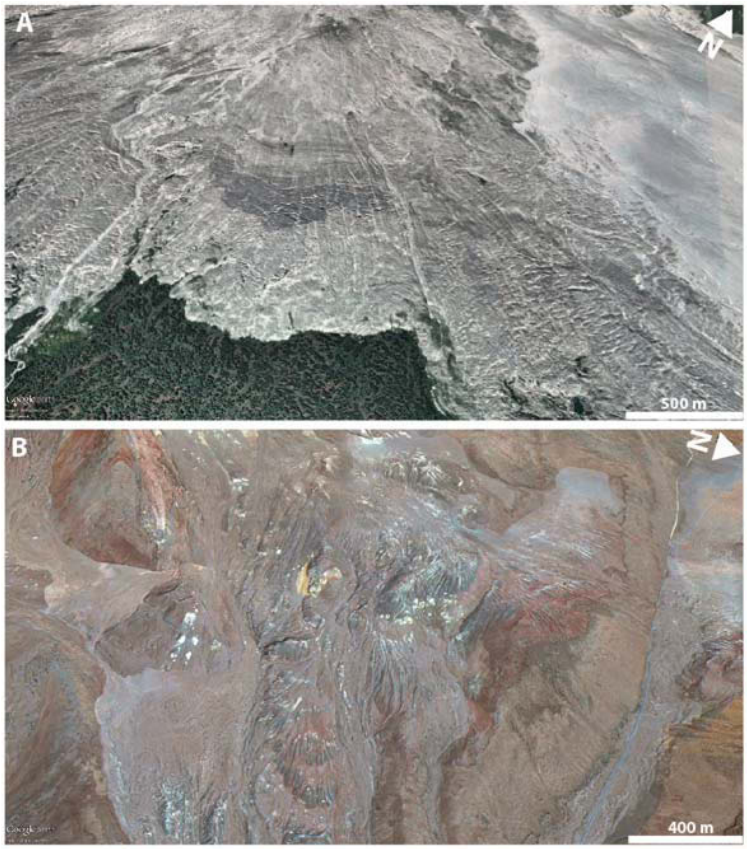

Figure 5: (A) Ridges found at the 1964 debris avalanche deposit at Shiveluch volcano (Belousov et al., 1999). (B) Ridges found at the ˜1800 AD debris avalanche deposit at Tutupaca volcano.

5. The Peruvian volcanic context and the Tutupaca volcano

In southern Peru, the Quaternary volcanic arc is located in the Western Cordillera of the Andes, is oriented NW-SE and forms part of the Central Volcanic Zone of the Andes (CVZ,

da Silva and Francis, 1990). In this segment, there are a dozen of active or potentially active volcanoes, which include, from NW to SE, the stratovolcanoes of Sara Sara, Coropuna, Ampato-Sabancaya, Chachani, Misti, Ubinas, Huaynaputina, Ticsani, Tutupaca, Yucamane and Casiri, and the monogenetic volcanic field of Andahya-Huambo. Of these volcanoes at least 5 have experienced historical activity after the Spanish conquest (i.e. 1532 BP). These volcanoes are the Ampato-Sabancaya, Misti, Ubinas, Huaynaputina and Tutupaca (Siebert et al., 2011). Apart from the Quaternary volcanic edifices, there are numerous Tertiary volcanoes and volcanic terrains that are also prone to instability, even if the volcanic centers are extinct.

The Peruvian volcanic arc results from the subduction of the oceanic Nazca plate beneath the continental South American plate, a process that began in the Upper Jurassic times and continues to the present day (Allmendinger et al., 1997; Ramos and Aleman, 2000). In the Central Andes, near latitude 22°S, subduction rates reached a maximum of 150 mm/y between 20 and 25 Ma and it has steadily declined from 20 Ma to present. It is estimated that the present subduction rate at this latitude is about 63-79 mm/y and that the convergence angle has an azimuth of N79°E (Kendrick et al., 2003; Somoza, 1998; Norabuena et al., 1999).

From north to south, the Benioff plane geometry along the Peruvian subduction system varies:

- The *Northern and Central Peru Zone*, in which the Benioff plane has a dip of 10-15°. From a certain distance from the trench (100 km), Benioff plane becomes almost horizontal, forming what is called a "flat slab". As a result, this segment is characterized by the absence of active volcanism (Wörner, 1992).

- The *Southern Peru Zone* is characterized by a steeply dipping Benioff plane 25-30° on the continent, and there is the so-called asthenospheric wedge located between the continental lithosphere and the Benioff plane. In this region the active volcanoes of southern Peru are located (Wörner, 1992).

From a petrological point of view, the Peruvian segment of the CVZ is characterized by andesitic and dacitic compositions, although rhyolitic composition are also found, while more basic compositions, such as basaltic andesites and basalts are rare or absent (Zbar, 1991). The Tutupaca volcano is one of the 5 active volcanoes in the Peruvian volcanic arc of southern

Peru. Based on historical reports, this volcano might have experienced several eruptive events during the last centuries (1787-1789, 1802, Zamacola & Jauregui, 1804) but this was questioned by several authors (cf. de Silva & Francis, 1990) who suggested that probably those eruptions were from the neighbor volcano, Yucamane. As we will demonstrate in Chapter 2, however, these eruptions are from Tutupaca. On the other hand, volcanic monitoring studies clearly show that the Tutupaca presents some persistent fumarolic activity (Masías et al., 2011). Because of this recent activity, it is necessary to provide a comprehensive study of this edifice, including the reconstruction of its volcanological evolution and the identification of its eruptive dynamics. For this reason, the INGEMMET (Peru) and IRD (France) launched a research program on this edifice, which includes the reconstruction of the eruptive chronology, the petrological characterization of its volcanic products, and the related hazard assessment. In addition, the present thesis reports detailed studies of the two main volcanic events that affected the Tutupaca, the Azufre (Chapter 2) and Paipatja (Chapter 3 and 4) debris avalanches, based on recent geological studies that revealed at least two major recent debris avalanches.

It is important to note that due to the very dry and cold weather conditions and location of Tutupaca (above 5,000 meters) the deposits associated to the debris avalanches are in perfect state of conservation, which makes this volcano ideal for this type of investigation.

6. Scientific context and outline of the thesis

Debris avalanches and large volcanic landslides occur at both active and extinct volcanoes. and commonly have a high mobility, which represent severe natural hazards. A debris avalanche may destroy villages, cut communications means, dam rivers and cause violent floods, lahars and tsunamis (e.g. Carrasco-Nuñes et al., 2011). Examples are collapse-induced lahars at Casita, Nicaragua; tsunamis induced by collapse at Mayuyama, Japan (Bernard et al., 2009; Evans et al., 2007; Kerle and van Wyk de Vries, 2001; Siebert, 2002); tsunamis at Tenerife, Canary Islands, triggered by the Guimar debris avalanche (Giachetti et

al., 2011); and effects on the landscape and sedimentation in Mt. Taranaki, New Zealand (Procter et al., 2009).

In Peru, many cities and important infrastructure are close to volcanic complexes. The case of the Arequipa city is the most notable, with almost 1 million inhabitants at the foot of Misti, a volcano that has several old collapse structures. Similarly, the Ubinas is the most active volcano in Peru. Its southern flank generated at least two avalanches that covered the valley of Ubinas. If a similar event occurred, hundreds of hectares of crops would be seriously affected and more than a dozen villages would be buried, including the town of Ubinas (3725 inhabitants). Deposits of old avalanches have also been reported at other volcanoes like Ticsani (Mariño et al., 2009; Bernard, 2008), and Pichu Pichu (Legros et al., 2000).

In this context, the main objective of this thesis is to provide a detailed study of deposits of debris avalanches resulting collapse of volcanic domes at Tutupaca, in order to discuss the emplacement dynamics. The work focuses on surface structures that are distinct from the hummocky terrain most usually found on debris avalanche deposits: the so-called "ridges" of the Tutupaca deposits. These structures were investigated and in the field and also through analogue laboratory experiments. The latter were performed to better understand the origin and development of these surface structures that are found in many other debris avalanches deposits. The experimental results are then compared qualitatively to natural data in order to discuss the possible mechanisms of the debris avalanche at Tutupaca volcano.

In *Chapter 2*, we examine the processes that affected the younger Tutupaca western edifice and that caused the generation and emplacement of the Azufre avalanche. We analyze the geological history of the volcanic dome complex, emphasizing the formation and destabilization of the youngest domes. This chapter also reports estimated velocities of the avalanche and discusses the mechanisms that triggered the avalanche.

Chapter 3 is an article published in the *Bulletin of Volcanology* and for which I am co-author. We report the geological history and petrographic characteristics of the last major eruption and volcanic debris avalanche of Tutupaca that occurred 200-230 years ago. In

addition, this chapter discusses the pre-eruptive processes and conditions that triggered the avalanche.

Chapter 4 is another article published in the *Bulletin of Volcanology* for which I am the lead author. We studied in particular the surface ridges and their of the younger avalanche of Tutupaca. We describe in detail the sedimentological characteristics of the ridges and propose that they can result from granular segregation fingering.

Chapter 5 presents a laboratory study on granular flows. We present the methodology, materials, and device used and report the results of experiments on granular segregation, fingering and generation of ridges. We discuss the most favorable conditions required for the formation of longitudinal ridges by a granular flow. Finally, we compare the structures formed in the experiments with those observed in the deposits of the most recent debris avalanche at Tutupaca volcano described in Chapter 3.

Finally, *Chapter 6* presents the summary, conclusions and perspectives of this thesis.

Chapter 2:

DESTABILIZATION OF AN EXTINCT, HYDROTHERMALLY ALTERED VOLCANO BY RENEWED ACTIVITY: THE AZUFRE DEBRIS AVALANCHE, TUTUPACA VOLCANO (SOUTHERN PERU)

1. Introduction

Volcanic flank collapses and their consequents landslides or avalanches are among the most relevant eruptive events during the evolution of a volcano. Volcanic debris avalanches are huge masses of rock that slide down at high velocities, can travel tens of kilometers from its source and cover areas of hundreds of square kilometers (Van Wyk de Vries and Davies, 2015). Volcanic debris avalanches can have major catastrophic consequences (e.g. Mount St. Helens, Bandai, Volcán Casita, and many others) and they are responsible for many historic disasters and thousands of associated fatalities (Siebert, 1992). The Holocene eruptive chronology of Tutupaca volcano is marked by at least two major volcanic avalanches (Manrique, 2013; Samaniego et al., 2015). The younger one, which occurred just 200-230 years ago, is probably the youngest volcanic debris avalanche in the Andes (Chapter 3, Samaniego et al., 2015). In this chapter, we present the first field data corresponding to another debris avalanche event that affected Tutupaca. Given that several neotectonic fault scarps are close to the Tutupaca volcanic complex, and that the recent dome complex is constructed on top of an older hydrothermally altered edifice, there is a high likelihood of subsequent landslides, especially if the recent dome complex reactivates.

2. Geological setting

The Peruvian volcanic arc results from the subduction of the oceanic Nazca plate beneath the South-American continental lithosphere. This volcanic province, which belongs to the Central Volcanic Zone (CVZ) of the Andes, is formed upon the Western Cordillera of the Peruvian Andes, and it comprises at least 12 late Pleistocene and Holocene volcanic centers and several monogenetic fields (Simkin and Siebert, 1994). The Tutupaca volcano (17° 01′ S, 70° 21′ W) is one of the 7 active volcanoes that are present in the south of Peru, and is located at the southern end of the Peruvian arc, 25–30 km to the north of Candarave village (Tacna Department, Southern Peru). Historical chronicles reported by Hantke and Parodi (1966) indicate that several volcanic eruptions affected this part of the Andes in AD 1780, 1787, 1802, 1862, and 1902. These authors suggested that the source of these eruptions was Tutupaca volcano, however, based on the youthful and uneroded morphology

of the nearby Yucamane volcano, several authors attributed these eruptions to the latter (Simkin and Siebert, 1994; de Silva and Francis, 1990).

Around Tutupaca there are many villages that could be affected in case of a possible reactivation of this volcano. In particular, worth mentioning is the village of Candarave (3174 inhabitants). As a whole, there are a total of 15766 inhabitants who live within 60-70 km away from the volcano (INEI, 2008). Near Tutupaca there is also important infrastructure such as the Peru – Bolivia Binational road (Ilo - Desaguadero - La Paz), the Pastogrande dam and its related irrigation system, the Suches, Vizcachas, Loriscota, Vilacota lakes and the Locumba river basin that supply water to nearby villages, and large porphyry-cooper mining projects such as Cuajone, Toquepala and Quellaveco at Moquegua province. (Figure 1).

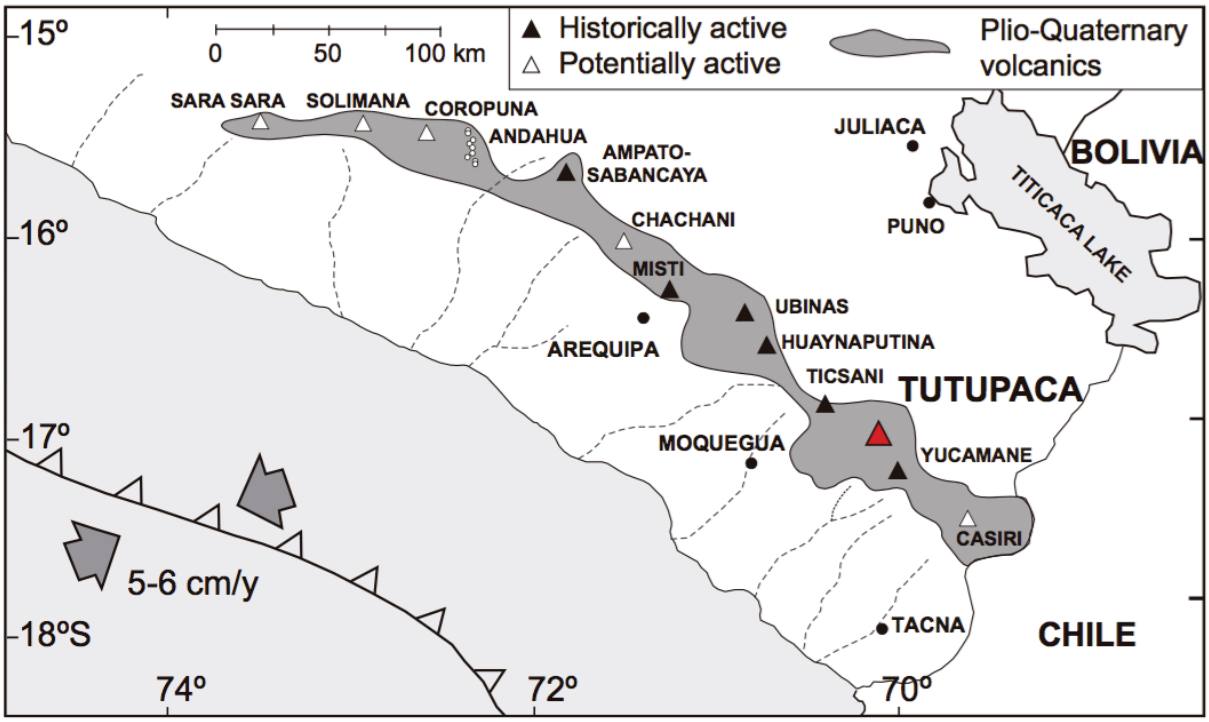

Figure 1. Location of Tutupaca volcanic complex in the Peruvian volcanic arc.

3. Eruptive chronology of Tutupaca volcanic complex

The Tutupaca volcanic complex rises from the basement at 4400–4600 m above sea level and is composed of an old, highly altered and eroded basal edifice and two younger twin peaks, located in the northern part of the complex (the Western and Eastern Tutupaca; Samaniego et al., 2015). Several fault systems have been identified in this part of the Andean

cordillera, the main one being a series of normal faults with a sinistral component that has been mapped around the Suches lake and that displays a roughly N140 direction (Manrique et al., 2013).

Basal Tutupaca

This edifice is the oldest part of the complex (Figure 2). This is a highly eroded edifice, consisting of a succession of lava flows, although several pyroclastic flow deposits have also been described. Based on the radial distribution and dips of these lavas, we infer that the former summit was located 2–3 km to the south of the current Tutupaca peaks. The summit zone has an uneven topography and displays a strong hydrothermal alteration. This central part of the edifice has multiple peaks consisting of lava sequences cut by intense Pleistocene glacial erosion resulting in the highly eroded morphology and glacial U-shaped, radially oriented valleys. Major moraine deposits (up to 100 m thick) were stacked mostly in the southern part of the complex, as well as in the Callazas and Tacalaya valleys. These moraines were probably formed during the Last Glacial Maximum (LGM), which has been broadly dated at 17–25 ka in the Western Cordillera of the Peruvian Andes (Smith et al., 2008; Bromley et al., 2009). A thick ignimbrite deposit of dacitic composition outcrops on the southern and western flanks of the edifice and records a major explosive phase that probably occurred at the end of edifice evolution.

The lavas of the Basal Tutupaca are porphyritic, dark grey andesites, with some lava flows having xenoliths or enclaves. Towards the south of the construction a series of small domes of 250-750 m in diameter and heights of 20 to 50 m, aligned NNW-SSE direction were emplaced. These domes have been dated by K/Ar method at 0.26 ± 0.2 Ma (Fidel and Zavala, 2001). Given that these domes are aligned along a roughly NW-SE direction; we hypothesize that the previously mentioned fault system influenced the structural development of the volcanic complex.

Western Tutupaca

This edifice overlies the Basal Tutupaca, and consists of lava sequences, domes and debris avalanche deposits (Figure 2). It is formed by several domes, which have a diameter of 1-1.5 km and a height of 400-500 m. The domes are of dacite composition (64.4 – 67.1 wt.% SiO_2) with a porphyritic texture comprising plagioclase, amphibole, biotite, Fe-Ti oxides and traces of sphene and quartz. Dark gray magmatic, microcrystalline enclaves have been identified mostly composed of plagioclase and amphibole. Overlying the domes, a lava sequence has been identified showing a metric stratification, reaching more than 200 m thick and forming the upper part of the cone. These sequences are widely affected by glacial erosion. A sequence of tephra fallout deposits outcropping in the distal south-western part of the volcano shows that this edifice experienced voluminous plinian to subplinian eruptions during its history. A debris avalanche deposit, which is located on the western side of the volcano, has a minimum thickness of 100 to 150 m and displays a block-rich facies. This deposit outcrops along the Tacalaya valley and is covered by old moraine deposits, and it has an undulated and eroded surface.

Eastern Tutupaca

The youngest edifice of Tutupaca volcanic complex (Figure 2) is composed of several lava domes and its associated deposits, among which are block-and-ash pyroclastic flow deposits, and debris avalanche deposits. It is composed of at least 7 coalescing lava domes (named Dome I to VII; Manrique, 2013), which are cut by a 1-km-wide horseshoe-shaped amphitheater open to the NE. It is worth noting that the direction of opening of the amphitheater is almost orthogonal to the N140 regional faults that cut the edifice. We identified two debris avalanche deposits associated with this edifice: an older deposit that is channelized in the valleys located to the E and SE of the volcano (The Azufre debris avalanche deposit, this chapter) and a younger deposit that outcrops immediately to the NE of the amphitheater (Chapter 3, Samaniego et al., 2015).

Two escarpments have been observed in this edifice. The younger and conspicuous amphitheater is a 1-km-wide horseshoe-shaped open to the NE. An older amphitheater is 1.7 km wide and cuts the domes located in the north and also some volcanic units of the

Western Tutupaca edifice (Figure 2). All domes display the same dacitic composition and mineral assemblage which are composed of plagioclase, biotite and amphibole encompassed in a microcrystalline paste of porphyritic texture (Manrique, 2016). We briefly describe the Eastern Tutupaca domes, which were numerated following an anticlockwise direction from north to south (Figure 3):

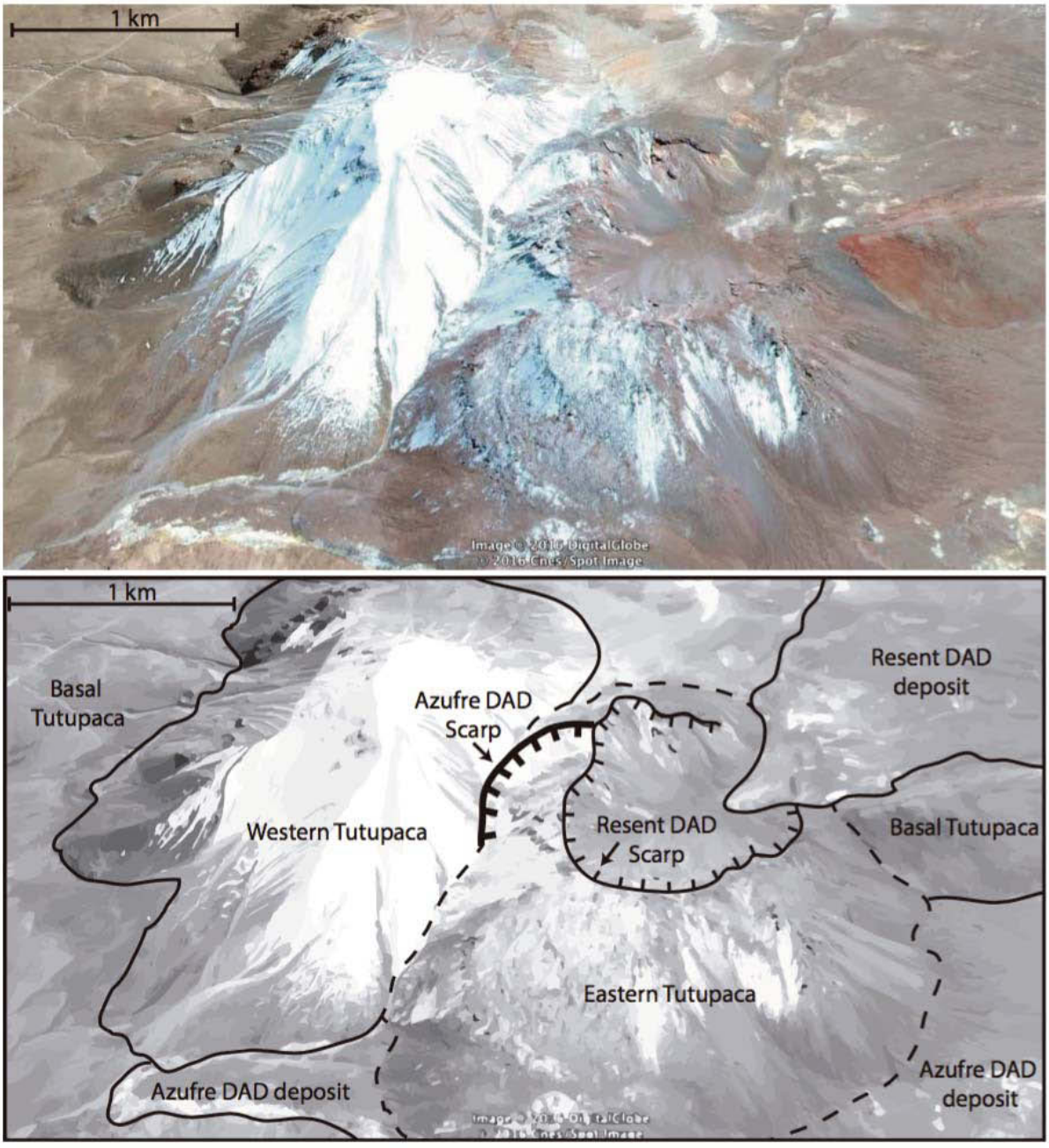

Figure 2: Satellite image and sketch of Tutupaca Volcanic Complex. The wider black line shows the Azufre debris avalanche scarp. The Recent debris avalanche scarp and the three volcanic edifices are also shown.

Dome I: It is located on the northwest flank of the Eastern Tutupaca edifice, close to Western Tutupaca, and it is constructed on top of the highly hydrothermalized lavas of the Basal Tutupaca Edifice. This dome has an elongated shape with a ~22^{o} surface slope, measuring 600 m long at east-west direction, and having a thickness of 400 m. By its stratigraphic position, this dome is considered the oldest dome of Eastern Tutupaca, i.e. it underlies the Domes II and III and it was emplaced directly on the remnants of the Basal edifice and Western Tutupaca lavas.

Dome II: Located southwest of Dome I, it has a slightly elongated north-south morphology. It is 180 m wide and 380 m long in the north-south direction. This dome is approximately 240 m thick. It overlies Dome I.

Dome III: Located to the east of Dome I, this dome has an ellipsoidal shape with a maximum size of about 1 km, and a height of 500 m. This dome is affected by the two collapse scarps: the ancient escarpment associated with the Azufre debris avalanche and the most recent one associated with the historical debris avalanche.

Dome IV: It is located southwards of Domes II and III and at the northwest of Dome V. It is slightly elongated in the north-south direction, has a maximum size of 900 m and a thickness of 240 m. This dome is affected by the younger collapse escarpment and fills the structure associated with the old collapse scarp (Azufre).

Dome V: It is located to the south of the dome complex and is the most voluminous dome of the recent edifice. It merges with a thick lobe, which has an elongated shape from south to east and is approximately 1.6 km long with a thickness of about 200 m. Dome V has a rough surface. It is elongated, with lengths of 2 km and 1 km in the East-West and North-South directions, respectively, and it has a height of 780 m. This dome is also affected by the recent collapse scarp.

Dome VI: It is located east of Dome V, has an elongated shape, a rough surface and it is 700 m long and 550 m thick.

Dome VII: It is located to the north of the Dome VII is the youngest of all domes. It has a width of 550 m and a maximum height of 600 m.

4. The Azufre debris avalanche deposit

Deposits: distribution, facies, stratigraphic relations

The Azufre debris avalanche deposit is found in the S and SE sectors of the Tutupaca volcanic complex, with important branches to the W and E (Figure 3). It was first mapped by Fidel and Zavala (2001) who identified these volcanic deposits but did not discuss their origin. The main characteristic of this debris avalanche deposit is that it is channelized into four valleys, reaching 3.4 km in the Zuripujo valley, 2.2 km in Tutupaca valley, 1.1 km in Río Negro valley, and 2.6 km in Río Blanco valley (Figure 3).

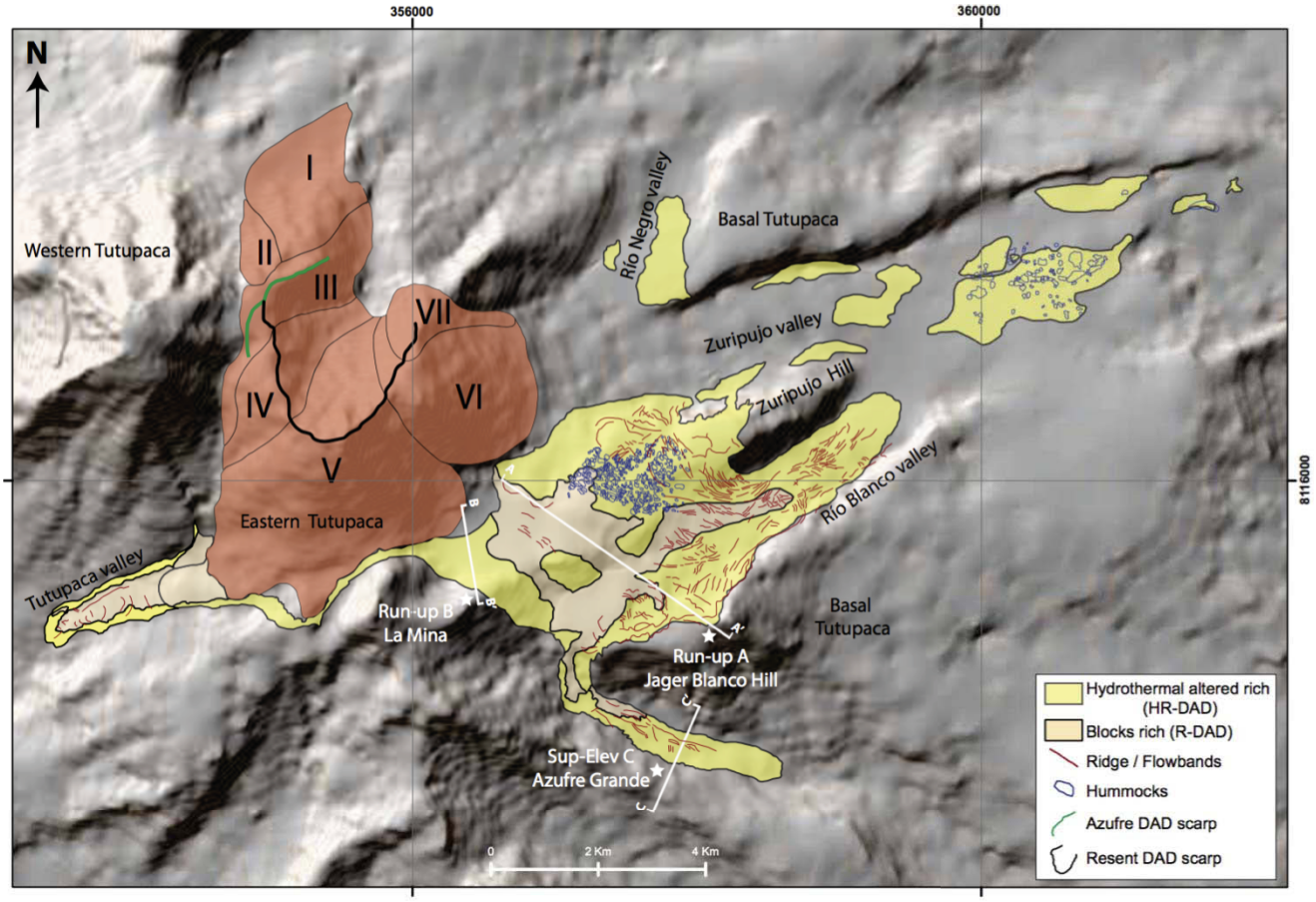

Figure 3: Geological map of the Tutupaca volcanic complex. HR-DAD correspond to the Hydrothermal-Rich sub-unit, while BR-DAD correspond to the Block-rich sub-unit.

This debris avalanche deposit has two different sub-units (Figure 4). The main sub-unit, hereafter called Hydrothermal-rich debris avalanche deposit (HR-DAD) is a whitish-yellow volcanic breccia with hetero-lithological and heterometric facies. It is unconsolidated, massive, and matrix supported (60-70 vol.% matrix), with a maximum thickness of 30-40 m in the bottom of the filled valleys (Figure 3). The matrix of the deposit is constituted by fractured hydrothermal ash-size material. The blocks frequently show evidence of fracturing and cataclasys and are of two different types: aphanitic blocks without alteration and hydrotermalized blocks, which correspond to the Tutupaca Basal edifice, and sub-angular to angular fresh dome blocks from centimeters up to 3 meter of diameter.

In the proximal part, the hydrothermal-rich deposit is covered by a second block-rich sub-unit, hereafter called Block-rich debris avalanche deposit (BR-DAD), which has variable thickness ranging from 5 to 15 m (Figures 3 and 4). This deposit is block-supported, non-consolidated, massive and shows cataclasys and shearing structures. It is constituted by 60-70 vol.% blocks and 40-30 vol.% matrix. The blocks have maximum diameters of 5 m and are generally angular to sub angular with frequent show jigsaw fractures. Also, they show prismatically jointed blocks structures (PJB) that indicate that they were still hot when they emplaced.

Figure 4. Detailed view of the contact between the Hydrothermal-rich debris avalanche deposit (HR-DAD) and the Block-rich debris avalanche deposit (BR-DAD)

Run-up and super-elevations

The Azufre debris avalanche deposit has frequent run-up and super-elevation structures (Figure 3). Such structures are acquired when a high velocity granular or hyper concentrated flow is suddenly diverted because of abrupt changes in the valley direction and/or topographic barriers. At these places, the granular mass runs up and deposits above the top of the main flow. In the Azufre DAD we identified two run-ups and one super-elevation zone that permitted us to estimate the velocity of the avalanche. A moving mass generates a "run-up" when the motion material is capable of rise uphill of a mountain side, hill or valley flank oriented perpendicularly to the flow path (Pierson et al., 1985). A “super-elevation” in this case is applied to channelized flows. This is based on the tilting of the mass in motion over one of the channel edges due the action of a centrifugal force due to changes in the general direction of the channel.

Run-up "A". It is located in the Río Blanco valley (Figure 3). Here the DAD is oriented E-SE and makes a run-up above the Yager Blanco Hill, which is composed by lavas from Tutupaca Basal edifice. The run-up is 34 m above the adjacent bottom valley level, and even partially surpasses the Yager Blanco Hill, generating a small deposit that descends in direction to Azufre Grande valley (Figure 5a). Based on valley morphology, we estimate a debris avalanche thickness of at least 20 m. Distally, the avalanche changed its direction, produced another super-elevation at the Zuripujo hill and eventually spread onto the upper part of the Zuripujo valley (Figure 3) where it left a 50-100 m thick deposit.

Run-up "B". It is located SE of Eastern Tutupaca edifice (Figure 3). The block-rich avalanche generated a series of run-up against a hill formed by ancient lavas of the Tutupaca Basal edifice in an area called La Mina. Distinct thin debris avalanche deposit layers on the hill show that at least two pulses of the avalanche were emplaced in this area. The maximum height of the run-up from the first pulse is 124 m from the bottom of the valley (Figure 5b) and the height of the second one is 54 m.

Super-elevation "C". We found a remarkable super-elevation feature in the Azufre Grande valley, 43 m above the valley floor on the left flank (Figure 5c), which was produced by impact of the avalanche against the Yager Blanco hill (Super-elevation A) generating that part of the motion mass enter the channel valley changing drastically its direction. This valley contains a very well developed and channelized lobe.

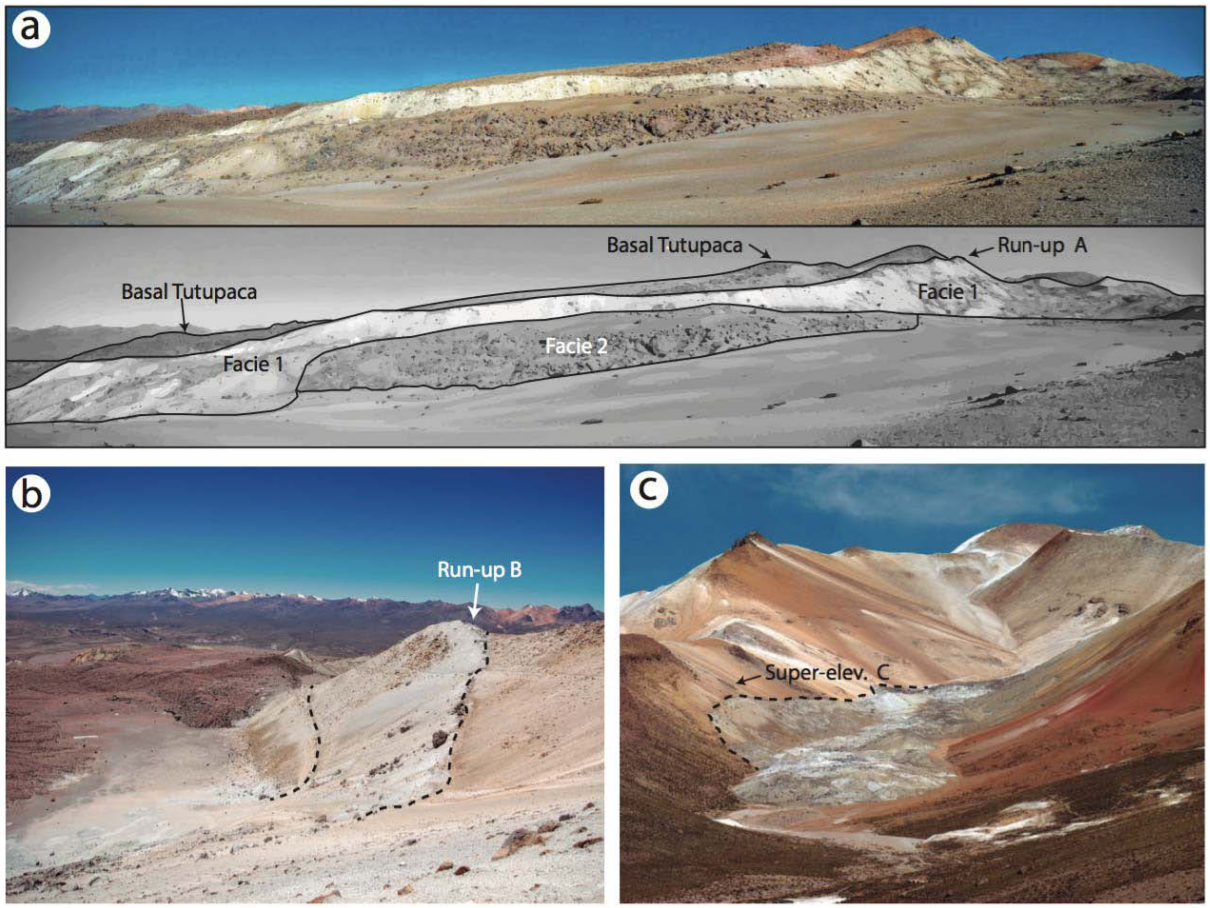

Figure 5: Super-elevations and run-up of the Azufre debris avalanche. a) Photographs and sketch of run-up A, showing also the two facies of the debris avalanche deposit and the ancient flank valley formed by lavas of the Tutupaca Basal. b) Run-up B formed by two pulses of the hydrothermal-rich DAD material. c) Super-elevation C of the debris avalanche material in the glacial valley of Azufre Grande.

Hummocks and other structures

Hummocks were formed as a result of the stretching of the avalanche material (Paguican et al., 2014). These structures have diameters from 2-3 m up to 50 m of and heights of 2 m up to 10 m. The summit of the Zuripujo hill shows an area with more than about a hundred small-scale (2-3 m high) hummocks that were produced by the spreading of the avalanche over this topographic high. These hummocks are represented predominantly by the HR-DAD facies with altered material, and less BR-DAD facies with fresh dome rocks (Figure 6).

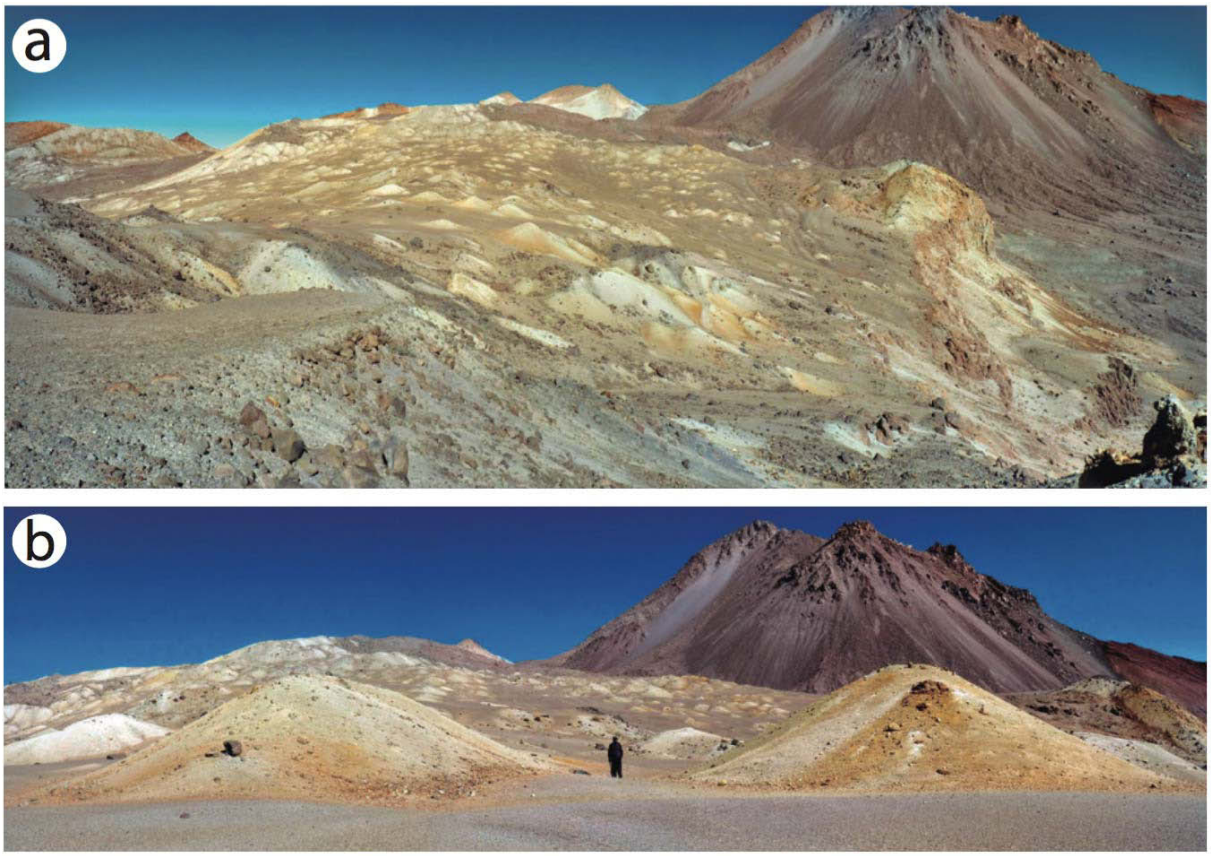

Figure 6: Hummocks at Zuripujo hill. a) Panoramic view with the younger edifice of Tutupaca volcano in background. b) Detailed view, with person for scale.

In the middle part of the Zuripujo valley we found another area of hummocks, which were higher and larger (50 m of maximum diameter and up to 10 m high) than the ones described above (Figure 7). These hummocks are part of the distal lobe of the avalanche. In this area, the hummocks have a mixed nature since the two facies of the debris avalanche are found in a same hummock, which indicates that both facies had mingled even in the distal parts of the avalanche (Figure 7B and 7C).

Figure 7: a) Panoramic view of the hummocks in the Zuripujo valley. These hummocks have heights up to 10 m.b, c) Detailed view of the distal hummocks in the Zuripujo valley, with contact between the two facies of the debris avalanche deposit.

We found elongated structures in the central part of the deposit. These were hard to identify in the field but appear clearly on high resolution satellite images. Following the terminology of Dufresne and Davies (2009) these elongated structures are classified as flowbands because, unlike ridges (or elongated ridges, Valderrama et al., 2016, Chapter 4),

these structures do not rise much above the general surface of the deposit with length/height and length/width aspect ratios of ~18 and ~103, repectively (with typical heights H= 2 m, length L= 209 m and width W= 10 m. Figure 3 shows a map of these structures made using a high resolution (5 m pixel size) satellite image. These flowbands are assumed to be parallel to the flow direction, and their orientation suggests changes in flow direction.

5. Dynamical constraints

Field evidence show that the Azufre debris avalanche travelled fast enough to leave high run-up and super-elevations. Several authors have used similar features to estimate the velocity of an avalanche based on the equations presented by Pierson (1985) to treat the 1980 Mount St. Helens post-avalanche lahars and which are simplified equations of those proposed by Chow (1959) and Apmann (1973). The first equation used to calculate the velocity (U) that is necessary for a run-up (Pierson 1985):

$$U = (2gh)^{\frac{1}{2}} \qquad (1)$$

where g is the gravitational acceleration and h is the height of the run-up. This equation is applied to run-ups A (Yager Blanco Hill) and B (La Mina), (Figure 8a and b).

The super-elevation formula is based on the supposed tilting of the motion mass in a bend due to centrifugal force (Figure 8c):

$$U = \left(\frac{g\Delta h r_c}{b}\right)^{\frac{1}{2}} \qquad (2)$$

where r_c is the centerline radius of curvature and b is the channel width and Δh is the height difference between the lowest point of the deposit inside the channel and the maximum elevation at one edges. This equation is used in the super-elevation C (Azufre Grande valley). Equations 1 and 2 do not consider the effect of the channel roughness, resistance of the

bend, increased density of the flowing mass or internal resistance to the flow, water loss or bulking process; therefore, these equations should provide only maximum estimates of velocity values.

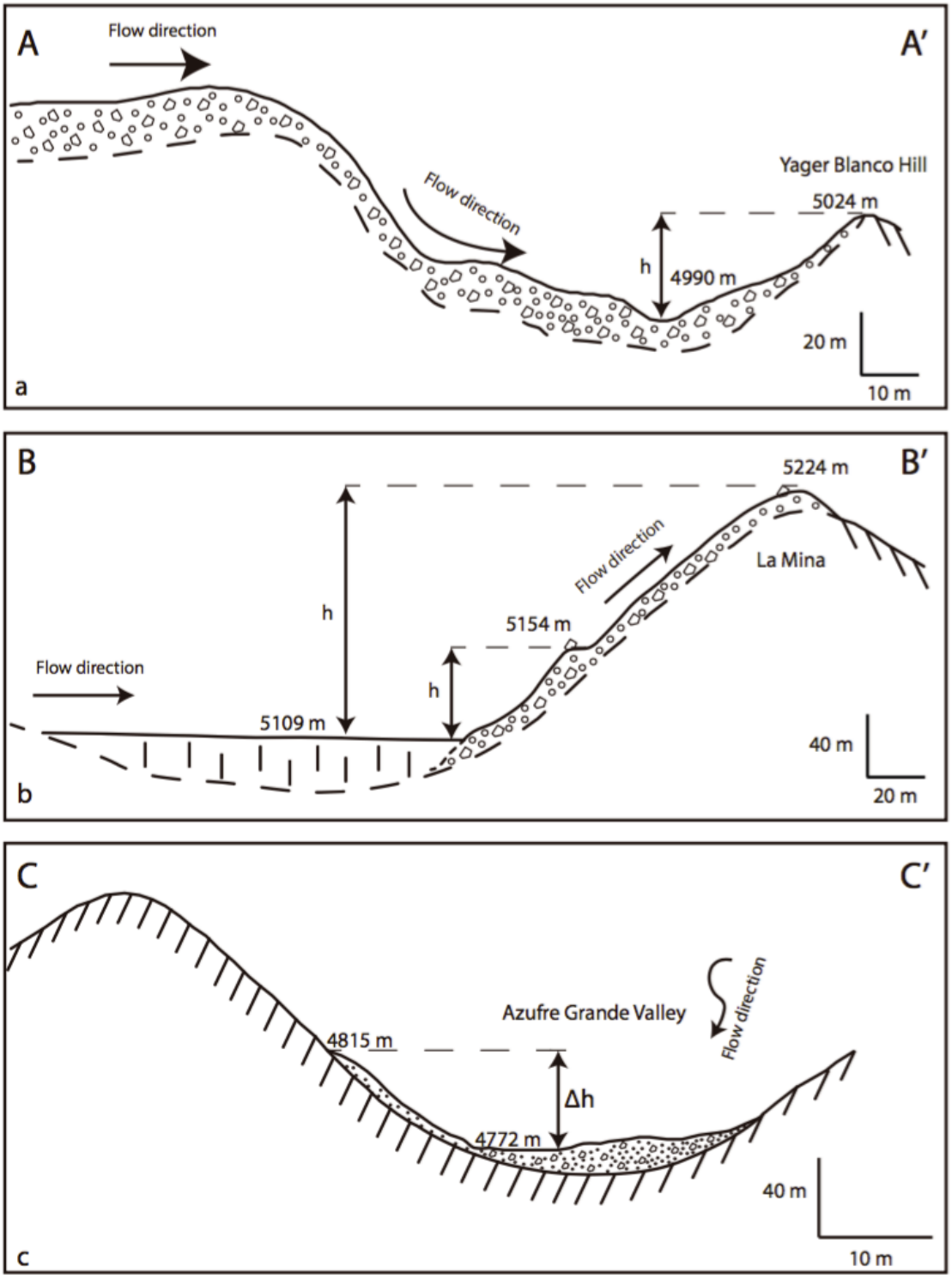

Figure 8: a) Cross-section of run-up A area; h shows the difference of elevation between the bottom of the valley and the highest mark of the DAD deposit up to Yager Blanco Hill. b) Cross-section of run-up B in La Mina area; the highest pulse reached the altitude of 5224 m asl and the smaller reached 5154 m asl. c) Cross-section of super-elevation C at Azufre

Grande valley showing the difference of altitude between the deposit at the bottom of the valley and the mark leaving for the deposit on the right side of the valley (left side in the picture).

Table 1 shows the parameters and results of equations 1 and 2. For run-up A (Yager Blanco hill) the velocity is 25.8 m/s and for run-up B (Basal Tutupaca) the velocity is 47.4 m/s. The velocity for super-elevation C (Azufre Grande valley) is 69.8 m/s. The velocity values are in agreement those reported for other debris avalanches in the literature like Mt. Meager: from 3 to 117 m/s (Allstadt 2013), Mt Saint Helens: from 50 to 70 m/s (Voight, 1981) or Soufrière Hills: mean of 27 m/s (Voight et al., 2002) and Bezymianny: maximum of 60 m/s (Belousov et al. 2007).

	h (m)	△h (m)	g (m/s^2)	b (m)	rc (m)	U (m/s)	U (km/h)
Run-up A	34	--	9.8	--	--	25.8	92.9
Run-up B	115	--	9.8	--	--	47.4	170.9
Super-elevation C	--	43	9.8	198.0	2293.1	69.8	251

Table 1. Super elevations and run-up at Azufre avalanche deposits. Parameters and results. U= velocity, g = gravitational acceleration and h = height of the run-up, r_c = centerline radius of curvature and b = channel width

6. Discussion

The Azufre DAD in the framework of the Eastern Tutupaca development

The Eastern Tutupaca edifice is a dacitic dome complex that, based on its young morphology and the lack of glacial erosion, is considered of Holocene age. The relics of the older domes of this edifice are represented by domes I, II and III, located in the northern part of the complex (Figure 9). These domes were affected by a sector collapse that triggered the Azufre debris avalanche. A remnant of this escarpment is found in the northern part of the complex. Due to the presence of PJB blocks of BR-DAD facies of the Azufre DAD, we consider that these domes were still hot at the time of collapse. After the Azufre DAD, in this newly formed amphitheater, dome growth resumed and formed the Domes IV and V, which are mostly located to the S and SE of the former amphitheater. Then, the Domes VI and VII were

emplaced directly upon the Azufre DAD. This newly reconstructed Eastern Tutupaca edifice was affected by a second sector collapse that produced the current amphitheatre and the Paipatja DAD that spread-out to the NE of the dome complex (Chapter 3).

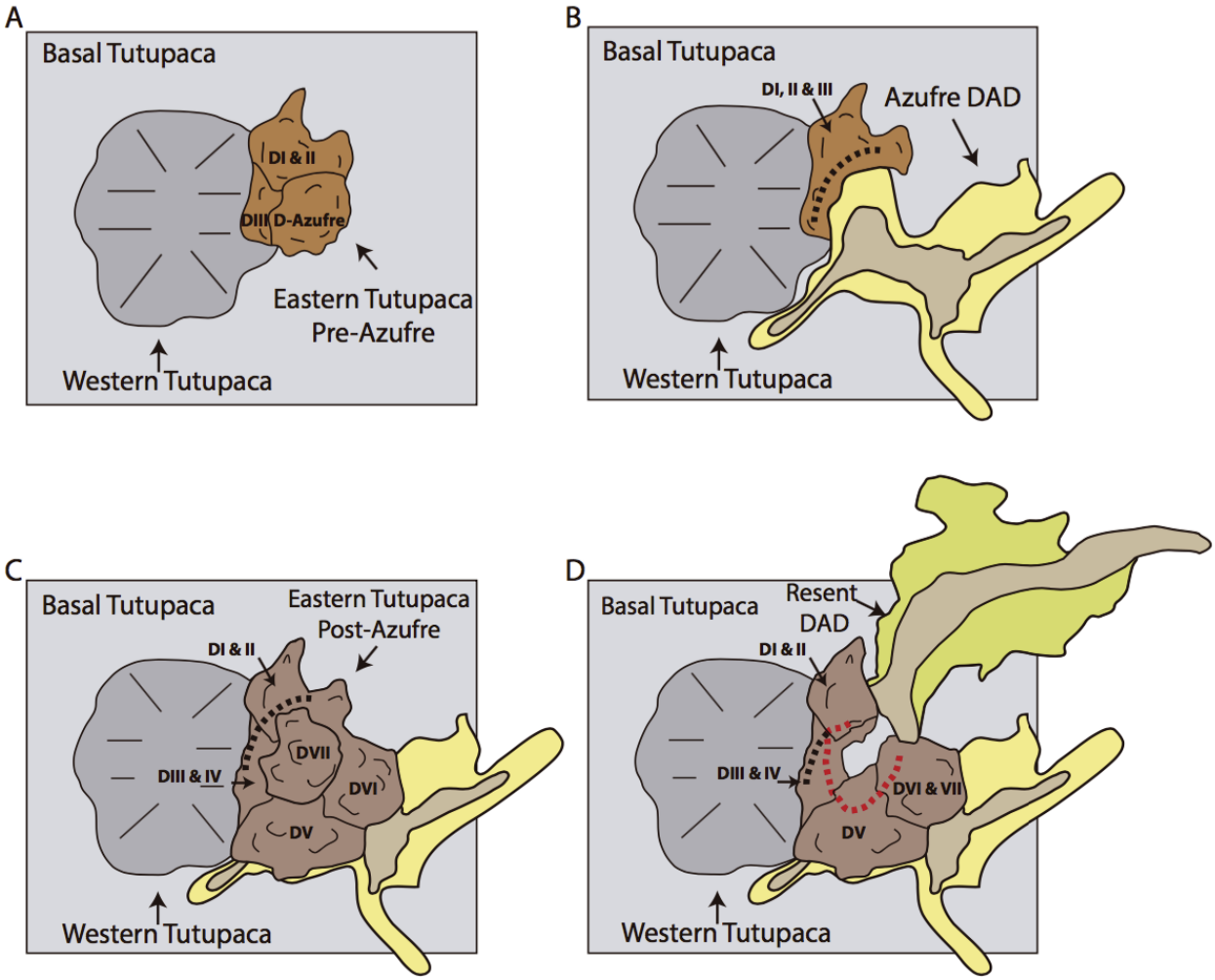

Figure 9: Sketches showing the evolution of Tutupaca volcano before and after the two modern avalanches that affected the youngest edifice. Also shown is the spatial distribution of both debris avalanches deposits.

Triggering mechanism of Azufre DAD

The Tutupaca Basal edifice shows signs of frequent deep seated landslides and so it would have been easily deformed and destabilized by intruding magma. The DAD Azufre occurred soon after the eruption of the firsts domes, and as it is mostly composed by Basal Tutupaca material, the dome would only have been relatively small; the collapse was thus predominantly a destabilization of the older edifice. The collapse could have been caused by

loading from the new dome, pushing of magma intruding the edifice, or from increasing pore pressure due to the reactivating hydrothermal system. The presence of an active fault system crossing the complex open the possibility of a fault associate earthquake as a trigger of the collapse. The avalanche spread over a highly irregular topography and was channeled into four valleys, where super-elevation and run-ups give maximum velocities of about 40-60 m/s.

Although the Azufre avalanche is clearly older than the historical one (Chapter 3), it is very little altered by erosion so that detailed field work and interpretation of the surface structures (hummocks, flowbands) permitted us to find the source of the avalanche. A partially exposed segment of the Azufre avalanche scarp is located between the two youngest edifices of the volcanic complex (Figure 2), and is possible to appreciate how a segment of the Azufre avalanche scarp also includes the recent avalanche scar, showing an evident weak area, controlled by the faults system before described.

7. Conclusions

The geological history of the Eastern Tutupaca edifice, which was constructed on top of a highly hydrothermalized edifice and traversed by an active fault system, created the conditions for the destabilization and collapse of the volcanic edifice at least two times during its recent volcanic history. Thus, the triggering mechanism for collape of theTutupaca edifice seems to be the extrusion of huge dacitic domes on an unstable and deformed substratum (Figure 9).

The Azufre debris avalanche occurred as part of the Holocene, Eastern Tutupaca dome activity. Given the extremely fresh nature of its deposits, we consider a Holocene age, although it is certainly older than the Patpatja DAD, dated at 218±14 yBP (Samaniego et al., 2015).

Reactivation of highly altered volcanoes is likely to occur at other places in the Andes as there are many hydrothermally altered edifices and as disperse magmatism is ongoing (e.g. Tutupaca, Ticsani, Huaynaputina in historical times). Thus the type of scenario we present here for Tutupaca is likely to occur again. The Ubinas volcano, while erupting a more

basic magma (Rivera et al., 2010), could also suffer this type of event as it is strongly altered and eroded on its southern side. The ancient avalanche of Ticsani (Mariño, 2002, Bernard, 2008, Byrdina et al., 2013) is an example of a much more voluminous type of collapse than at Tutupaca.

Chapter 3:

THE HISTORICAL (218 ± 14 YBP) ERUPTION OF TUTUPACA VOLCANO (SOUTHERN PERU)

Summary

The Tutupaca volcanic complex is a little known volcanic centre located in southern Peru. This dacitic dome complex has experienced at least two mayor large mass-movement events that compromise and determinate its geological evolution during Holocene times. The last mayor event occurs only 218 ± 14 years before present (yBP) and is one of the larger explosive volcanic events to have occurred in southern Peru during historical times. On the basis of an important fieldwork and additional radiocarbon datings, we were able to reconstruct the eruptive dynamism associated with the last eruption of this volcano and correlate the studied deposits with some rare historical reports of volcanic activity in this part of the Andean range. This chapter correspond to a paper that I co-authored and that was recently published at *Bulletin of Volcanology* (Samaniego et al., 2015).

The most striking characteristic of this recent edifice is the ~1-km-wide collapse amphitheater open to the NE and a related hummocky and ridged debris avalanche deposit that spreads out on the north-eastern adjacent highlands. The sector collapse scarp at Tutupaca has an inner bowl shape, opening to a shallow outer scar and slide plane. The inner upper walls of the scar consist of unaltered dome lava, underlain by reddish altered dome lavas, both correlative with Eastern Tutupaca domes, and highly altered lavas of the lower Tutupaca Basal edifice. The scar opens onto a 25° inclined slope on which similarly inclined basal volcano strata outcrop under a partial cover of later collapse breccia. The base of the outer scar is composed of slightly altered lavas and intensely hydrothermally altered white and yellow zones.

The debris avalanche deposit (<1 km^3) is genetically and spatially associated with a pyroclastic density currents deposits. Both units were emplaced synchronously and spread onto the Paipatja plain situated to the northeast of Tutupaca volcano. Based on the spatial and temporal relationship between this recent debris avalanche and the pyroclastic density current deposits, coupled with the petrological similarity between the juvenile fragments in the debris avalanche, the pyroclastic density current deposits and the pre-avalanche domes we propose that juvenile magma was involved in the sector collapse. Thus, the ascent of a

magma, coupled with the fact that the new Tutupaca dome complex was constructed inside of the amphitheatre leave by the Azufre avalanche, on top of an older, altered volcanic sequence, probably induced the destabilisation of the hydrothermally active edifice. This triggering mechanism differs from that described for Azufre debris avalanche (Chapter 2) for which no explosive phase accompanied the sector collapse.

This eruption probably represents the youngest debris avalanche in the Andes and was accompanied by one of the larger explosive events to have occurred in Southern Peru during historical times.

Bull Volcanol (2015) 77:51
DOI 10.1007/s00445-015-0937-8

RESEARCH ARTICLE

The historical (218±14 aBP) explosive eruption of Tutupaca volcano (Southern Peru)

Pablo Samaniego[1] · Patricio Valderrama[1,2] · Jersy Mariño[2] · Benjamín van Wyk de Vries[1] · Olivier Roche[1] · Nélida Manrique[2] · Corentin Chédeville[1] · Céline Liorzou[3] · Lionel Fidel[2] · Judicaëlle Malnati[1]

Received: 22 January 2015 / Accepted: 14 May 2015

Abstract The little known Tutupaca volcano (17° 01′ S, 70° 21′ W), located at the southern end of the Peruvian arc, is a dacitic dome complex that experienced a large explosive eruption during historical times. Based on historic chronicles and our radiometric data, this eruption occurred 218±14 aBP, probably between 1787 and 1802 AD. This eruption was characterised by a large sector collapse that triggered a small debris avalanche (<1 km^3) and an associated pyroclastic eruption whose bulk volume was 6.5–7.5×10^7 m^3. Both units were emplaced synchronously and spread onto the plain situated to the northeast of Tutupaca volcano. The spatial and temporal relationship between the debris avalanche and the pyroclastic density current deposits, coupled with the petrological similarity between the juvenile fragments in the debris avalanche, the pyroclastic density current deposits and the pre-avalanche domes, indicates that juvenile magma was involved in the sector collapse. Large amounts of hydrothermally altered material are also found in the avalanche deposit. Thus, the ascent of a dacitic magma, coupled with the fact that the Tutupaca dome complex was constructed on top of an older, altered volcanic sequence, probably induced the destabilisation of the hydrothermally active edifice, producing the debris avalanche and its related pyroclastic density currents. This eruption probably represents the youngest debris avalanche in the Andes and was accompanied by one of the larger explosive events to have occurred in Southern Peru during historical times.

Keywords Tutupaca · Peru · Central Andes · Explosive activity · Sector collapse · Volcanic hazards · Historical activity

Editorial responsibility: S. De la Cruz-Reyna

✉ Pablo Samaniego
pablo.samaniego@ird.fr

[1] Laboratoire Magmas et Volcans, Université Blaise Pascal-CNRS-IRD, 5 rue Kessler, 63038 Clermont-Ferrand, France

[2] Observatorio Vulcanológico del INGEMMET, Dirección de Geología Ambiental y Riesgo Geológico, Urb. Magisterial B-16, Umacollo, Arequipa, Peru

[3] Université de Brest, CNRS, UMR 6538 Domaines Océaniques, Institut Universitaire Européen de la Mer, Place Copernic, F-29280 Plouzané, France

Introduction

The Peruvian volcanic arc results from the subduction of the oceanic Nazca plate beneath South-American continental lithosphere. This volcanic province, which belongs to the Central Volcanic Zone of the Andes, is formed upon the Western Cordillera of the Peruvian Andes, and it comprises at least 12 Late Pleistocene and Holocene volcanic centres and several monogenetic fields (Siebert et al. 2010). Among these volcanic centres, seven volcanoes have experienced eruptive activity since the arrival of the Spanish conquistadors in the sixteenth century. These edifices include the well-know El Misti, Ubinas, Sabancaya and Huaynaputina volcanoes, as well as other lesser-studied edifices such as Ticsani, Tutupaca and Yucamane (Fig. 1).

On the basis of numerous studies over the last decades, the eruptive chronologies of a number of these volcanic centres are well constrained. The two last major explosive events in this part of the Andes were the large 2-ka BP plinian eruption of El Misti volcano (Volcanic Explosive Index-VEI of 5; Thouret et al. 2001; Harpel et al. 2011; Cobeñas et al. 2012) and the 1600 AD explosive eruption of Huaynaputina volcano which was the biggest historical explosive eruption in the

Published online: 24 May 2015

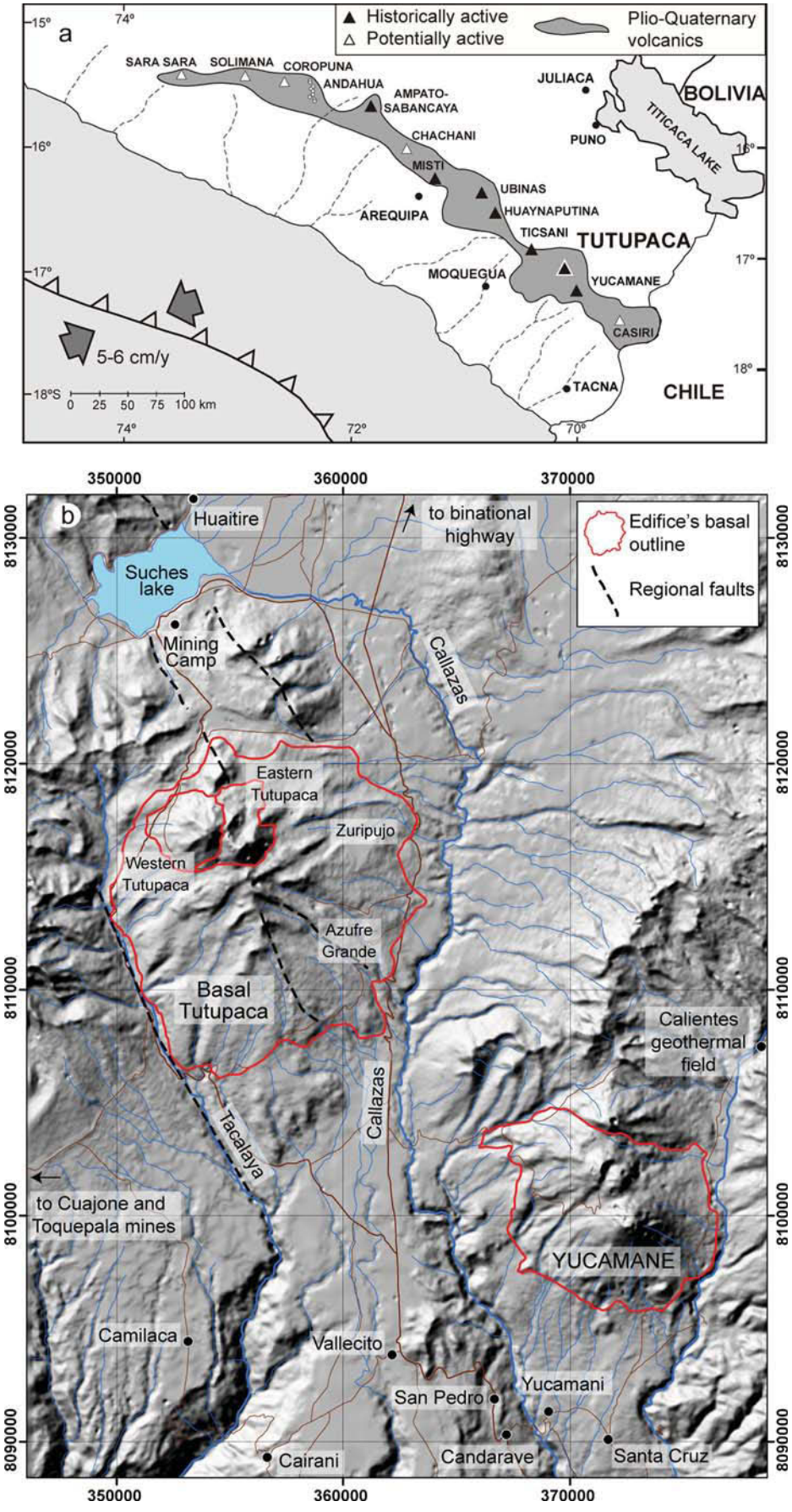
a
Historically active
Potentially active
Plio-Quaternary volcanics
SARA SARA
SOLIMANA
CORPUNA
ANDAHUA
AMPATO-SABANCAYA
CHACHANI
MISTI
UBINAS
HUAYNAPUTINA
TICSANI
TUTUPACA
YUCAMANE
CASIRI
AREQUIPA
MOQUEGUA
TACNA
JULIACA
PUNO
TITICACA LAKE
BOLIVIA
CHILE
5-6 cm/y
b
Huaitire
to binational highway
Edifice's basal outline
Regional faults
Suches lake
Mining Camp
Callazas
Eastern Tutupaca
Zuripujo
Western Tutupaca
Azufre Grande
Basal Tutupaca
Calientes geothermal field
Tacalaya
to Cuajone and Toquepala mines
YUCAMANE
Camilaca
Vallecito
San Pedro
Yucamani
Cairani
Candarave
Santa Cruz

◀ **Fig. 1** **a** Location of Tutupaca volcano in the Peruvian volcanic arc. **b** Regional map showing the location of the Tutupaca and Yucamane volcanoes

Andes (VEI 6, Thouret et al. 1999; Adams et al. 2001). Other small to moderate explosive events occurred at El Misti in the 15th century (Thouret et al. 2001), as well as at the frequently active Ubinas edifice that experienced at least 25 eruptive episodes since the 16th century (Thouret et al. 2005; Siebert et al. 2010) including a moderate-size eruption in 1667 AD and the recent eruptions of AD 2006–2009 and 2013–2015 (Rivera et al. 2014). Last, rare historical accounts suggest that Sabancaya volcano was also active in the 18th century (AD 1750, 1784), and more recently, vulcanian explosive activity was described in AD 1988–1997 (Siebert et al. 2010; Gerbe and Thouret 2004). All this information shows that the Peruvian segment of the Andean Central Volcanic Zone experienced significant explosive activity through the last few centuries.

Tutupaca volcano (17° 01′ S, 70° 21′ W) is located at the southern end of the Peruvian arc (Fig. 1), 25–30 km to the north of Candarave village (Tacna Department, Southern Peru). Historical chronicles reported by Hantke and Parodi (1966) indicate that several volcanic eruptions affected this part of the Andes in AD 1780, 1787, 1802, 1862, and 1902. These authors suggested that the source of these eruptions was Tutupaca volcano. However, based on the youthful and uneroded morphology of the contiguous Yucamane volcano, several authors attributed these eruptions to the latter (Siebert et al. 2010; de Silva and Francis 1990). In this manuscript, we present results of a detailed study of recent Tutupaca eruptive products, which include field descriptions of the main volcanic units, petrologic characterisation of juvenile material, radiocarbon dating and correlation with historical records. With these results, we reconstruct the eruptive sequence associated with the last eruption of Tutupaca, which is an unidentified historical explosive event in the Andes.

Overall structure of Tutupaca volcano

The Tutupaca volcanic complex is constructed on top of a high volcanic plateau consisting of volcanic and volcano-sedimentary rocks, which include thick Mio-Pliocene ignimbritic deposits (Fidel and Zavala 2001; Mamani et al. 2010). This sequence is well exposed in the Callazas and Tacalaya valleys located at the eastern and western parts of the complex (Fig. 1). The Tutupaca volcanic complex rises from the basement at 4400–4600 m above sea level (m asl) and is composed of a big basal edifice and two small "twin" peaks (the Western and Eastern Tutupaca), which are located at the northern part of the volcanic complex and constructed on the remnants of the basal volcano (Figs. 1 and 2). Several fault systems have been identified in this part of the Andean cordillera, the main one being a series of normal faults with a sinistral component that has been mapped around the Suches lake and that displays a roughly N140 direction (Benavente et al. 2010). These faults affected the volcanic complex and seem to have influenced its structural development (Fig. 1).

The *Basal Tutupaca* edifice is mostly composed of andesitic and dacitic lava flows. Based on the radial distribution and dips of these lavas, we infer that the former summit was located 2–3 km to the south of the current Tutupaca peaks. The summit zone is characterised by an uneven topography and strong hydrothermal alteration (Figs. 1 and 2). This edifice was strongly affected by Pleistocene glaciation, resulting in the highly eroded morphology and glacial modification of several radially oriented valleys. As a result, major moraine deposits (up to 100 m thick) were stacked mostly in the southern part of the complex, as well as in the Callazas and Tacalaya valleys. These moraines are probably formed during the Last Glacial Maximum (LGM), which has been broadly dated at 17–25 ka in the Western Cordillera of the Peruvian Andes (Smith et al. 2008; Bromley et al. 2009). In addition, a thick ignimbrite deposit of dacitic composition outcrops on the southern and western flanks of the edifice and represents a major explosive phase that probably occurred at the end of edifice evolution. This ignimbrite deposit is covered by the

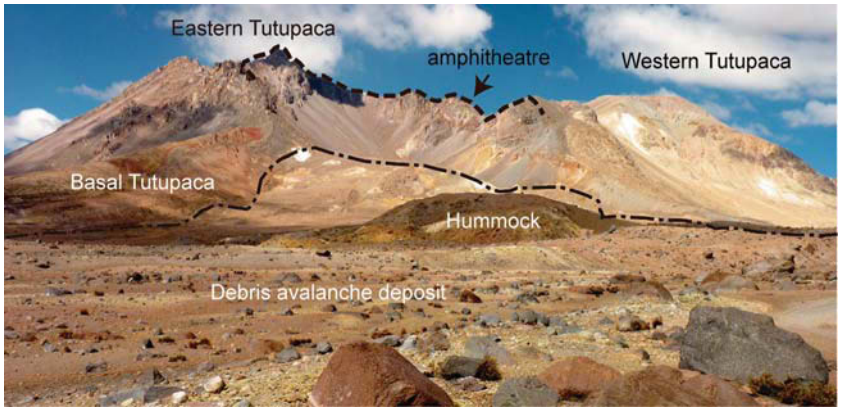

Fig. 2 Panoramic view of the north-east of Tutupaca volcano and its amphitheatre

LGM moraines, suggesting an age older than 25 ka. The less massive *Western Tutupaca* peak (5815 m asl) is mostly composed of lava flows and domes of siliceous andesitic and dacitic compositions. This edifice was also eroded by the Late Pleistocene glaciers. A sequence of tephra fallout deposits outcropping in the distal south-western part of the volcano shows that this edifice experienced powerful plinian to subplinian eruptions during its history. Last, the younger *Eastern Tutupaca* peak (5790 m asl) is a dacitic dome complex characterised by a lack of glacial erosion, suggesting a Holocene age. It is composed of at least 7 coalescing lava domes (Manrique 2013), which are cut by a 1-km-wide horseshoe-shaped amphitheatre open to the NE (Fig. 1b). It is worth noting that the direction of opening of the amphitheatre is almost orthogonal to the N140 regional faults that cut the edifice. We identified at least two debris avalanche deposits associated with this edifice: an older deposit that is channelised in the valleys located to the E (Zuripujo) and SE of the volcano (e.g. Azufre Grande) and a younger deposit that outcrops immediately to the NE of the amphitheatre and that will be described in detail in this work.

The recent eruptive products

The north-eastern part of Eastern Tutupaca edifice (Figs. 2 and 3) exhibits a remarkably well-preserved volcanic sequence characterised by abundant surface structures. Here, we describe the main characteristics of these deposits in stratigraphic order. The detailed descriptions of these deposits and their surface structures, as well as their dynamic implications, are beyond the scope of this manuscript and are discussed in a companion paper (Valderrama et al. 2014).

The Zuripujo pyroclastic density current deposit (Z-PDC)

Exposed in the lower part of the Zuripujo valley, 8–10 km from the Eastern Tutupaca edifice, is a 2–5-m-thick unit composed of at least two or three block-and-ash flow deposits, which are interlayered with centimetre-thick ash-rich layers showing cross-bedding and lamination (Figs. 3, 4 and 5). The block-and-ash flow deposits are massive, matrix-supported, with 20–30 vol.% angular and subangular blocks in an unconsolidated, grey, medium ash matrix. The block sizes range from 5 to 10 cm, although 1-m diameter blocks are also locally observed. The deposit is mostly polylithologic, but the most common lithology is dark grey, unaltered, dense dacitic blocks with plagioclase, amphibole and biotite in a vitreous groundmass. These blocks, and the breadcrust bombs also locally observed, are interpreted as representing a collapsing dome. A large amount of slightly altered, dark grey, pyroxene-rich andesitic blocks are also present in the deposit and are interpreted as blocks entrained from underlying units of the older edifice. The most striking characteristic of this deposit, however, is the relatively large amount (5–10 vol.%) of centimetre-size, white-yellowish, highly altered, friable lava fragments that are also present as smaller clasts in the matrix of the deposit (Fig. 5). Three charcoal samples collected in this unit have been dated and yielded almost identical ages (190± 30, 220±30 and 230±30 aBP; Table 1). At the Zuripujo valley, the Z-PDC unit is overlain by an up to 1-m-thick (Figs. 4 and 5), locally reworked, grey-reddish ash-rich layer that includes some breadcrust bombs at the top and is interpreted as a lateral facies of the Paipatja pyroclastic density current deposit (P-PDC, see below). The contact between these two units is commonly flat, although in rare outcrops, we observed erosive features as well as a 10–30-cm-thick layer of reworked material.

The upper part of the Zuripujo valley exposes a 3–5-m-thick sequence of block-and-ash flow deposits that covers an older debris avalanche deposit. This block-and-ash unit, which can be traced up to the eastern foot of the Tutupaca domes, displays a rough surface morphology characterised by an enrichment in metric-size angular blocks and flow structures such as the fan observed at the Zuripujo valley bifurcation, 4–5 km from the Eastern Tutupaca summit. The spatial continuity between the proximal and distal deposits at Zuripujo valley, its stratigraphic position (both covered by the Paipatja PFD) and the petrography of the blocks indicate that they are parts of the same volcanic unit.

The Tutupaca debris avalanche deposits

This unit is exposed towards the northeast of the Tutupaca dome complex, in a zone between the amphitheatre and the Villaque and Taipicirca hills (Fig. 3), over an area of around 12–13 km^2. In the proximal zone (i.e. the first 3 km from the Tutupaca amphitheatre), a heterogeneous breccia is exposed, composed of two successive units interpreted as debris avalanche deposits. At the foot of the amphitheatre, the lower unit forms a massive, Toreva block-like structure 1–1.5 km in diameter and 150–200 m high that is flanked by two 1.5-km-long levees diverging from the amphitheatre. Downhill, the deposit consists of several 200–700-m-long, 20–40-m-high megablocks, as well as smaller 100–200-m-long hummock-like hills (Figs. 3, 4 and 6). These features are composed of a heterogeneous, polymict breccia, which, following Glicken's (1991) facies terminology, is a block facies consisting of highly cataclased, metric-size blocks with abundant jigsaw cracks in a fine-medium sand matrix. Lava blocks are mostly highly altered (hydrothermally altered), yellow-reddish andesites, although other petrographic types are observed and include oxidised, reddish-grey andesites, and scarce, unaltered, dark grey andesites and dacites. Given the high amount of altered fragments, we call this unit the Hydrothermally-Altered Debris Avalanche Deposit (HA-DAD, Fig. 6).

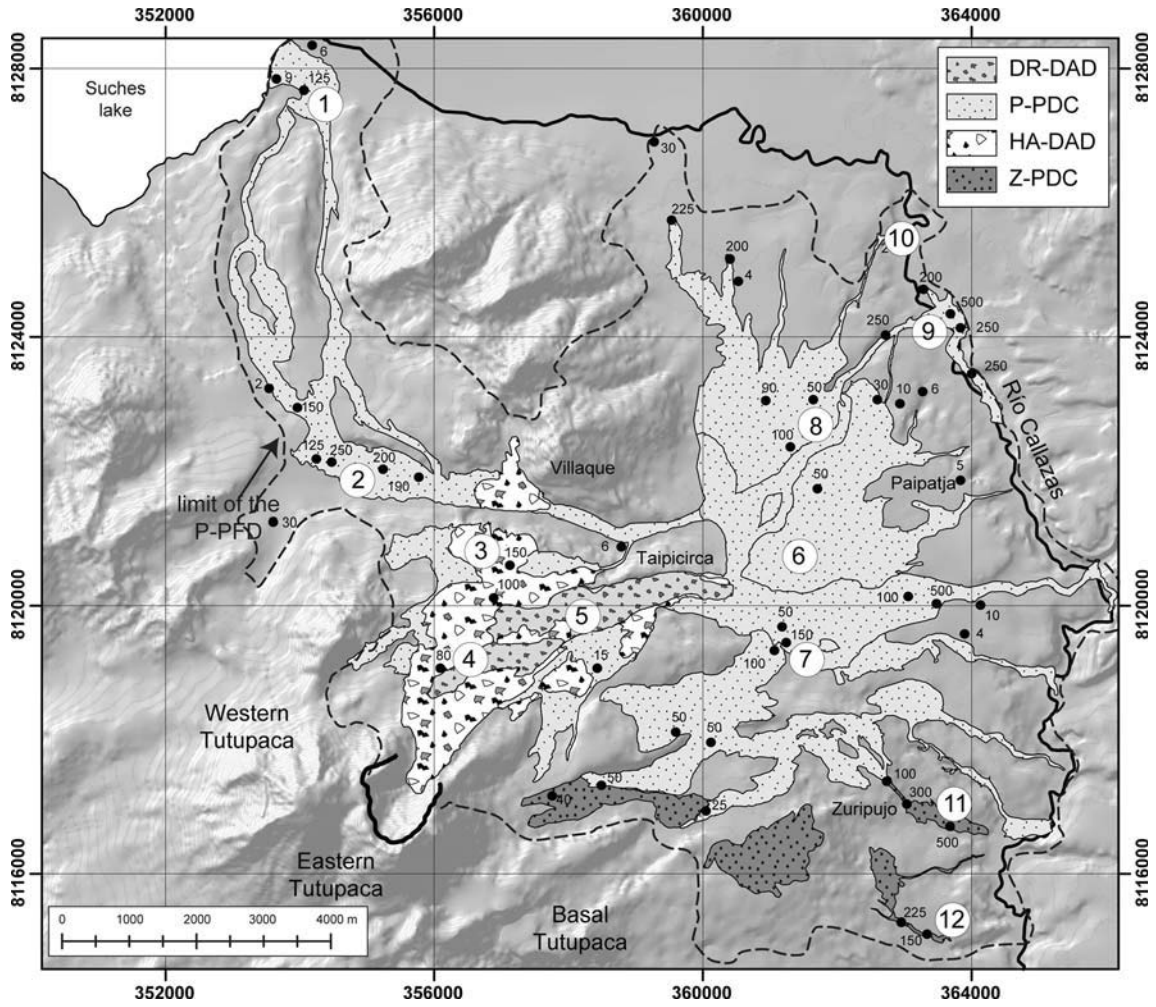

Fig. 3 Simplified geological map of the Recent Tutupaca deposits. Location of main stratigrafic sections is shown. *Z-PDC* Zuripujo pyroclastic density current deposit, *HA-DAD* hydrothermally altered debris avalanche deposit, *P-PDC* Paipatja pyroclastic density current deposit, *DR-DAD* dome-rich debris avalanche deposit. The area delimited by the *black dashed line* corresponds to the lateral and distal deposits related to the ash-cloud accompanying the P-PDC. *Dots* correspond to minimum thickness (in cm) of P-PDC

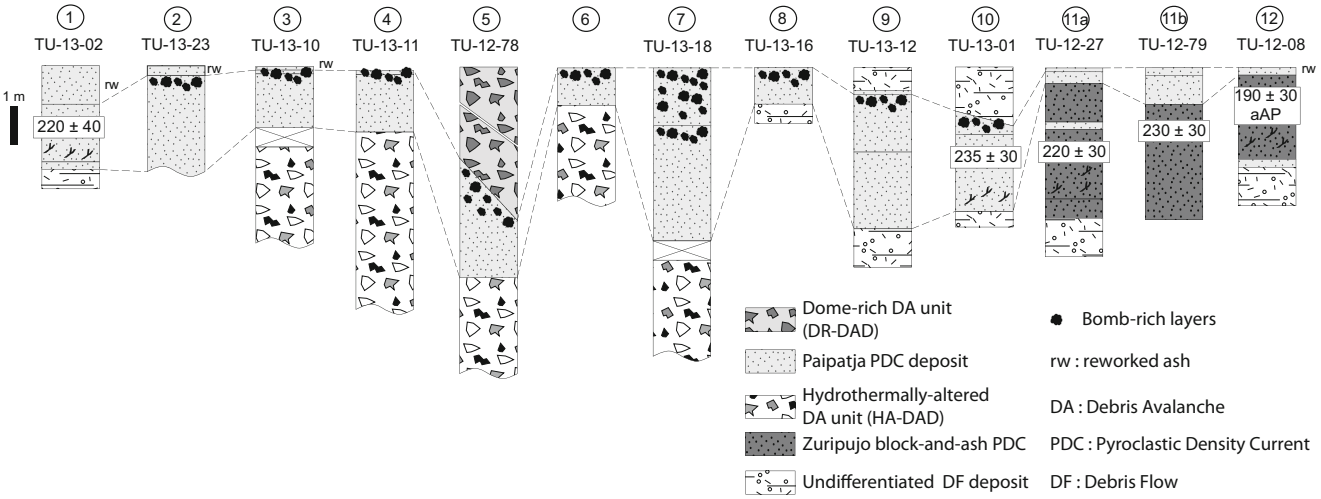

Fig. 4 Composite stratigraphic sections of the Tutupaca debris avalanche deposits and related pyroclastic flow deposits. Location of the stratigraphic sections is shown in Fig. 3

Fig. 5 Photos of the Zuripujo pyroclastic density current deposit (Z-PDC). **a** Outcrop of 4–5-m-thick outcrop of Z-PDC in the Zuripujo valley (site 11, samples TU-12-27 and TU-12-79, Fig. 3). **b** The upper 2 m of outcrop (**a**) showing the Z-PDC overlain by the Paipatja pyroclastic density current deposit (P-PDC). Note the presence of breadcrust bombs in the Z-PDC. **c** The Z-PDC at a small ravine located to the south of the main Zuripujo valley (site 12, sample TU-12-08, Fig. 3). **d** Detail of the matrix of the Z-PDC deposit showing a charcoal fragment. Note also the abundance of light-coloured hydrothermally altered fragments

In the medial zone (i.e. roughly 3 to 6 km from the amphitheatre), the debris avalanche deposit is characterised by a rough surface morphology consisting of longitudinal, elongated ridges that commonly diverge with distance from the amphitheatre (Figs. 3 and 6). These ridges are 5–10 m wide, 150–400 m long and 2–5 m high (for a detailed description of these structures, the reader is referred to the companion paper of Valderrama et al. (2014)). In this medial zone, the debris avalanche deposit is exposed along two corridors. The first one follows an NNE direction, reaching the Taipicirca valley and defining an 80-m-high run-up onto the Villaque hill, whereas the second corridor is between two old moraines and follows an NE direction to reach the Paipatja plain. In this latter part, the HA-DAD unit is overlain by an upper deposit, which is mainly composed of unaltered (fresh) dark grey dome rocks of dacitic composition (Dome-Rich Debris Avalanche Deposit, DR-DAD, Fig. 6). This upper unit shows scarce evidence of cataclasis (such as jigsaw cracks), but instead shows abundant prismatically jointed blocks, indicating an origin in a still-hot dome complex. In between these two DAD units, we observed the Paipatja pyroclastic flow deposit described below.

Last, in the distal zone (i.e. more than 6 km from the amphitheatre), on the Paipatja plain and up to the Callazas river, the debris avalanche deposits are mostly covered by the Paipatja pyroclastic flow deposits (see below). Several big (>1 m in diameter) blocks distributed on the plain, whose bases are surrounded by the Paipatja pyroclastic flow deposit, suggest, however, that there is an underlying debris avalanche deposit up to a distance of 7–8 km from the amphitheatre. We estimate a volume of 0.6–0.8 km^3 on the basis of the mapped surface of the debris avalanche deposits and an average thickness of 25–40 m. This estimate probably represents a minimum volume, given that the Tutupaca debris avalanche deposit is covered by the Paipatja pyroclastic flow deposits.

Table 1 ^{14}C age results obtained in this study

Sample No.	Lab code	Locality	UTM Easting	UTM Northing	Unit	Type of sample	^{14}C age (a BP)	$\partial^{13}C$ (o/oo)	Calendar age range (cal AD) - 1 sigma -	Relative area (%)	Calendar age range (cal AD) - 2 sigma -	Relative area (%)
TU-12-08A	GrA 55325	Candarave-Huaytire road	363234	8114941	Zuripujo PDC	charcoal	190±30	−22.12	1670-1700	25	1664-1816	68
									1722-1782	42	1828-1893	20
									1795-1809	12		
									1838-1845	4		
									1867-1878	6		
TU-12-27B	GrA 54421	Qda. Zuripujo	363116	8116729	Zuripujo PDC	charcoal	220±30	-	1665-1679	15	1645-1700	27
									1733-1800	85	1721-1810	67
TU-12-79B	GrA 56328	Qda. Zuripujo	363178	8116684	Zuripujo PDC	charcoal	230±30	−21.80	1662-1675	17	1641-1698	30
									1738-1798	83	1723-1808	69
TU-13-01A	GrA 60691	Paipatja plain	362912	8125348	Paipatja PDC	charcoal	235±35	-	1654-1675	26	1636-1700	32
									1739-1798	74	1721-1810	64
TU-13-02B	GrA 57883	Suches lake	354047	8127482	Paipatja PDC	charcoal	220±40	-	1652-1688	28	1642-1712	28
									1728-1804	72	1717-1814	56
											1834-1891	10
Average							218±14		1671-1675	7	1662-1680	15
									1739-1783	85	1731-1802	85
									1795-1798	8		

These AMS ages were calculated at the Center for Isotope Research of the University of Groningen, Netherlands by the team of the Prof. J. van der Plicht. UTM coordinates correspond to the WGS 1984 projection (zone 19)

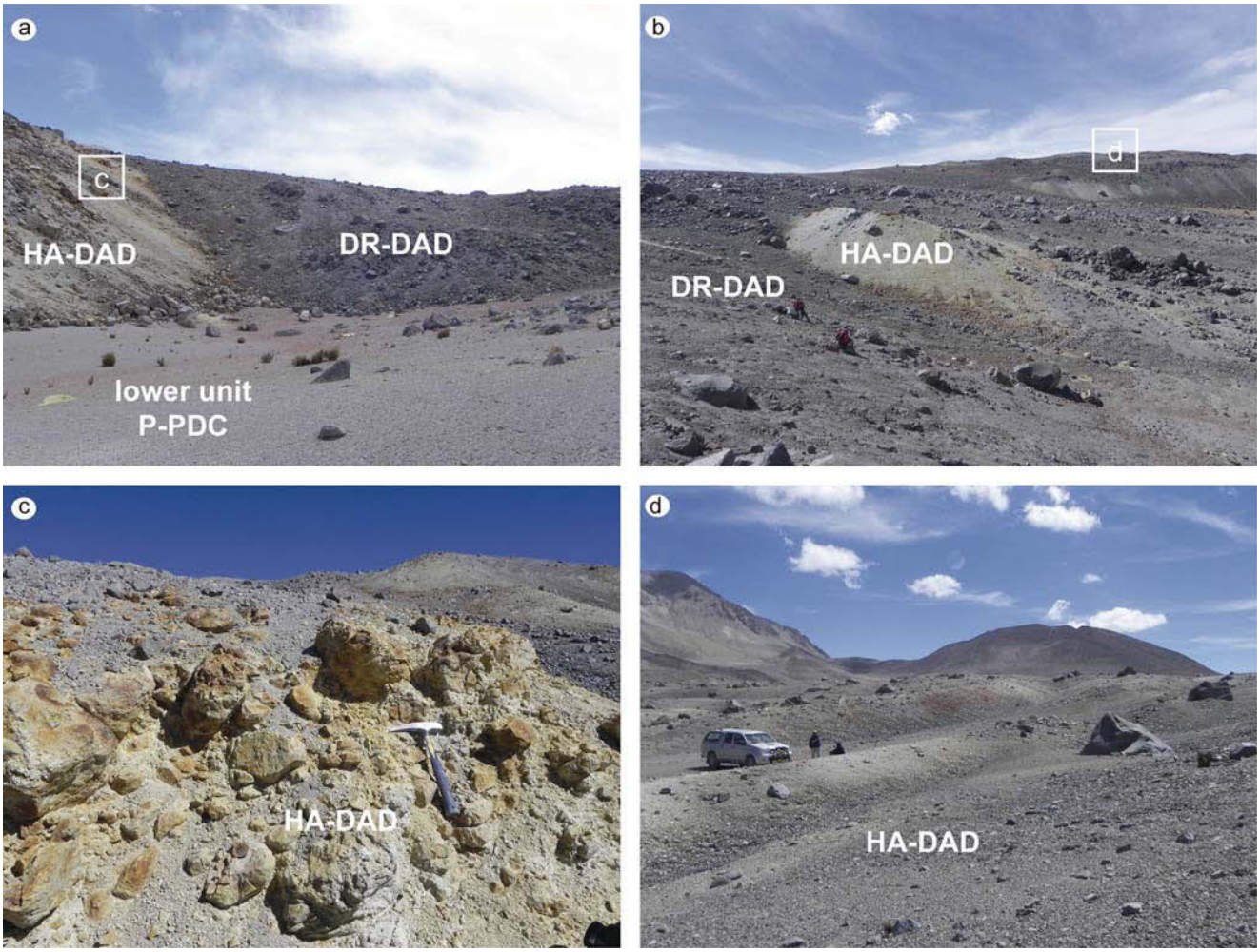

Fig. 6 Photos of the debris avalanche deposit (DAD) corresponding to the proximal-medial zone (site 5, Fig. 3). **a**, **b** Lower hydrothermally altered unit (HA-DAD) and upper dome-rich unit (DR-DAD). We also note the deposits of the P-PDC. **c** Detail of the HA-DAD showing the large amount of altered blocks. **d** Surface structures (ridges) observed at HA-DAD

The Paipatja pyroclastic density current deposit (P-PDC)

Distribution and stratigraphic relations

This unit spreads to the northeast of Tutupaca, reaching the Paipatja plain and the Callazas valley 8–10 km from the vent. A secondary branch of this unit reaches Suches lake 10–12 km from the vent (Fig. 3). In the proximal and medial zones (up to 6 km from the amphitheatre), this unit overlies the lower debris avalanche deposit unit (HA-DAD) and is covered by (and in some places interstratified with) the upper debris avalanche deposit unit (DR-DAD). In the distal zone (i.e. beyond 6 km from the amphitheatre), the P-PDC deposit also covers the main HA-DAD unit and appears to be mainly channelised in the numerous valleys draining the Paipatja plain, although an ash-rich, 10–20-cm-thick, over-bank deposit is also observed (Fig. 3). On the Paipatja plain, we observed two successive P-PDC units (Figs. 4 and 7). The widespread, lower unit covers the entire Paipatja plain and reaches the Callazas valley, whereas the upper unit is characterised by 1–1.5-m-thick bomb-rich lobes that overlie the lower unit (Figs. 4 and 7).

The thickness of the P-PDC unit is highly variable, ranging from 0.5 to 2 m thick on the Paipatja plain and around Suches Lake, to 2–5 m in the channelised distal zone in the Callazas valley. In addition, given that the P-PDC unit overrides the lower debris avalanche unit in the medial zone, it is less thick on the ridges than between them. As a result, large thickness variations (from around 10 cm to 1 m) are also observed on a scale as small as ~10 m. We stress that due to a lack of erosion, no cross sections exist in the flat area of the Paipatja plain and thus thickness measurements are scarce.

Deposit description and dating

Over the whole Paipatja plain, the P-PDC deposit is massive, matrix-supported, with 20–40 vol.% of angular to subangular lava blocks and bombs in a dark grey, medium-to-coarse ash matrix. Block size ranges from ~3 to 20 cm, although

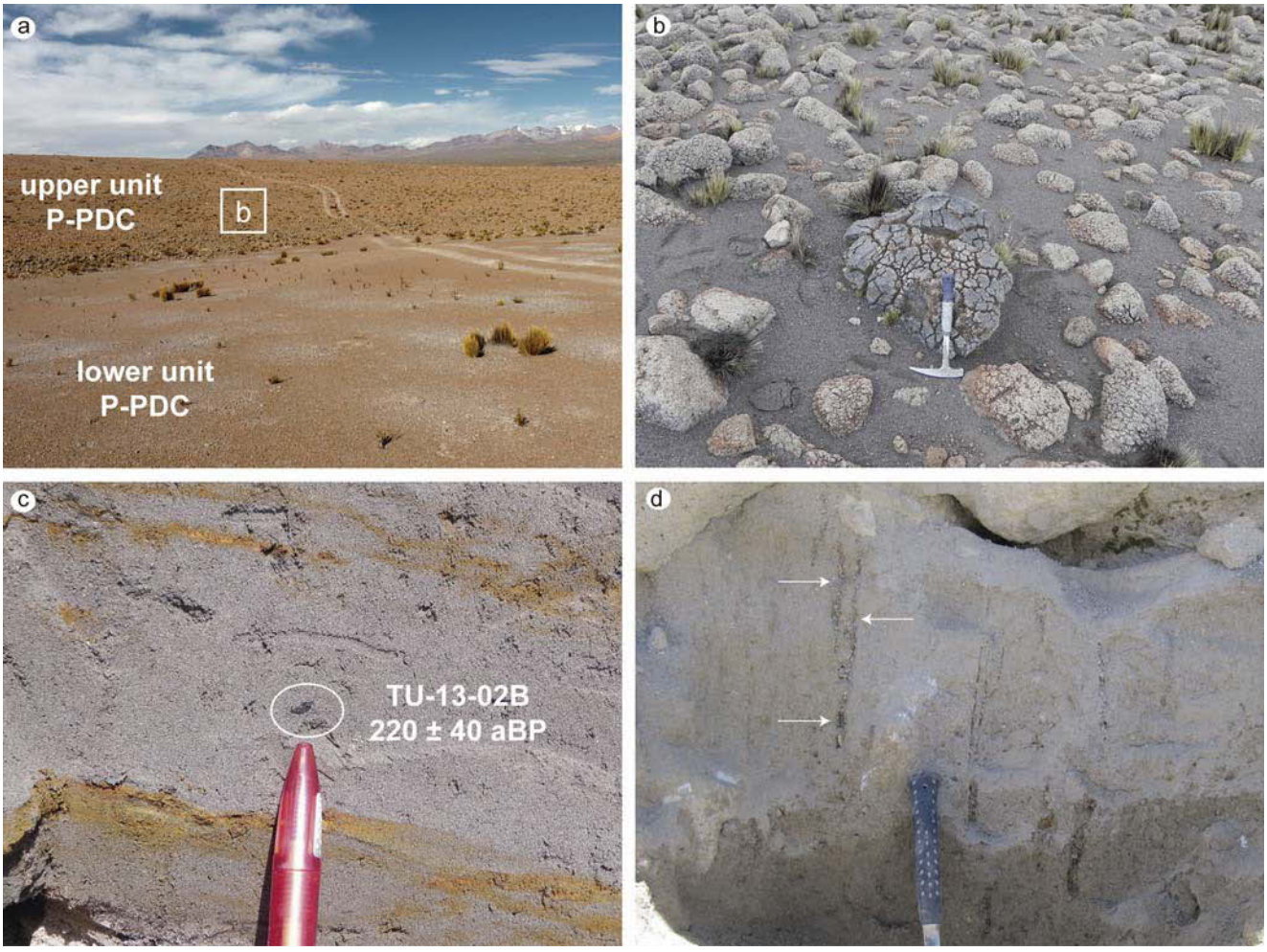

Fig. 7 Paipatja pyroclastic density current deposit (P-PDC). **a** Lower and upper units of P-PDC at Paipatja plain (site 7, Fig. 3). **b** Detail of the upper P-PDC deposit showing the enrichment in decimeter-size cauliflower- and breadcrust-like bombs. **c** Detail of the P-PDC deposit at the Suches lake (site 1, Fig. 3). Note the crude stratification of the fine grained matrix and the presence of many charred twigs and Andean grass (TU-13-02, age indicated). **d** Detail of the P-PDC at the distal end at Callazas valley (site 9, Fig. 3). Note the presence of gas escape pipes (marked by *arrows*)

occasional blocks 0.5–1 m in diameter are also observed. Bombs vary from 10 to 50 cm in size, and they are mostly observed at the deposit's surface. The deposit exhibits slight normal grading overall. No clear differences in the amount of blocks and bombs are observed between the proximal and distal parts of the deposit. In contrast, a progressive decrease in block size is observed with distance.

Extensive exposures of P-PDC unit exist in the Callazas valley, which hosts the maximum deposit runout (sites 9 and 10 at 8–10 km from the amphitheatre, Figs. 3 and 4). There, the P-PDC unit rests on a volcano-sedimentary sequence that includes debris flow deposits and fine-grained lacustrine deposits. The P-PDC deposit is composed of two main layers. The lower layer is mostly ash-rich, whereas the upper layer is highly enriched in bombs at the top of the deposit, with many centimetre-size gas escape pipes. Debris flow deposits comprising reworked material cover the P-PDC unit. Charcoal is extremely scarce in the Paipatja plain deposits, probably because outcrops exposing the base of the deposit are rare. However, at site 10 (Figs. 2 and 3), we found plenty of carbonised grass that yielded an age (235±35 aBP; Table 1), which is radiometrically indistinguishable from those obtained for the Zuripujo PDC deposits (190–230 aBP).

The northern branch of the P-PDC unit outcrops between the Villaque hill and Suches lake (Fig. 2). In this zone, the unit is topographically constrained, 1–2 m thick and appears as a grey, massive layer mostly composed of medium-to-coarse ash with scattered dense lapilli. Its base is composed of a 20–25-cm-thick layer exposing a crude planar stratification with some decimetric lenses of coarser and in places altered (oxidised) material. Overlying this basal layer, the bulk of the deposit does not have any laminations but shows a slight reverse grading. The fact that the P-PDC deposit is exposed in this zone suggests that at least the upper part of the PDC was able to surmount the Villaque hill. In this context, the deposits at Suches lake may have been formed by sedimentation from

the uppermost, more dilute part of the PDC, following the scenario described by Druitt et al. (2002) at Soufrière Hills volcano. The lower part of the unit bears plenty of charred twigs as well as carbonized grass that yield a very similar age to those of the Paipatja plain (i.e. 220±40 aBP; Table 1).

Granulometry and componentry

Grain size analysis was carried out on 14 selected samples from the P-PDC deposit. In the absence of natural, deep cross sections, we sampled the matrix of the deposit by digging (down to 150 cm) in flat areas from the proximal to distal parts of the deposit. Selected grain size histograms (Fig. 8) show that the deposit consists of fine ash to lapilli fragments (−4φ to +5φ), showing a large grain size distribution. Proximal (i.e. sites 11, 10) and central-distal (i.e. sites 12, 13) deposits have similar grain size distributions, which are clearly different from those of lateral deposits (i.e. sites 15C, 02D). In fact, the size distribution of the lateral facies, such as those in the Suches and Zuripujo valleys is almost unimodal, with a fines-enriched trend and good sorting (σ_φ~1-2), whereas central deposits are characterised by a "flat" distribution and poor sorting (σ_φ>2). The P-PDC deposits define a narrower grain size range and tend to be less well sorted than well-known blast deposits (Hoblitt et al. 1981; Druitt 1992; Belousov et al. 2007; Komorowski et al. 2013; Bernard et al. 2014), and fall instead (Fig. 8) into the "pyroclastic flow" field defined by Walker (1983).

Three main types of blocks are observed in the P-PDC deposit, the most abundant being angular to subangular,

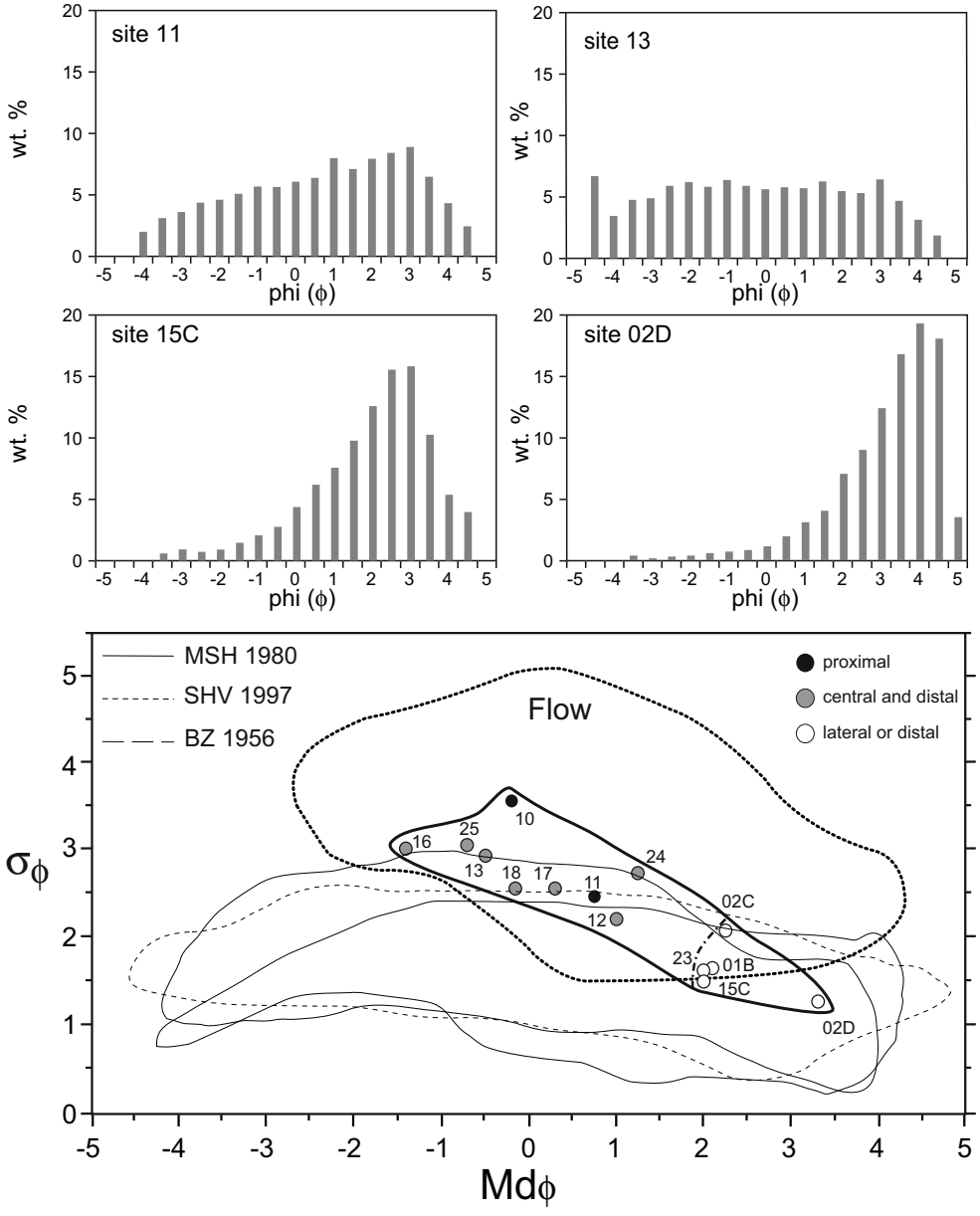

Fig. 8 **a–d** Selected grain size histograms for P-PDC samples. **e** Mdϕ vs σϕ diagram including the "Flow" field (Walker 1983) as well as the fields for different blast deposits (from Belousov et al. 2007). Mount St. Helens (MSH 1980), Bezymianny (BZ 1956) and Soufrière Hills (SHV 1997)

dense, porphyritic dacite blocks with many prismatically jointed fractures. A less abundant component corresponds to vesicular and highly porphyritic cauliflower- and breadcrust-type bombs, which are mostly observed on top of the deposit. A last, minor component corresponds to altered andesitic blocks interpreted as fragments entrained from the basement (*cf.* Roche et al. 2013). For the deposit matrix, we carried out a componentry analysis based on the methodology developed by Eychenne and Le Pennec (2012) in which at least 300 grains were chosen for fractions of −3φ to +1φ. We studied the same 14 samples as for the granulometric analyses, which are distributed from the proximal to distal zones. Three main classes of components were identified: fresh dome fragments, free crystals and altered lava fragments, the latter being interpreted as fragments from the old domes and the basal edifice. Fresh dome fragments range from 57 to 72 wt.%, free crystals (mostly present in the 0φ and +1φ classes) vary from 6 to 18 wt.% and altered fragments range from 20 to 48 wt.%.

Summary of petrologic characteristics

Based on 30 whole-rock major and trace element analyses, the Holocene eruptive products of Tutupaca volcano are classified as high-K calc-alkaline dacites (Fig. 9). All samples from the Eastern Tutupaca domes display a very restricted dacitic composition (64.4–66.1 wt.% SiO_2, normalised to an anhydrous basis, Table 2, Fig. 9), as well as the lava blocks included in the debris avalanche deposits and in the Z-PDC deposits, which show similar chemical characteristics (64.5–65.9 wt.% SiO_2). In contrast, the blocks and bombs of the P-PDC deposits have slightly higher silica contents (65.1–68.0 wt.% SiO_2), especially the scarce pumiceous samples, which have silica-rich compositions (67–68 wt.% SiO_2). For most major and trace elements, Eastern Tutupaca samples lie on the trend defined by the whole Tutupaca volcanic complex (Fig. 9). However, the Eastern Tutupaca rocks display a slight enrichment in some trace elements, namely the light rare earth elements (e.g. La) and a notable depletion in heavy rare earth elements (e.g. Yb), which leads to high La/Yb ratios for these Eastern Tutupaca samples (Fig. 9). A detailed petrological study is in progress, but our current hypothesis is that these characteristics are due to high-pressure crustal processes such as fractionation of amphibole and/or garnet and/or assimilation of deep crustal rocks (*cf.* Thouret et al. 2005; Mamani et al. 2010; Rivera et al. 2014).

Lava samples from the Eastern Tutupaca domes as well as those from the debris avalanche deposit are dark-grey, highly

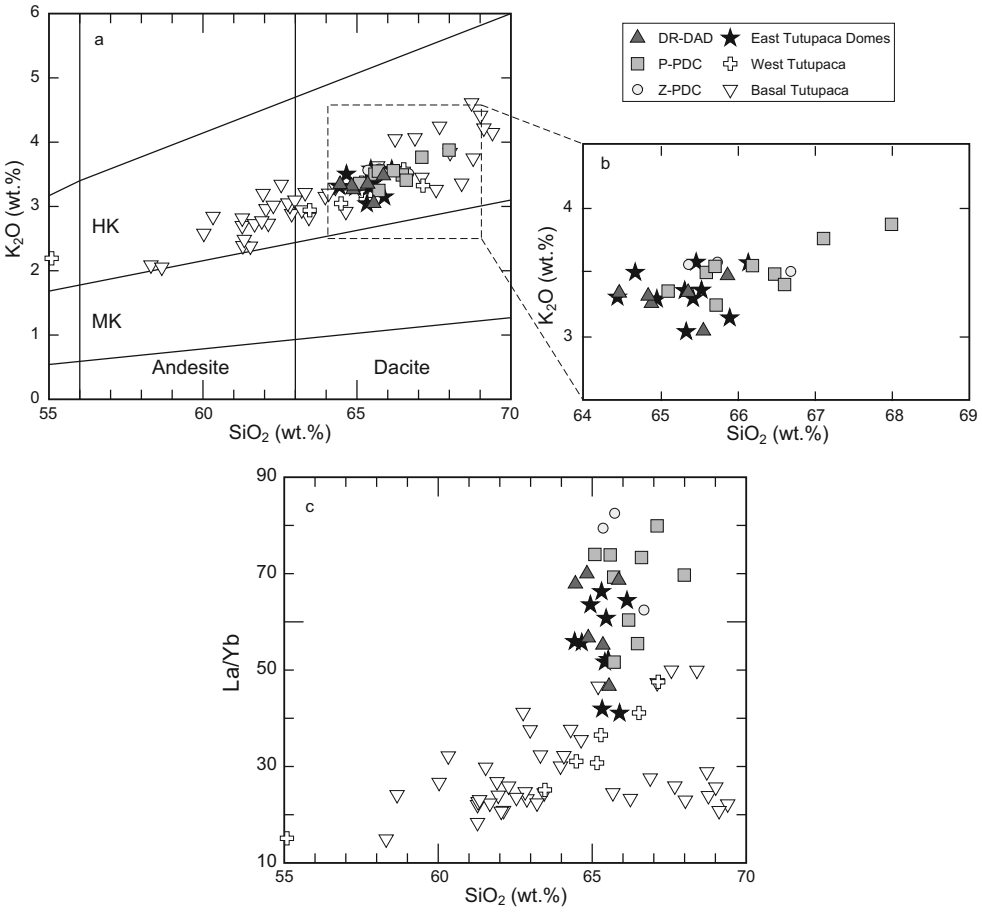

Fig. 9 Selected geochemical data for Tutupaca. **a**, **b** SiO_2 vs K_2O diagram and **c** SiO_2 vs La/Yb

Table 2 Selected whole-rock major (wt.%) and trace element (ppm) analyses of recent Tutupaca eruptive products

Sample no.	TU-12-14	TU-12-18	TU-12-04B	TU-12-09	TU-12-06A	TU-12-06C	TU-12-79A
UTM-Northing	8117106	8116280	8120200	8119422	8119537	8119537	8116684
UTM-Easting	356850	356820	358990	357418	361158	361158	363178
Unit	Recent dome	Recent dome	DR-DAD	HA-DAD	P-PFD	P-PFD	Z-PFD
Description	Lava block	Lava block	Lava block	Lava block	Cauliflower Bomb	Block	Breadcrust bomb
SiO_2 (wt.%)	63.72	64.42	63.39	64.41	64.57	64.06	66.63
TiO_2	0.72	0.72	0.79	0.77	0.70	0.73	0.73
Al_2O_3	15.81	15.80	15.99	15.31	15.56	15.98	15.74
Fe_2O_3*	4.30	4.35	4.40	4.17	4.34	4.35	3.90
MnO	0.06	0.06	0.06	0.06	0.06	0.05	0.05
MgO	1.80	1.61	1.76	1.59	1.64	1.57	1.52
CaO	3.87	3.79	3.91	3.61	3.51	3.76	3.36
Na_2O	4.34	4.30	4.47	4.18	4.15	4.35	4.20
K_2O	3.23	3.32	3.29	3.40	3.49	3.30	3.51
P_2O_5	0.27	0.28	0.30	0.30	0.27	0.27	0.27
LOI	0.21	−0.04	0.23	0.51	0.95	0.17	0.64
TOTAL	98.33	98.61	98.58	98.31	99.24	98.60	100.56
Sc (ppm)	6.55	5.56	6.67	5.79	5.39	5.52	5.37
V	91.00	93.20	92.60	82.70	88.33	90.52	75.33
Cr	11.75	11.62	12.80	9.43	10.94	11.75	10.26
Co	11.71	11.20	11.33	13.99	12.21	10.03	12.30
Ni	11.92	10.66	10.12	7.38	11.18	9.79	6.74
Rb	104.68	104.11	97.83	102.77	109.82	102.35	115.51
Sr	764.15	763.48	836.36	774.71	716.60	798.88	714.95
Y	8.21	8.30	9.06	8.85	7.37	7.88	8.73
Zr	128.04	138.62	148.80	134.70	134.36	134.31	143.19
Nb	7.50	7.78	8.51	8.97	6.82	8.26	8.83
Ba	1289.39	1309.65	1275.39	1334.10	1235.74	1320.77	1324.95
La	35.74	37.32	39.54	40.57	35.46	37.32	38.71
Ce	69.20	70.62	78.71	79.53	67.32	69.97	94.22
Nd	27.80	28.60	31.78	32.05	26.29	28.67	30.23
Sm	4.73	5.54	5.99	5.21	4.16	4.96	5.23
Eu	1.09	1.13	1.31	1.32	1.15	1.28	1.24
Gd	3.16	3.10	3.46	3.58	3.07	2.99	3.58
Dy	1.81	1.88	2.00	1.82	1.57	1.65	2.03
Er	0.65	0.58	0.71	−0.03	0.61	0.47	0.95
Yb	0.56	0.56	0.58	0.59	0.51	0.50	0.62
Th	8.30	8.41	8.28	9.73	9.10	8.03	9.90

Analyses were performed at the Laboratoire des Domaines Océaniques, Université de Bretagne Occidentale, Brest (France), by ICP-AES, except Rb, performed by flame atomic emission spectrometry, following the procedure of Cotten et al. (1995). Relative standard deviations are <2 and 5 % for major and trace elements, respectively

LOI loss on ignition

*Total iron as Fe_2O_3

porphyritic (30–40 vol.%) dacites containing plagioclase (10–20 vol.%), amphibole (10 vol.%), biotite (5 vol.%) and Fe-Ti oxides (2–3 vol.%). We also found ortho- and clinopyroxene, sphene, quartz and apatite as accessory phases (≤1 vol.%). Two populations of plagioclase were observed, the main group corresponding to euhedral, fresh, zoned phenocrysts (up to 4 mm), and the subordinate group (<3–4 vol.%) consisting of subhedral crystals with frequent disequilibrium textures such as reaction rims and dusty concentric zones and cores. The second most abundant mineral is amphibole, which appears as fresh, euhedral crystals (<1 mm) or is partially to completely replaced by a microcrystalline assemblage

composed of oxides (opacite). Biotite, which appears as euhedral to subhedral phenocrysts (up to 1–2 mm), represents the third main phase, frequently showing intergrowth textures with amphibole, plagioclase and Fe-Ti oxides. These phases, together with the other accessory minerals, are included in a vitreous to intersertal groundmass with a maximum of 5–10 vol.% vesicles. The dense blocks from the P-PDC deposit have a texture and a mineral assemblage similar to that of the lava dome blocks described above. In contrast, the bombs are more vesiculated (up to 40 vol.%) and display a high crystallinity (15–20 vol.% phenocryst) and the same mineral assemblage as the dense blocks. In conclusion, the geochemical and petrographical characteristics are useful tools to discriminate Eastern Tutupaca eruptive products from older products of Western and Basal Tutupaca edifices. We stress the strong homogeneity of the recent Tutupaca dacites and the fact that the young domes, the blocks from the DA deposit (namely those from the DR-DAD), and the juvenile samples from the P-PDC deposit share the same geochemical and petrographical characteristics.

Discussion

Historic chronicles and age of the Tutupaca sector collapse

Historical chronicles reported by Fidel and Zavala (2001) clearly point to an explosive eruption of Tutupaca volcano during the last few centuries. Zamacola y Jaúregui (1804) describes that "*now 15 years* (i.e. around 1789 AD) *burst* (a volcano) *close to the village of Candarave, distant 60 leagues from this city (*i.e. Arequipa; 1 Castellan league is about 4.2 kilometres)*, since that time, it has been smoking incessantly; but there will be two years* (i.e. in 1802 AD), (the volcano) *made a formidable explosion that its ashes and noise reached more than 100 leagues*" (this text and the next one were translated by the authors from the original texts in Spanish). Valdivia (1847) is more explicit since he mentions that "*on March, 20 1802 burst Tutupaca, leaving for five months ash in the air, (and) getting dark the atmosphere as far as Locumba, Tacna and Arica* (cities located in the south-western coastal zone)". These chronicles are corroborated by the oral tradition of the Candarave inhabitants, who consider Tutupaca as "the villain", in comparison to the "the good" Yucamane. This perception seems clearly related to the past explosive eruptions of Tutupaca and their impacts on local communities (Zora Carvajal 1954). These chronicles clearly show that Tutupaca experienced a strong explosive episode that started around 1787 AD and whose paroxysm probably occurred in 1802 AD.

The historic information is corroborated by the five radiocarbon ages (Table 1) we obtained from charcoal samples from the Z-PDC deposit in the Zuripujo valley and the P-PDC deposit on the Paipatja plain and nearby Suches lake. Samples from the Z-PDC deposit yield two well-constrained ages (220±30 and 230±30 aBP, Table 1), and a third slightly younger one (190±30 aBP), whereas the two samples from the P-PDC deposits give very close ages (220±40 and 235±35 aBP, Table 1). We calibrated these conventional ^{14}C ages to calendar ages using the Calib 6.0 code (Stuiver and Reimer 1993; Stuiver et al. 2005) and the Southern Hemisphere calibration curve (SHCal04, McCormac et al. 2004), which is suitable for this region and is available back to 11 ka cal BP (Fig. 10). Results of this calibration procedure show that the five samples are statistically identical at a 95 % confidence level with a pooled mean of 218±14 aBP. The calibrated calendar age for this average ^{14}C age yields two age spans, the most important being 1731–1802 cal AD period (with a relative area of 85 %). We emphasise that the two historic eruptions (1787–89 and 1802 AD) reported by Zamácola y Jaúregui (1804) and Valdivia (1847) fall at the end of this period.

Unfortunately, radiocarbon data are unable to discriminate between the pre-collapse flows (i.e. the Zuripujo event) and the syn-collapse pyroclastic event (i.e. Paipatja event). However, the stratigraphic evidence unambiguously shows that the Zuripujo event (Z-PDC) preceded the sector collapse and the associated explosive phase (DAD and P-PDC). Thus, we can state that the time between these two volcanic events was too short to be resolved using the radiocarbon method (i.e. some years to a few decades).

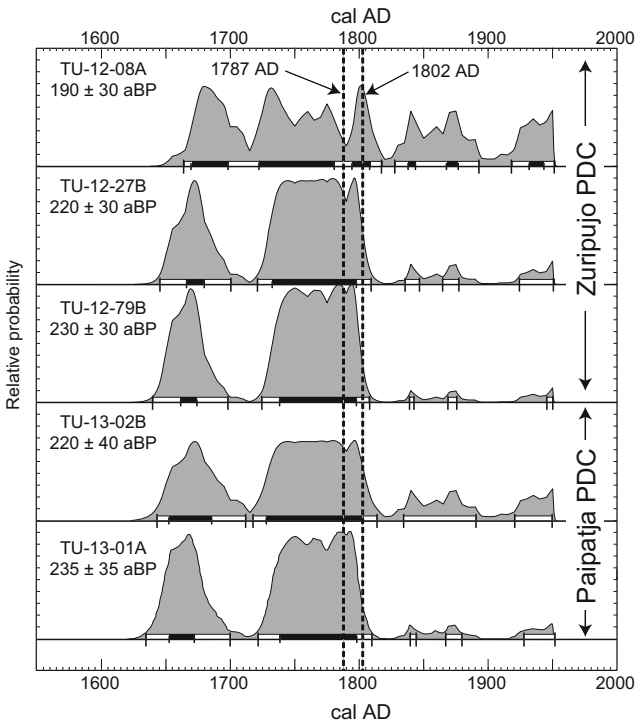

Fig. 10 Density probability functions for the calibrated radiocarbon ages of the last Tutupaca explosive eruption

Magnitude of the explosive phase

With the aim of estimating the magnitude of the explosive phase accompanying the debris avalanche of Tutupaca, we estimated the volume of the Paipatja pyroclastic density current (P-PDC) deposit. Satellite image inspection, coupled with detailed fieldwork including almost 300 GPS points, led to the establishment of a detailed map and made it possible to constrain the whole area covered by the P-PDC deposits (Fig. 3). In addition, we also mapped the mostly reworked, distal and lateral deposits of the P-PDC, which are interpreted as the related derived ash-cloud surge deposit. As a result, the main unit of the P-PDC covers an area of ~35–40 km^2, whereas the distal and lateral deposits have a larger distribution, covering an area of ~100–105 km^2. Last, in absence of natural, deep cross sections, we estimated an average thickness by digging in flat areas representative of the different parts of the deposit (75 holes for the whole P-PDC unit). On the Paipatja plain we found an average thickness of ~0.5-1 m, whereas in the valleys descending to the Rio Callazas, we observed a thickness range of 2–5 m. Based on these estimates, we obtained a volume of ~$5–6\times10^7$ m^3 for the main P-PDC deposit. For deposits of the uppermost ash-cloud layer, we estimate an average thickness of 15 cm and obtain a volume of ~1.5×10^7 m^3. Thus, the total bulk volume for the P-PDC is of the order of ~$6.5–7.5\times10^7$ m^3, corresponding to a VEI 3 eruption. We did not find proximal tephra fallout deposits associated with this eruption. Historical chronicles, however, suggest that distal fine ash fallout occurred in the coastal region at Locumba (77 km to the SW of Tutupaca), Tacna (110 km to the S) and Arica (165 km to the S). Because we have no constraints on the extent of these distal fine ash fallout deposits, the total eruption volume is underestimated. Considering such uncertainties, the bulk volume was probably greater than that calculated for the preserved deposits, implying that the eruption might well rank as a VEI 4. In summary, this eruption probably represents the youngest debris avalanche in the Andes and was accompanied by one of the larger explosive events in Peru during historical times.

Eruptive dynamics of the pyroclastic density currents

Explosive eruptive activity frequently accompanies sectorial collapse of volcanic edifices, especially in the case of violent decompression of a shallow magma body (see Belousov et al. 2007, for review and references therein). As a result, the explosive eruption produces so-called lateral or directed blast-generated pyroclastic density currents. Thus, blast deposits are intimately associated with debris avalanche deposits. This association formed during the recent eruptions of Bezymianny in 1956 (Belousov 1996), Mount St. Helens in 1980 (Hoblitt et al. 1981) and Soufrière Hills, Monserrat in 1997 (Voight et al. 2002). It is important to note that at Bezymianny and Mount St. Helens, the source of the explosion was a cryptodome that triggered the flank failure, whereas at Soufrière Hills, Monserrat, the source of the explosion was a growing lava dome. A similar scenario was described by Macías et al. (2010) at Tacaná volcano (southern México). In this case, however, the debris avalanche was associated with block-and-ash flows without a blast.

Explosive events also occur when the magma reservoir is too deep to produce a lateral blast. In these cases, decompression of the upper part of the magmatic system triggers a sustained plinian eruption and related pumice-rich pyroclastic flows. This occurred during the 1964 eruption of Shiveluch volcano (Belousov et al. 1999). In this case, a time delay exists between the sector collapse and the subsequent explosive activity. As a result, the contact between the debris avalanche deposits and the covering pyroclastic deposits is well-defined.

Lateral explosions producing similar blast-generated pyroclastic density currents are also associated with growing lava domes with no sector collapse. This occurred during the well-known eruption of Montagne Pelée, Martinique in 1902 (Bourdier et al. 1989), and recently during the 2010 Merapi eruption (Komorowski et al. 2013). This scenario also occurred during the explosive destruction of a lava dome at Chachimbiro volcanic complex, Ecuador (Bernard et al. 2014). In these cases, the growing lava dome exploded as a result of a high extrusion rate, which prevented efficient outgassing. It is also important to note that, in these examples, no associated debris avalanche deposits have been described.

In the case of the Tutupaca sector collapse, there is no plinian fallout deposit associated with the debris avalanche and the pyroclastic density current deposits. However, several pieces of evidence suggest that magmatic activity was intimately linked with the sector collapse. These include the intimate stratigraphic relations between the DA deposit and the P-PDC deposits, the fact that the P-PDC deposits cover a sector whose angle coincides with the that of the DA deposit (Fig. 11), the presence of prismatically jointed blocks in the DR-DAD, and the petrological similarity between the juvenile clasts in the DA, the P-PDC deposits and the recent Tutupaca domes. Figure 11 depicts the deposit of the lateral blasts that accompanied the Bezymianny, Mount St. Helens, and Soufrière Hills (Monserrat) sector collapses. At Tutupaca, the PDC deposits cover an area similar to that at Soufriere Hills, Montserrat, in agreement with the estimated bulk volumes (8×10^7 m^3 for Tutupaca, and 3×10^7 m^3 for Montserrat, Belousov et al. 2007). We also observe a similarity between Tutupaca and Mount St. Helens in terms of the blast propagation angle and the digitate shape of the devastation zone. This last feature, however, is probably related to the fact that the Mount St. Helens blast deposit was mapped in greater detail compared with the Bezymianny and Soufrière Hills blast deposits (note that the latter extend into the sea in distal areas). However, the sedimentological characteristics of the P-PDC

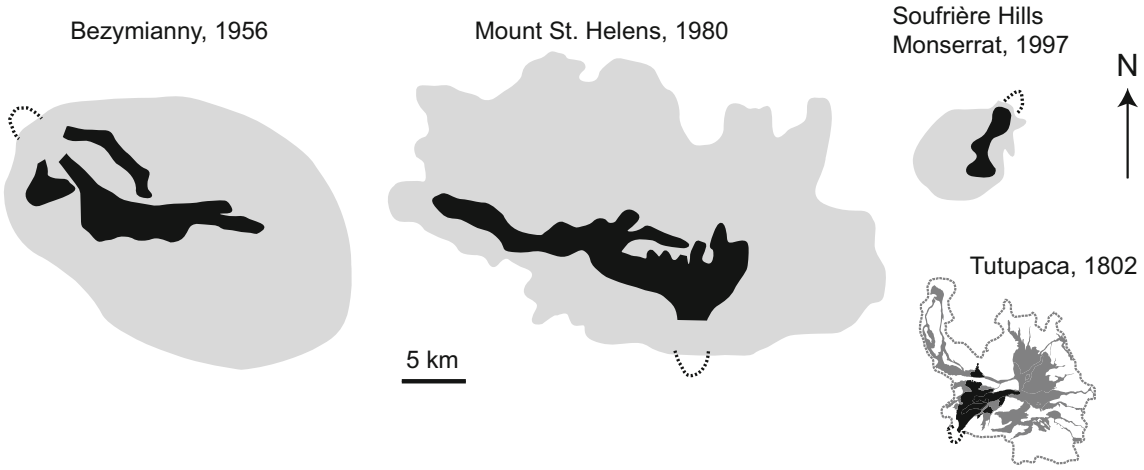

Fig. 11 Distribution of the blast deposits (*grey*) associated with well-known debris avalanches (*black*). *Dotted lines* represent the amphitheatre. Modified from Belousov et al. (2007)

deposit do not match those of the above-mentioned blast deposits as reported by Belousov et al. (2007). These authors report that blast deposits are characterised by three distinct units: (i) a basal layer with evidence of material entrainment from the substrate, (ii) a thicker, middle layer that is fines-depleted, normally graded and well sorted, and (iii) an upper, fines-rich layer with frequent planar and wavy laminations. This three-layer sequence may reflect emplacement of a dilute, turbulent and erosive current with a possible lower layer of higher particle concentration. The P-PDC deposits associated with the Tutupaca debris avalanche do not show the deposit sequence identified by Belousov et al. (2007). Instead, the field observation and the sedimentological characteristics suggest a fairly concentrated basal flow (Fig. 8) with an associated dilute cloud that was able to overpass topographic barriers (for instance the Villaque hill). Thus, we propose that the P-PDC deposits result from pyroclastic density currents formed during a lateral eruption by asymmetrical fountain collapse associated with the Tutupaca sector collapse. A last point to be stressed is that after the sector collapse and its associated pyroclastic density currents, no magmatic activity occurred at Tutupaca. This fact is in sharp contrast with what has been described at other volcanoes that experienced sector collapses (such as Bezymianny, Mount St. Helens or Soufriere Hills).

Reconstruction of the eruptive events

The Eastern Tutupaca dome complex consists of at least 7 coalesced dacitic domes that grew during Holocene times on top of an old, hydrothermally altered basal edifice (Manrique 2013). This dome complex was active in the late 18th century and was affected, between 1787 and 1802 AD, by a major sector collapse that produced a debris avalanche and the associated pyroclastic density currents whose deposits are described in this manuscript. This event was preceded by the block-and-ash flows whose deposits outcrop in the Zuripujo valley to the SE of the Eastern Tutupaca summit (the Z-PDC deposits). These deposits have a limited lateral extent, and mostly outcrop in an almost orthogonal position with respect to the NE-opening amphitheatre, which may reflect a focused flow direction from the source area. In addition, the Z-PDC deposits are overlain by a partially reworked ash-rich layer that represents the lateral facies of the later Paipatja pyroclastic density current deposits (P-PDC, Fig. 5). On the basis of these constraints, we propose that the Z-PDC represents a volcanic event that preceded the Tutupaca sector collapse. This inference is also supported by the fact that charcoal fragments are abundant in the Z-PDC deposits but are extremely rare in the P-PDC deposits, which suggests that the Z-PDC charred and covered the rare vegetation (mainly grass and small bushes) of this high Andean plateau. An additional point to be taken into consideration concerns the fact that the Z-PDC deposit contains a large amount of altered (hydrothermal) components, which contrasts with the rather scarce juvenile material that has been observed in the P-PDC. Thus, the Z-PDC was probably associated with vent clearing explosions occurring in a pressurised lava dome and its subsequent collapse along a sliding plane that was deep enough in the dome to significantly affect the hydrothermal system. As a result, parts of the dome with large amounts of hydrothermally altered material collapsed, producing the pyroclastic flow deposits of the Zuripujo valley. This type of activity has been described at other andesitic and dacitic domes such as Galeras, Colombia (Calvache and Williams 1992) and Soufrière Hills, Monserrat (Sparks et al. 2002).

Dome growth activity proceeded on the Eastern Tutupaca edifice and culminated with the sector collapse that affected its NE flank, following a scenario that was described for the 1997 sector collapse of Soufrière Hills, Monserrat (Sparks et al. 2002) as well as at Tacaná volcano, México (Macías et al.

2010). In the case of Tutupaca, the sector collapse affected the dome complex and the hydrothermally altered lavas of the basal edifice. As a result, a relatively small (<1 km^3) debris avalanche spread at the foot of the amphitheatre and reached the Paipatja plain 6–8 km away. The debris avalanche had two main units. The first unit is mainly composed of hydrothermally altered rocks (HA-DAD) from the basal edifice, although it also includes non-altered dome blocks. This lower unit (Unit 1 in Valderrama et al. 2014) is the more voluminous and shows morphological features such as megablocks and hummocks. The upper part of this unit indicates a different dynamical behaviour, expressed by the presence of surface ridges (Unit 2a of Valderrama et al. 2014). The second unit (DR-DAD) also displays frequent surface ridges (Unit 2b of Valderrama et al. 2014), covers the previous one and comprises unaltered dacitic blocks with frequent prismatically jointed blocks, which attest to thermal contraction. This suggests that the second debris avalanche pulse was associated with the collapse of an active dome complex located at the former Tutupaca summit.

In between these debris avalanche units, the voluminous ($6.5–7.5 \times 10^7$ m^3) Paipatja pyroclastic density current deposit (P-PDC) extends up to 10–12 km down the Callazas river (to the NE) and the Suches lake (to the N). This pyroclastic sequence overlies the HA-DAD and is interstratified with (or covered by) the DR-DAD, which shows that the debris avalanche and the pyroclastic flows were generated quasi-synchronously.

Comparison with other debris avalanche deposits in the Central Andes

Based on satellite image analysis, Francis and Wells (1988) published an inventory of the most prominent debris avalanche deposits in the Central Andes. Since then, many detailed field-based studies have been focused on these deposits, which rank among the most spectacular debris avalanches on earth. Examples include the debris avalanche deposits of Socompa (van Wyk de Vries et al. 2001; Kelfoun et al. 2008), Parinacota (Clavero et al. 2002), Tata Sabaya (de Silva et al. 1993), Ollagüe (Clavero et al. 2004) and Llullaillaco (Richards and Villeneuve 2001). Compared with these examples, the Tutupaca debris avalanche differs in its small areal coverage (12–13 km^2) and volume (<1 km^3); its area is one order of magnitude smaller that the huge surfaces covered by the Socompa (490 km^2), Tata Sabaya (~300 km^2), Parinacota (140 km^2), Ollagüe (~100 km^2) or Llullaillaco (165 km^2) debris avalanche deposits. In spite of its modest size, the Tutupaca debris avalanche deposit is important for two main reasons. First, because at Tutupaca, the debris avalanche deposits are intimately associated with a sequence of pyroclastic density current deposits, pointing clearly to a magmatic origin for the sector collapse. Second, due to its young age and high degree of preservation, Tutupaca is a unique place for studying the origin and implications of the elongate ridges that characterise this deposit (cf. Valderrama et al. 2014).

Conclusions

The younger (Eastern) edifice of the Tutupaca volcanic complex is a Late Holocene dacitic dome complex that was affected by a sector collapse in historical times. The collapse triggered a small (<1 km^3) debris avalanche and associated pyroclastic density currents whose deposits have a bulk volume of about $6.5–7.5 \times 10^7$ m^3, which ranks this eruption as at least a VEI 3 event. Both deposits, of the avalanche and the pyroclastic density currents, were emplaced synchronously and spread onto the plain NE of Tutupaca volcano. The ^{14}C age determinations obtained for the pyroclastic flow deposits yield a mean age of 218±14 aBP, which corresponds to an eruption that occurred in the 18th century (1731–1802 cal AD). This age is in agreement with the historical chronicles that report major explosive activity at Tutupaca in the period between 1787 and 1802 AD.

The spatial and temporal relationships between deposits of the debris avalanche and the Paipatja pyroclastic density currents (P-PDC), coupled with the petrological similarity between the juvenile fragments in both deposits, indicate that juvenile magma was involved in the sector collapse. A pressurised dome complex triggered the first pyroclastic density currents (Z-PDC). Then, ascent of a dacitic magma batch, coupled with the fact that the Tutupaca dome complex was constructed on top of a highly altered and hydrothermally active volcanic system, triggered the destabilisation of the edifice, producing the debris avalanche and its related pyroclastic density currents represented by the P-PDC.

On the basis of our work on the most recent eruption at Tutupaca, a future eruption of this volcano may display similar eruptive dynamics characterised by viscous dome growth and related block-and-ash pyroclastic flows. This scenario is corroborated by the pre-historical activity of Tutupaca, which shows a frequent pattern of dome growth and collapse as well as at least one other, older debris avalanche event. During the past eruptions of Tutupaca, the eruptive products affected uninhabited areas of the high Andes in Peru, and tephra fallout had only a minor regional impact. However, if a large eruption occurred today, it could affect a much larger population of at least eight to ten thousand inhabitants living within a 25-km radius of the volcano, as well as the important mining (Toquepala, Cuajone) and geothermal (Calientes) infrastructures located in the proximity of Tutupaca.

Acknowledgments This work is part of a Peruvian–French cooperation programme carried out between the Instituto Geológico, Minero y Metalúrgico (INGEMMET, Peru) and the Institut de Recherche pour le Développement (IRD, France). It was partially founded by a "Jeunes Equipes Associées à l'IRD" (JEAI) project that is an initiative designed to promote and strengthen new research teams in developing countries. We warmly thank Etienne Medard, Pierre Delmelle, Marie Detienne, Karine Bernard, Marco Rivera and Jean-Luc Le Pennec for fruitful discussions on the field and Fran van Wyk des Vries for the english improvement of the manuscript. We are grateful to the two anonymous reviewers for their comments and with S. De la Cruz-Reyna and J.D.L. White for the editorial handling. This research was financed by the French Government Laboratory of Excellence initiative no. ANR-10-LABX-0006, the Région Auvergne and the European Regional Development Fund. This is Laboratory of Excellence ClerVolc contribution no. 159.

References

Adams NK, de Silva SL, Self S, Salas G, Schubring S, Permenter JL, Arbesman K (2001) The physical volcanology of the 1600 eruption of Huaynaputina, southern Peru. Bull Volcanol 62:493–518

Belousov A (1996) Pyroclastic deposits of March 30, 1956 directed blast at Bezymianny volcano. Bull Volcanol 57:649–662

Belousov A, Belousova M, Voight B (1999) Multiple edifice failures, debris avalanches and associated eruptions in the Holocene history of Shiveluch volcano, Kamchatka, Russia. Bull Volcanol 61:324–342

Belousov A, Voight B, Belousova M (2007) Directed blasts and blast-generated pyroclastic density currents: a comparison of the Bezymianny 1956, Mount St. Helens 1980, and Soufrière Hills, Montserrat 1997 eruptions and deposits. Bull Volcanol 69:701–740

Benavente C, Carlotto V, del Castillo B (2010) Extensión en el arco volcánico actual del Sur de Perú. XV Congreso Peruano de Geología, Extended abstracts. Sociedad Geológica del Perú, Lima

Bernard B, Hidalgo S, Robin C, Beate B, Quijozaca J (2014) The 3640–3510 BC rhyodacite eruption of Chachimbiro compound volcano, Ecuador: a violent directed blast produced by a satellite dome. Bull Volcanol 76:849. doi:10.1007/s00445-014-0849-z

Bourdier JL, Boudon G, Gourgaud A (1989) Stratigraphy of the 1902 and 1929 nude ardente deposits, Mt. Pelée Martinique. J Volcanol Geotherm Res 38:77–96

Bromley GRM, Schaefer JM, Wincler G, Hall BL, Todd CE, Rademaker CKM (2009) Relative timing of last glacial maximum and late-glacial events in the central tropical Andes. Quat Sci Rev 28: 2514–2526

Calvache ML, Williams SN (1992) Lithic-dominated pyroclastic flows at Galeras volcano, Colombia – an unrecognized volcanic hazard. Geology 20:539–542

Clavero JE, Sparks RSJ, Huppert HE, Dade WB (2002) Geological constraints on the emplacement mechanism of the Parinacota debris avalanche, Northern Chile. Bull Volcanol 64:40–54

Clavero JE, Polanco E, Godoy E, Aguilar G, Sparks S, van Wyk de Vries B, Pérez de Arce C, Matthews S (2004) Substrata influence in the transport and emplacement mechanisms of the Ollagüe debris avalanche, Northern Chile. Acta Vulcanol 16:59–76

Cobeñas G, Thouret JC, Bonadonna C, Boivin P (2012) The c.2030 yr BP Plinian erup- tion of El Misti volcano, Peru: eruption dynamics and hazard implications. J Volcanol Geotherm Res 241–242:105–120

Cotten J, Le Dez A, Bau M, Caroff M, Maury RC, Dulski P, Fourcade S, Bohn M, Brousse R (1995) Origin of anomalous rare-earth element and Yttrium enrichments in subaerial exposed basalts: evidence from French Polynesia. Chem Geol 119:115–138

de Silva SL, Francis P (1990) Potentially active volcanoes of Peru: observations using Landsat Thematic Mapper and space shuttle photography. Bull Volcanol 52:286–301

de Silva SL, Davidson JP, Croudace IW, Escobar A (1993) Volcanological and petrological evolution of Volcan Tata Sabaya, SW Bolivia. J Volcanol Geotherm Res 55:305–335

Druitt TH (1992) Emplacement of the 18 May 1980 lateral blast deposit ENE of Mount St. Helens, Washington. Bull Volcanol 54:554–573

Druitt TH, Calder ES, Cole PD, Hoblitt RP, Loughlin SC, Norton GE, Ritchie LJ, Sparks RSJ, Voight B (2002) Small-volume, highly mobile pyroclastic flows formed by rapid sedimentation from pyroclastic surges at Soufrière Hills Volvano, Monserrat: an important volcanic hazard. In: Druitt T, Kokelaar BP (eds), The eruption of Soufrière Hills Volcano, Montserrat, from 1995 to 1999. Mem Geol Soc London 21: 263–279

Eychenne J, Le Pennec JL (2012) Sigmoidal particle density distribution in a subplinian scoria fall deposit. Bull Volcanol 74:2243–2249. doi:10.1007/s00445-012-0671-4

Fidel L, Zavala B (2001) Mapa preliminar de amenaza volcánica del volcán Tutupaca. Boletín 24, Serie C: Geodinámica e Ingeniería Geológica, INGEMMET, 109 p

Francis PW, Wells GL (1988) Landsat Thematic Mapper observations of debris avalanche deposits in the Central Andes. Bull Volcanol 50: 258–278

Gerbe MC, Thouret JC (2004) Role of magma mixing in the petrogenesis of lavas erupted through the 1990–98 explosive activity of Nevado Sabancaya in south Peru. Bull Volcanol 66:541–561

Glicken H (1991) Sedimentary architecture of large volcanic-debris avalanches. Sedimentation in Volcanic Settings. SEPM Spec Publ 45: 99–106

Hantke G, Parodi A (1966) Catalogue of the active volcanoes of the world, Part XIX, Colombia, Ecuador and Peru, IAVCEI Naples, Italy, 73 pp

Harpel CJ, de Silva S, Salas G (2011) The 2 ka eruption of Misti Volcano, Southern Peru—the most recent plinian eruption of arequipa's iconic volcano. Geol Soc Am Spec Pap 484:1–72. doi:10.1130/2011.2484

Hoblitt RP, Miller CD, Vallance JW (1981) Origin and stratigraphy of the deposit produced by the May 18 directed blast. In: Lipman PW, Mullineaux DR (eds) The 1980 eruptions of Mount St. Helens, Washington. USGS Prof Paper 1250:401–419

Kelfoun K, Druitt TH, van Wyk de Vries B, Guilbaud MN (2008) Topographic reflection of the Socompa debris avalanche, Chile. Bull Volcanol 70:1169–1187

Komorowski JC, Jenkins S, Baxter PJ, Picquout A, Lavigne F, Charbonnier S, Gertisser R, Preece K, Cholik N, Budi-Santoso A, Surono (2013) Paroxysmal dome explosion during the Merapi 2010 eruption: processes and facies relationships of associated high- energy pyroclastic density currents. J Volcanol Geotherm Res 261: 260–294. doi:10.1016/j.jvolgeores.2013.01.007

Macías JL, Arce JL, García-Palomo A, Mora JC, Layer PW, Espíndola JM (2010) Late-Pleistocene flank collapse triggered by dome growth at Tacaná volcano, México-Guatemala, and its relationship to the regional stress regime. Bull Volcanol 72:33–53. doi:10.1007/s00445-009-0303-9

Mamani M, Worner G, Sempere T (2010) Geochemical variations in igneous rocks of the Central Andean orocline (13°S to 18°S): tracing crustal thickening and magma generation through time and space. Geol Soc Am Bull 122:162–182

Manrique N (2013) Evolución Vulcanológica y Magmática del Edificio Reciente del Complejo Volcánico Tutupaca (Tacna). Universidad Nacional San Agustín de Arequipa. Tesis. 90 p

McCormac FG, Hogg AG, Blackwell PG, Buck CE, Higham TFG, Reimer PJ (2004) SHCal04 Southern Hemisphere Calibration 0–11.0 cal Kyr BP. Radiocarbon 46:1087–1092

Richards JP, Villeneuve M (2001) The Llullaillaco volcano, northwest Argentina: construction by Pleistocene volcanism and destruction by sector collapse. J Volcanol Geotherm Res 105:77–105

Rivera M, Thouret JC, Samaniego P, Le Pennec JL (2014) The 2006–2009 activity of Ubinas volcano (Peru): petrology of the 2006 eruptive products and insights into genesis of andesite magmas, magma recharge and plumbing system. J Volcanol Geotherm Res 270:122–141

Roche O, Niño Y, Mangeney A, Brandt B, Pollock N, Valentine GA (2013) Dynamic pore-pressure variations induce substrate erosion by pyroclastic flows. Geology 41:1107–1110

Siebert L, Simkin T, Kimberly P (2010) Volcanoes of the world. Third edition. Smithsonian Institution and University of California press. 551 p

Smith JA, Mark BG, Rodbell DT (2008) The timing and magnitude of mountain glaciation in the tropical Andes. J Quat Sci 23:609–634

Sparks RSJ, Barclay J, Calder ES, Herd RA, Luckett R, Norton GE, Pollard L, Robertson RA, Ritchie L, Voight B, Young SR, Woods AW (2002) Generation of a debris avalanche and violent pyroclastic density current: the Boxing Day eruption of 26 December 1997 at the Soufrière Hills volcano, Montserrat. In: Druitt T, Kokelaar BP (eds) The eruption of Soufrière Hills volcano, Montserrat, from 1995–1999. Mem Geol Soc London 21:409–434

Stuiver M, Reimer PJ (1993) Extended 14C database and revised CALIB radiocarbon calibration program. Radiocarbon 35:215–230

Stuiver M, Reimer PJ, Reimer RW (2005) CALIB 5.0. [WWW program and documentation]

Thouret JC, Davila J, Eissen JP (1999) Largest historic explosive eruption in the Andes at Huaynaputina volcano, south Peru. Geology 27: 435–438

Thouret JC, Finizola A, Fornari M, Suni J, Legeley-Padovani A, Frechen M (2001) Geology of El Misti volcano nearby the city of Arequipa, Peru. Geol Soc Am Bull 113:1593–1610

Thouret JC, Rivera M, Wörner G, Gerbe MC, Finizola A, Fornari M, Gonzales K (2005) Ubinas: the evolution of the historically most active volcano in southern Peru. Bull Volcanol 67:557–589

Valderrama P, Roche O, Samaniego P, van Wyk des Vries B, Bernard K (2014) The dynamic implications of ridged textures on a volcanic debris avalanche deposit at Tutupaca volcano, Southern Peru. Submitted to Geology (April 2015)

Valdivia JG (1847) Fragmentos para la historia de Arequipa. Folletín de "El Deber", Arequipa, 109–111 p

van Wyk de Vries B, Self S, Francis PW, Keszthelyi L (2001) A gravitational spreading origin for the Socompa debris avalanche. J Volcanol Geotherm Res 105:225–247

Voight B, Komorowski JC, Norton GE, Belousov AB, Belousova M, Boudon G, Francis PW, Franz W, Heinrich P, Sparks RSJ, Young SR (2002) The 1997 Boxing Day Sector Collapse and Debris Avalanche, Soufriere Hills Volcano, Montserrat, W.I. In: Druitt T, Kokelaar BP (eds), The eruption of Soufrière Hills Volcano, Montserrat, from 1995 to 1999. Mem Geol Soc London 21:363–407

Walker GPL (1983) Ignimbrite types and ignimbrite problems. J Volcanol Geotherm Res 17:65–88

Zamácola y Jaúregui JD (1804) Apuntes para la historia de Arequipa. Imp. De La Bolsa-Guañamarca, N. 49. 1888

Zora Carvajal F (1954) Tacna, Historia y Folklore. Second edition (1969), Editorial Santa María

Chapter 4:

DYNAMIC IMPLICATIONS OF RIDGES ON A DEBRIS AVALANCHE DEPOSIT

Summary

Elongated ridges (or flowbands following the terminology of Dufresne and Davies 2009) have been described at the debris avalanche deposits of Shiveluch volcano in Kamchatka (Belousov et al., 1999) as well as some other volcanic debris avalanche deposits in the Central Andes such as those of Socompa (Kelfoun et al., 2008; van Wyk de Vries et al., 2001), Llullaillaco (Richards and Villeneuve, 2001) and Lastarria (Naranjo and Francis, 1987). Similar features have been also described in non-volcanic environments, such as landslides (Shaller, 1991) and rock avalanches overriding glaciers (McSaveney, 1978), as well as in extraterrestrial environments (i.e. Mars, Luchitta, 1978; Shaller, 1991). This chapter correspond to a paper that was recently published at *Bulletin of Volcanology* (Valderrama et al., 2016).

The historical (218±14 yBP) debris avalanche deposit of Tutupaca volcano (Chapter 3) presents a coupled hydrothermal- and magmatic-related volcanic component. A typical debris avalanche hummocky unit is found, formed out of rock from the dome foot and the underlying hydrothermally altered lavas. This deposit has ridges 20–500-m long, 10–30-m wide and 1–5-m high, regularly spaced and that fan slightly outward. Cross sections exposed within the ridges reveal coarser cores and finer troughs, suggesting grain size segregation during emplacement. The ridges are also associated with large blocks that have evidence of differential movement compared with the rest of the flowing mass. The presence of both ridged and hummocky deposits in the same event shows that, as different lithologies combine and collapse sequentially, materials with different mechanical properties can coexist in one landslide, leading to contrasting emplacement dynamics.

The rock of the collapsing volcanic edifice can be hot and can contain water and gas while the hydrothermally altered material has abundant fines and clays as well as water. Both magmatic and hydrothermal materials may fragment easily to produce a wide range of particle sizes, which can control the emplacement mechanism of the avalanche. The incorporation of variable amounts of fresh rock, hot magma and parts of the hydrothermal

system is likely to cause different mechanical behaviors for different flowing sections of an avalanche.

Surface features on debris avalanche deposits have been used to determine their kinematics and to suggest their emplacement dynamics. While hummocks and faults have been carefully analyzed in debris avalanche deposits, ridges have not been examined in detail in the field in relation to structure and sedimentology, even though they are likely to provide clues to the processes involved in avalanche emplacement. For a detailed study, two trenches were excavated to expose the interior of the ridges and they showed a similar structure, with a central zone of slightly coarser breccia and steep sided contacts with an inter-ridge filling of later pyroclastic flow material.

Ridge-like structures showing particle grain size segregation have been observed to form in experiments on polydisperse granular flows exhibiting granular fingering. In such esperiments, small perturbations cause deflection of the trajectories of these large particles along the steepest surface slope, which causes formation of frontal lobes and emerging static lateral levees. We interpret the Tutupaca ridges as joint margins of the lateral levées of granular fingers where the large blocks were concentrated. In this context, inter-ridge depressions formed as the flowing granular mass drained the central part of the fingers that became progressively less elevated than the ridges, as shown for self-channeling granular flows depicting levée-channel morphology. These features are consistent with static levées bordering a channel in which the granular material flowed.

Bull Volcanol (2016) 78:14
DOI 10.1007/s00445-016-1011-x

RESEARCH ARTICLE

Dynamic implications of ridges on a debris avalanche deposit at Tutupaca volcano (southern Peru)

Patricio Valderrama [1,2] · Olivier Roche [2] · Pablo Samaniego [2] · Benjamin van Wyk de Vries [2] · Karine Bernard [2] · Jersy Mariño [1]

Received: 23 September 2015 / Accepted: 10 February 2016

Abstract Catastrophic volcanic landslides can involve different parts of a volcano that can be incorporated into any resulting debris avalanche. The different material properties may influence the mechanical behaviour and, hence, the emplacement mechanisms of the different avalanche units. We present data from a coupled hydrothermal- and magmatic-related volcanic landslide at Tutupaca volcano (Peru). Around AD 1802, the hydrothermal system under Tutupaca's growing dacite dome failed, creating a debris avalanche that triggered a large explosive eruption. A typical debris avalanche hummocky unit is found, formed out of rock from the dome foot and the underlying hydrothermally altered lavas. It is covered by a more widespread and remarkable deposit that contains remnants of the hot dome core and the inner hydrothermal material. This deposit has ridges 20–500-m long, 10–30-m wide and 1–5-m high, regularly spaced and that fan slightly outward. Cross sections exposed within the ridges reveal coarser cores and finer troughs, suggesting grain size segregation during emplacement. Ridge morphology and granulometry are consistent with fingering known to occur in granular flows. The ridges are also associated with large blocks that have evidence of differential movement compared with the rest of the flowing mass. The presence of both ridged and hummocky deposits in the same event shows that, as different lithologies combine and collapse sequentially, materials with different mechanical properties can coexist in one landslide, leading to contrasting emplacement dynamics. The different structures thus highlight the complexity of such hazardous volcanic events and show the difficulty we face with modelling them.

Keywords Tutupaca volcano · Debris avalanche · Flank collapse · Ridges · Granular fingering

Editorial responsibility: L. Capra

✉ Patricio Valderrama
pvalderrama@ingemmet.gob.pe

[1] Observatorio Vulcanológico del INGEMMET (OVI), Av. Canada 1470, San Borja, Lima, Peru

[2] Laboratoire Magmas et Volcans, Université Blaise Pascal - CNRS - IRD, OPGC, TSA 60026 - CS 60026, 6 Avenue Blaise Pascal, 63178 Aubière, France

Introduction

Volcanic landslides and debris avalanches associated with magmatic and hydrothermal activity, such as Mount St. Helens (1980) or Bandai San (1888), represent major volcanic hazards (Siebert 1984; Siebert et al. 1987). Because of the complex mix of different rock types, fluids and gasses, resulting debris avalanches are likely to have complex and variable mechanical properties that control avalanche emplacement and run out distance (e.g. Voight et al. 2002; Shea and van Wyk de Vries 2008; van Wyk de Vries and Davis 2014; Roverato et al. 2015). These mechanical differences to mobility must be taken into account when assessing their impacts. The rock of the collapsing volcanic edifice can be hot and can contain water and gas while the hydrothermally altered material has abundant fines and clays as well as water. Both magmatic and hydrothermal materials may fragment easily to produce a wide range of particle sizes, which can control the emplacement mechanism of the avalanche (Eppler et al. 1987; Glicken 1998; Voight et al. 2002; Legros 2002). Particle size segregation can promote segregation features, while in fine material with low hydraulic permeability, water and gas could provide interstitial pore fluid pressure for the moving mass as shown for example for debris flows (Iverson 1997). The incorporation of variable amounts of fresh

Published online: 17 February 2016

rock, hot magma and parts of the hydrothermal system is likely to cause different mechanical behaviours for different flowing sections of an avalanche.

Surface features on debris avalanche deposits have been used to determine their kinematics and to suggest their emplacement dynamics (Belousov et al. 1999; van Wyk de Vries et al. 2001; Kelfoun and Druitt 2005; Dufresne and Davies 2009; Paguican et al. 2014). These features are either hummocks and megablocks (e.g. Paguican et al. 2014), extensive fault and fold networks (e.g. Shea and van Wyk de Vries 2008), or elongated ridges (e.g. Belousov et al. 1999; Dufresne and Davies 2009). While hummocks and faults have been carefully analysed in debris avalanche deposits (Clavero et al. 2002; Paguican et al. 2014), ridges have not been examined in detail in the field in relation to structure and sedimentology, even though they are likely to provide clues to the processes involved in avalanche emplacement.

In this work, we describe the surface features observed in a young and well-preserved volcanic debris avalanche deposit of Tutupaca volcano in southern Peru. In particular, we report a quantitative analysis of ridge morphology, as well as granulometry in two selected trenches dug across the ridges. These data have been compared with those of experiments on granular flows that allow us to discuss the implications of ridge formation for debris avalanches emplacement dynamics.

The Tutupaca volcano and its recent deposits

The Tutupaca volcanic complex in southern Peru (Figs. 1 and 2) is composed of an old, highly altered and eroded and glaciated basal edifice and two younger twin peaks, located in the northern part of the complex (the western and eastern Tutupaca; Samaniego et al. 2015). The younger edifice of the complex, the eastern Tutupaca, is a dome complex that sits on top of the basal edifice and consists of at least seven dacitic domes with no discernible glacial erosion, which suggests that they have formed during the Holocene. The most striking characteristic of this recent edifice is the presence of a ~1-km-wide collapse amphitheatre open to the NE and a related hummocky and ridged debris avalanche deposit that spreads out on the adjacent highlands (Figs. 1 and 2).

The sector collapse scar at Tutupaca has an inner bowl shape, opening to a shallow outer scar and slide plane. The inner upper walls of the scar consist of unaltered dome lava, underlain by reddish altered dome lavas, both correlative with eastern Tutupaca domes, and highly altered lavas of the lower basal edifice. The scar opens onto a 25° inclined slope on which similarly inclined basal volcano strata outcrop under a partial cover of later collapse breccia. The base of the outer scar is composed of slightly altered lavas and intensely hydrothermally altered white and yellow zones.

Samaniego et al. (2015) described the recent deposits of Tutupaca (Fig. 3), which consist of (i) a debris avalanche deposit with two main units of different composition, structural characteristics and travel path, and (ii) a large pyroclastic density current deposit that covers the volcano's northwest base, which is interleaved with the debris avalanche deposit. Charcoal in this pyroclastic deposit has been dated at about 218 ± 14 aBP (P-PDC of Samaniego et al. 2015), which is consistent with historical accounts of eruptive activity during the eighteenth and nineteenth centuries. The stratigraphic relationship between the debris avalanche and the pyroclastic density current deposit, coupled with the petrological similarity between the juvenile fragments in the debris avalanche, the pyroclastic density current deposit and the pre-avalanche domes, indicates (1) that juvenile magma was involved in the sector collapse and (2) that the debris avalanche and the pyroclastic density currents are different phases of a single, albeit complex sequence of events. Samaniego et al. (2015) concluded that this eruption represents the youngest debris avalanche in the Andes and was accompanied by one of the largest explosive events to have occurred in Peru during historical times.

The debris avalanche deposit description

Unit characteristics and terminology

The debris avalanche deposit (DAD) is exposed in the NE part of Tutupaca between the amphitheatre and the Paipatja plain, reaching 6–8 km from its source and covering an area of 12–13 km^2 (Fig. 1). Based on stratigraphic and lithological data, Samaniego et al. (2015) described two distinct DAD units separated by the Paipatja pyroclastic density current deposits (P-PDC) (Fig. 3). The lower unit is mostly composed of hydrothermally altered lava fragments as well as minor amounts of oxidized dome lavas, and it is referred to as the hydrothermally altered debris avalanche deposit (HA-DAD, Fig. 3). The upper unit is mostly composed of unaltered (fresh) dome fragments, which grade from sand-size particles to several meters in size. This unit is characterized by abundant prismatically jointed blocks that have been interpreted to be juvenile dome fragments, and has been called the dome-rich debris avalanche deposit (DR-DAD, Fig. 3).

In this study, we define units based on surface features and structures rather than lithology because our aim is to discuss the emplacement dynamics of the debris avalanche from the characteristics of these structures (Fig. 3). Based on these morphological features, we distinguish two main DAD units. The lower unit 1 spreads between the amphitheatre and the Paipatja plain and is confined by the old glacial valleys over most of its path. At the foot of the amphitheatre, unit 1 is characterized by an inner 1–1.5-km-wide and 100–200-m-thick toreva-like structure and it grades outwards to a series of hectometric

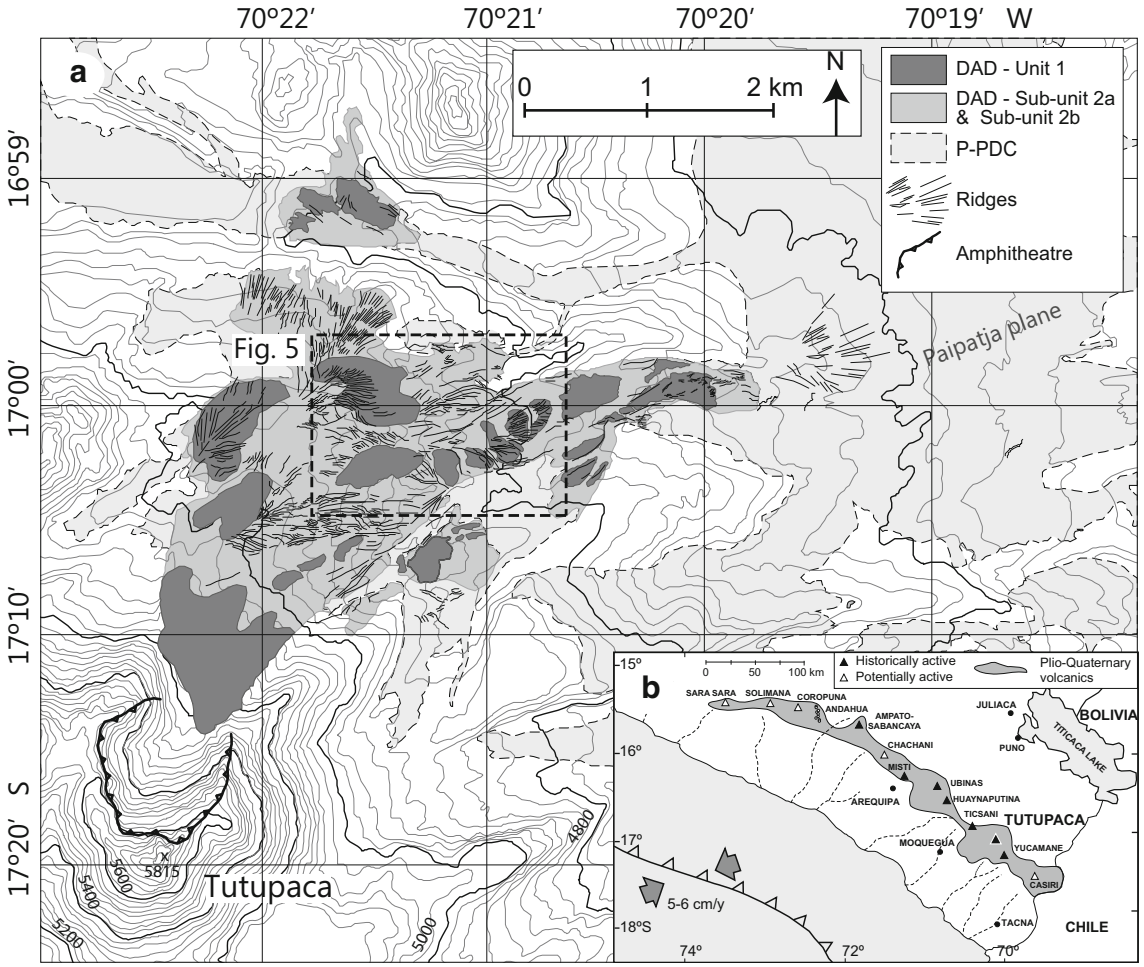

Fig. 1 **a** Map of Tutupaca debris avalanche deposit (DAD), showing the lower hummocky unit 1 and the more extended, upper ridged unit 2. *P-PDC* stands for the Paipatja pyroclastic density current deposit. Location of image presented in Fig. 5 is indicated. **b** Location of the Tutupaca volcano in the Peruvian volcanic arc

debris avalanche blocks (cf. Glicken 1991) as well as smaller hummock-like hills (Figs. 1 and 2). This hummocky debris avalanche deposit outcrops up to 4–6 km from the amphitheatre. The structures preserve the partially intact original stratigraphy (Figs. 2 and 3) with a lower hydrothermally altered layer overlain by a unit composed of older volcanic edifice and recent dome lava. This deposit has the characteristics of a classic volcanic debris avalanche (e.g. van Wyk de Vries and Davies 2014).

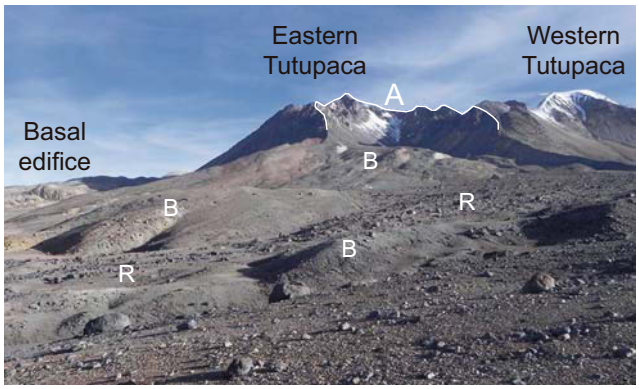

Fig. 2 Panoramic view of the Tutupaca volcano with amphitheatre (*A*) open to the NE, debris avalanche blocks (*B*) of Unit 1 and ridges (*R*) of the unit 2

In contrast, the thinner overlying breccia unit 2, that outcrops up to 5–7 km from the amphitheatre, is notable for its ridged surface (Figs. 1 and 2). This unit varies in surface lithology and is divided it into two sub-units (Fig. 3). The widespread sub-unit, 2a, mostly contains white and yellow hydrothermally altered lava, with clast fragments smaller than 10 cm, and sparse large, massive megaclast up to 5–10 m in diameter. The other sub-unit, 2b, is only found in the central part of the deposit, which is mostly channelized in a glacial valley running to the east from the Tutupaca base to the Paipatja plain (Fig. 3a). This sub-unit is composed of unaltered (fresh) dark grey dome rocks of dacitic composition. Neither sub-unit 2a nor sub-unit 2b has a clearly defined internal stratigraphic sequence, as can be seen from the two

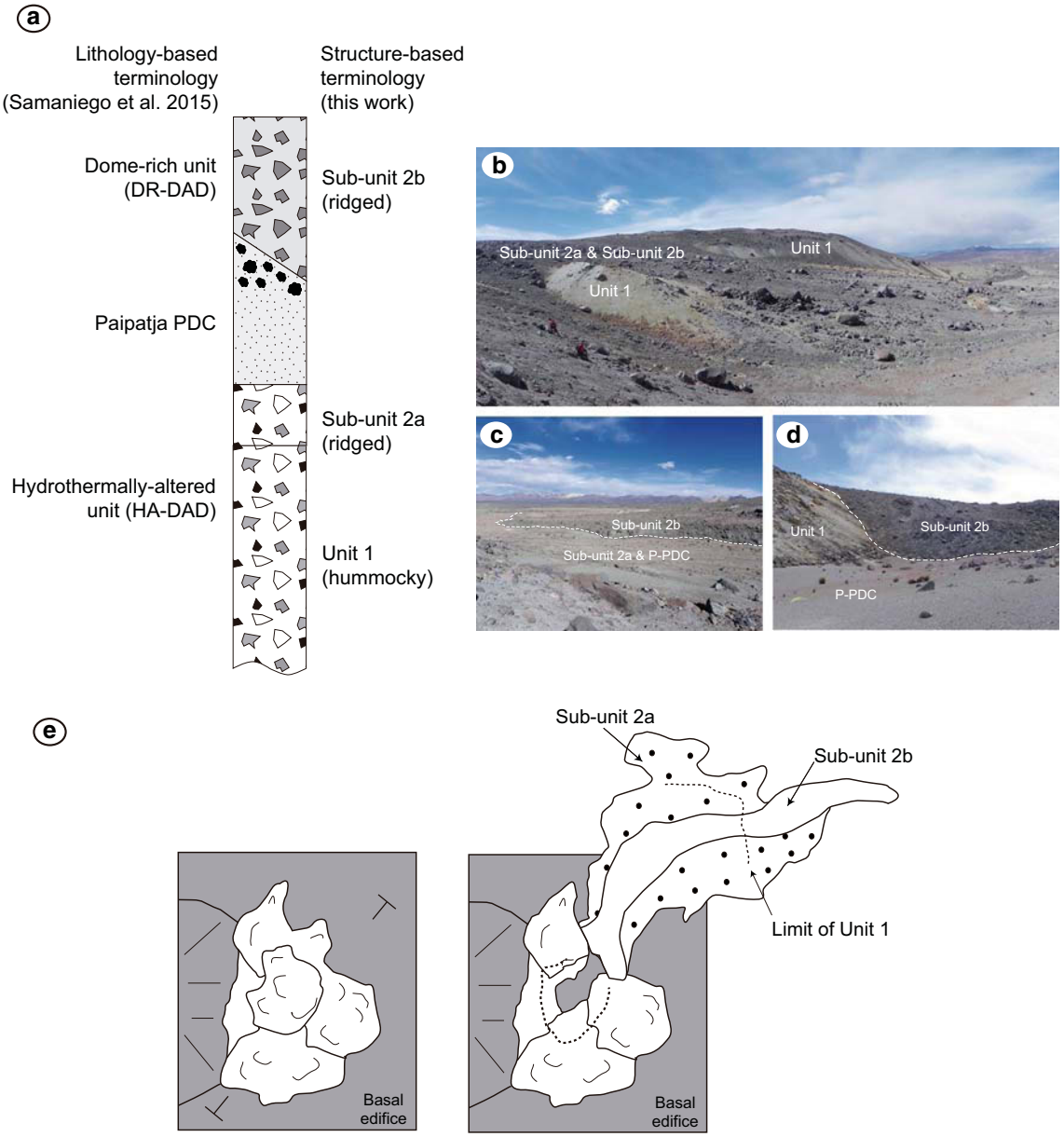

Fig. 3 **a** Composite stratigraphic section showing the units terminology used in this work and by Samaniego et al. (2015). **b** Panoramic view of both debris avalanche deposits: the lower hummocky unit 1 and the upper ridged unit 2 (sub-units 2a and 2b). **c**, **d** Photographs showing the contacts between the different units. **e** Simplified sketches showing the Tutupaca volcano before and after the collapse and the spatial distribution of the debris avalanche deposits

trenches we excavated and from few other exposures of the interior. It is worth noting that the contact between the underlying unit 1 and the overriding sub-units 2a and 2b can only be seen at scarce outcrops such as those shown in Fig. 3.

The lithologies present in the debris avalanche deposit units and their distribution correspond to lithologies in the scar. Unit 1 and sub-unit 2a (i.e. HA-DAD of Samaniego et al. 2015) fits with the lithologies seen in the lower part of the scar and the scar inner east side, which mostly correspond to the basal edifice or the lower part of the Tutupaca domes. In contrast, the lithologies observed in sub-unit 2b (i.e. DR-DAD of Samaniego et al. 2015) correspond to those observed in the scar inner west side, which correspond to the young Tutupaca domes.

Deposits of the P-PDC that accompanied the collapse are found on top of the avalanche unit 1 and sub-unit 2a in most areas, whereas they are overlain by the upper dome-rich sub-unit 2b (Fig. 3). These PDC deposits are thickest in the inter-ridge depressions, where we excavated down to 1.5 m without being able to find the avalanche deposit below. The P-PDC was deposited around large blocks and accentuates the appearance of the ridges.

Surface structures

Quantitative morphological data on the surface structures were measured from georeferenced Google Earth® Pro images with a pixel resolution of 5 m. The surface morphology of unit 1 is characterized by 200–700-m-long and 20–40-m-high debris avalanche blocks as well as smaller 100-200-m-long hummock-like hills (Fig. 2). These features outcrop in the medial zone, between ~2 and ~6 km from the amphitheatre. In contrast, unit 2 is composed of abundant ridges that are elongated, subparallel elevations separated by depressions on the surface of the avalanche deposit (Figs. 2, 3 and 4). These ridges are most abundant between 4 and 5 km from the scar, but are also present in the distal regions where they are partially buried by the P-PDC deposit (Fig. 1). In this study, 30–35 % of ridges are composed of the sub-unit 2a and the remaining 65–70 % occur within the dome-rich sub-unit 2b. The morphological characteristics of the ridges are presented in Fig. 5. The length of the ridges varies from a few meters to more than 500 m, with an average of 100 to 150 m (Fig. 5c). There is no relationship between the length of the ridges and their distance from the scarp (Fig. 5f). The ridges are 10–30-m wide, and the separation of the ridge axis (or wavelength) varies from ~30 to 35 m in the proximal area but reaches up to ~60 m at 6 km from the scar in open areas where the deposit has fanned out. The ridge height was measured in the field. They are typically 1–5-m high, and the largest ridges (>3-m high) are within the fresh sub-unit 2b near the proximal region. No relationship between the size and the ridge lithology is found.

A notable feature of the ridges in unit 2 is the concentration of larger blocks on the ridge crests (Figs. 3, 4 and 6). The ridge surfaces in the altered sub-unit 2a are smooth, either simple one-summit ridges with 10 to 20° side slopes, or multiple ridges, or flattopped ridges between two deep troughs. The height of the ridges increases progressively along strike after initiation and also tend to decrease gradually. Some ridges start abruptly downstream from large blocks (3–30-m wide), giving a tail-like aspect, while others have blocks up to 10 m in diameter along the axis of the ridge (Fig. 6).

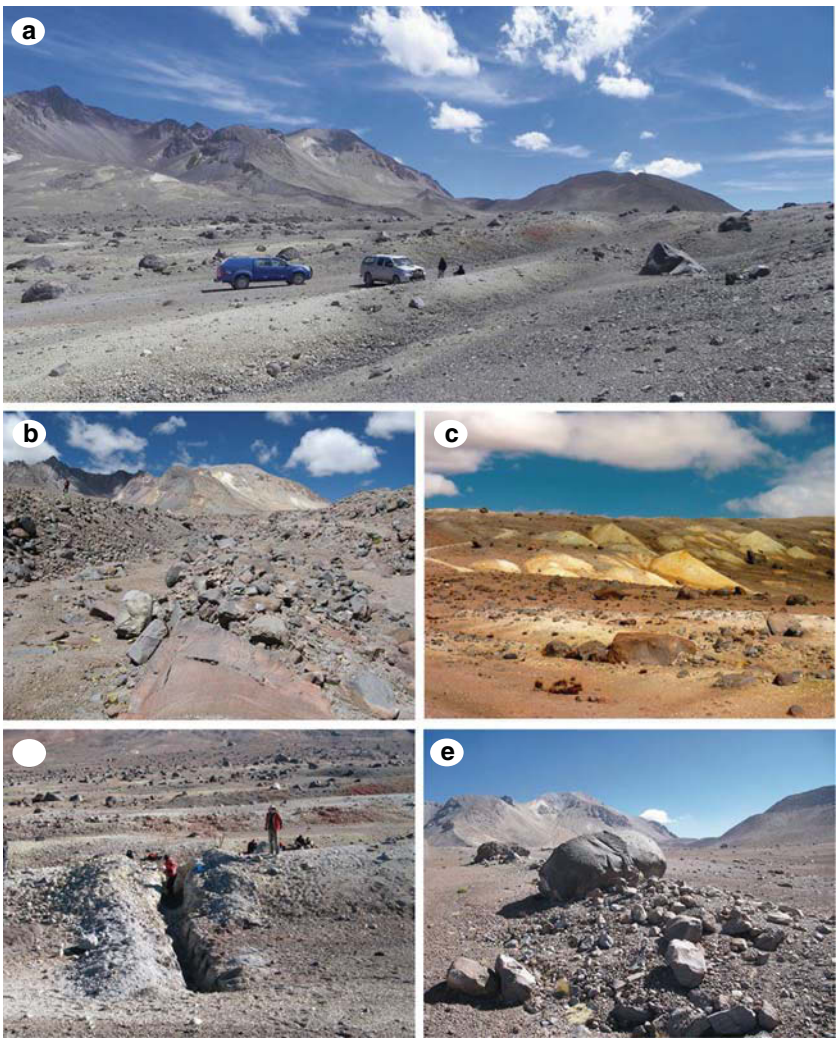

Fig. 4 Photograph showing the different surface morphologies of the DAD units 1, 2a and 2b. Note people and cars for scale. **a** Elongated ridges on sub-unit 2a. **b** Ridges on sub-unit 2b. Note the important amount of block on these ridges, compared with those of the sub-unit 2a. **c** Hummock field on unit 1 covered by ridged sub-unit 2a. **d** Trench dug in a ridge of the medial part of the DAD sub-unit 2a. **e** Blocks on top of the ridged sub-unit 2a

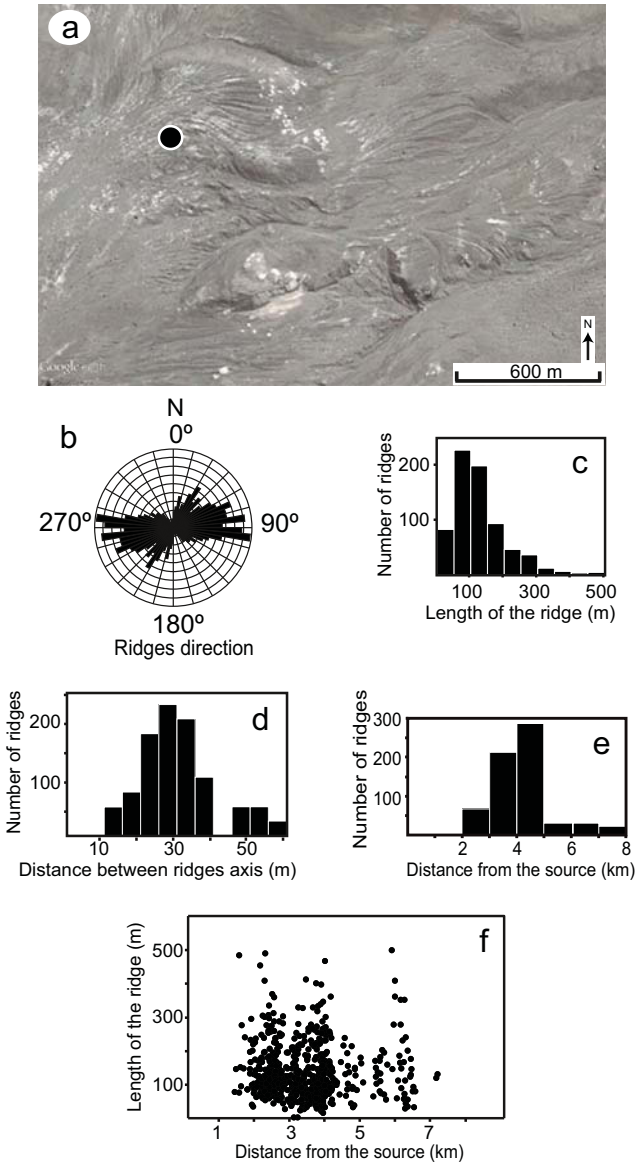

Fig. 5 **a** Google Earth® image of the ridges (location given in Fig. 1). The *black dot* corresponds to the location of the trenches dug across the ridges and presented in Fig. 7. **b** Rose diagram showing the ridge directions. **c**–**e** Histograms showing the morphological characteristics of ridges. **f** Diagram showing the length of the ridges as a function of the distance from the source

Concentrations of smaller blocks are found either downstream or upstream of the largest blocks. It was observed that these smaller blocks are pushed together, with trapped, brecciated blocks in between larger ones (Fig. 6). Impact marks were frequently seen. Some large blocks had zones of bulldozed matrix in front or behind the block, on all parts of the deposit.

Sedimentological data of elongated ridges

Two trenches were excavated to expose the interior of two ridges in the sub-unit 2a (Fig. 7). The internal upper 2 m of both ridges showed a similar structure, with a central zone of slightly coarser breccia and steep-sided contacts with an inter-ridge filling of later pyroclastic flow material. In both trenches, there was an altered upper layer at the centre that thinned at the ridge edge, and there were some indistinct lenses of different coloured breccia and some wedges or breccia-filled cracks. Facies exposed in the trenches were sampled and analysed for granulometry, component and textural analysis. Forty-nine, noncohesive samples were sieved to establish the grain-size distribution using the method of Blott and Pye (2001) and their Gradistat software. From this analysis, the matrix of the sampled material was defined at <32 mm.

The ridge structure and the material characteristics are shown in Fig 7. The contacts between the fresh and altered material in the central part of the ridge are lobate and steeply inclined outwards on the left side (facing uphill) where a red facies in the fresh breccia is also in contact with a brown material (Fig. 7a, b). On the right side (facing uphill) the contacts are convolute, with a fluidal-like mixing of brown fresh and yellow altered materials. The pyroclastic density current material is also involved in this mixing, down to a few centimetres below the contact (Fig. 7a, b). Histograms of the size distribution of the breccia matrix show that the samples are sand to gravel size dominated and fines poor (Fig. 7c). The pyroclastic density current deposit grain size distribution is notably different, with less sorting and more fines. The cumulative curves (Fig. 8) further show, with a few exceptions, a continuous change in size range from between the more poorly sorted and finer samples outside the ridge axis to the better sorted and coarser central breccias at the ridge axis. Angular andesitic breccia clasts with planar faces and subrounded cauliflower-like dense clasts are found to be predominant in the ridge axis (Fig. 7d). The breccia clasts are more rounded in the lateral parts of the ridge, where some clasts are coated in fine hydrothermal clays and deeply oxidized, giving a more rounded shape.

Discussion

The distribution of the lithologies within the deposits suggest that the debris avalanche at Tutupaca initiated with a failure of the lower hydrothermal system that allowed a frontal and basal avalanche unit (unit 1) to form (Fig. 9). Behind this, parts of the growing lava dome, with its hot magma carapace and part of the inner hydrothermal system, failed to produce units 2a and 2b. Such a sequence is similar to that seen in the Rosenquist slides of Mount St. Helens (Lipman and Mullineaux 1981) and reproduced in analogue models of Andrade and van Wyk de Vries (2010) and Paguican et al. (2014). We now discuss dynamical implications of the structures observed, focusing on the ridged deposits, that present a

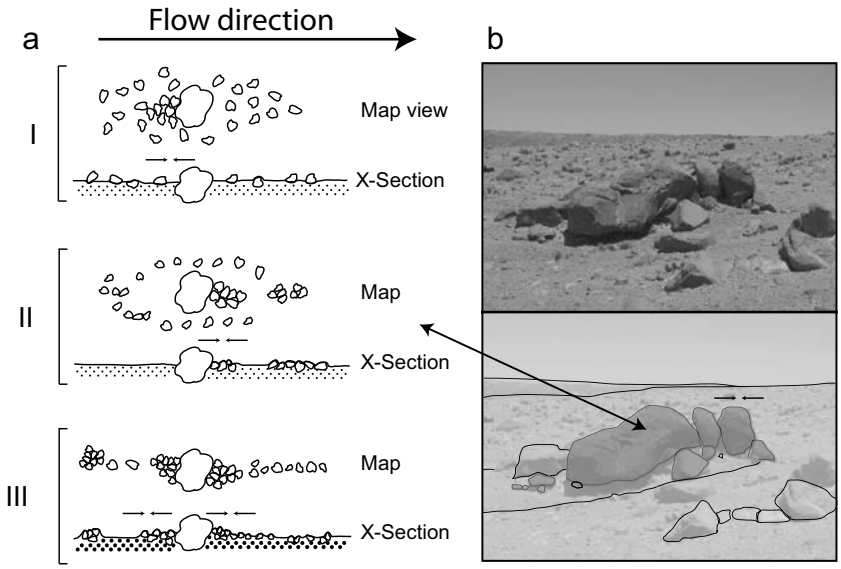

Fig. 6 Relationships between ridges and large (typically >10 m) blocks. The direction of movement is from the *left* to the *right*. **a** Map view and cross section of configurations I, II, and III between large and small blocks. Small blocks are concentrated downstream or upstream of the large blocks. **b** Photograph and interpretation of configuration II

significantly different type of surface structure to that seen on most hummocky volcanic debris avalanche deposits.

Comparison with other ridged debris avalanche deposits

Elongated ridges (or flowbands following the terminology of Dufresne and Davies 2009) have been described at the debris avalanche deposits of Shiveluch (Belousov et al. 1999) as well as some other volcanic debris avalanche deposits in the Central Andes such as those of Socompa (Kelfoun et al. 2008; van Wyk de Vries et al. 2001), Llullaillaco (Richards and Villeneuve 2001) and Lastarria (Naranjo and Francis 1987). Similar features have been also described in non-volcanic environments, such as landslides (Shaller 1991) and rock avalanches overriding glaciers (McSaveney 1978), as well as in extraterrestrial environments (i.e. Mars, Luchitta 1978; Shaller 1991). The 1964 Shiveluch deposits in particular show strong similarities with those of the Tutupaca debris avalanche. Like Tutupaca, the medial and distal part of the Shiveluch debris avalanche deposit display abundant elongated, subparallel ridges and depressions, whose dimensions (i.e. 1–30-m wide, 0.3–10-m high and up to 1-km long, Belousov et al. 1999) are of the same order of magnitude than at Tutupaca. Belousov et al. (1999) interpret these ridges and depressions as a result of unconfined spreading of a laminar plug flow that produces radial extension of the avalanche. However, Belousov et al. (1999) does not provide a detailed field description of the lithologies or internal structure of the ridges.

Interpretation of Tutupaca ridges

Ridge-like structures showing particle grain size segregation have been observed to form in experiments on polydisperse granular flows exhibiting granular fingering (Pouliquen et al. 1997; Pouliquen and Vallance 1999; Mallogi et al. 2006; Gray and Kokelaar 2010; Johnson et al. 2012). Flow fingers form when larger, more angular particles first segregate at the flow surface, as a response to size-induced percolation of fines and squeeze expulsion (Fig. 10). These larger particles then travel faster than the rest of the flowing mass and concentrate at the flow front. Small perturbations cause deflection of the trajectories of these large particles along the steepest surface slope, which causes formation of frontal lobes and emerging static lateral levées. Localized concentrations of these large particles result in a larger friction coefficient leading to local flow deceleration, which favours amplification of the instabilities and leads to the emplacement of granular fingers with lateral levées enriched in coarse material. Recirculation motion of the coarse particles (see also Johnson et al. 2012) can sustain the segregation process and favour the formation of long granular fingers. A notable result is that the fingers (i) are enriched in large particles at their joint margins that eventually form streamwise elongated ridges in the granular mass and (ii) have a nearly constant width, which defines a typical wavelength (i.e. length between consecutive parallel ridges).

We interpret the Tutupaca ridges as joint margins of the lateral levées of granular fingers where the large blocks were concentrated. In this context, inter-ridge depressions formed as the flowing granular mass drained the central part of the fingers that became progressively less elevated than the ridges, as shown for self-channelling granular flows depicting levée-channel morphology (Félix and Thomas 2004; Lube et al. 2007; Mangeney et al. 2007; Jessop et al. 2012). These depressions served as preferential pathways for the pyroclastic flows whose deposits accumulated there and thinned towards the ridge core. The segregation process observed in experiments can explain most of the observed Tutupaca ridges, particularly those whose axis separation reveals a well-defined wavelength. Furthermore, the sedimentological data show that

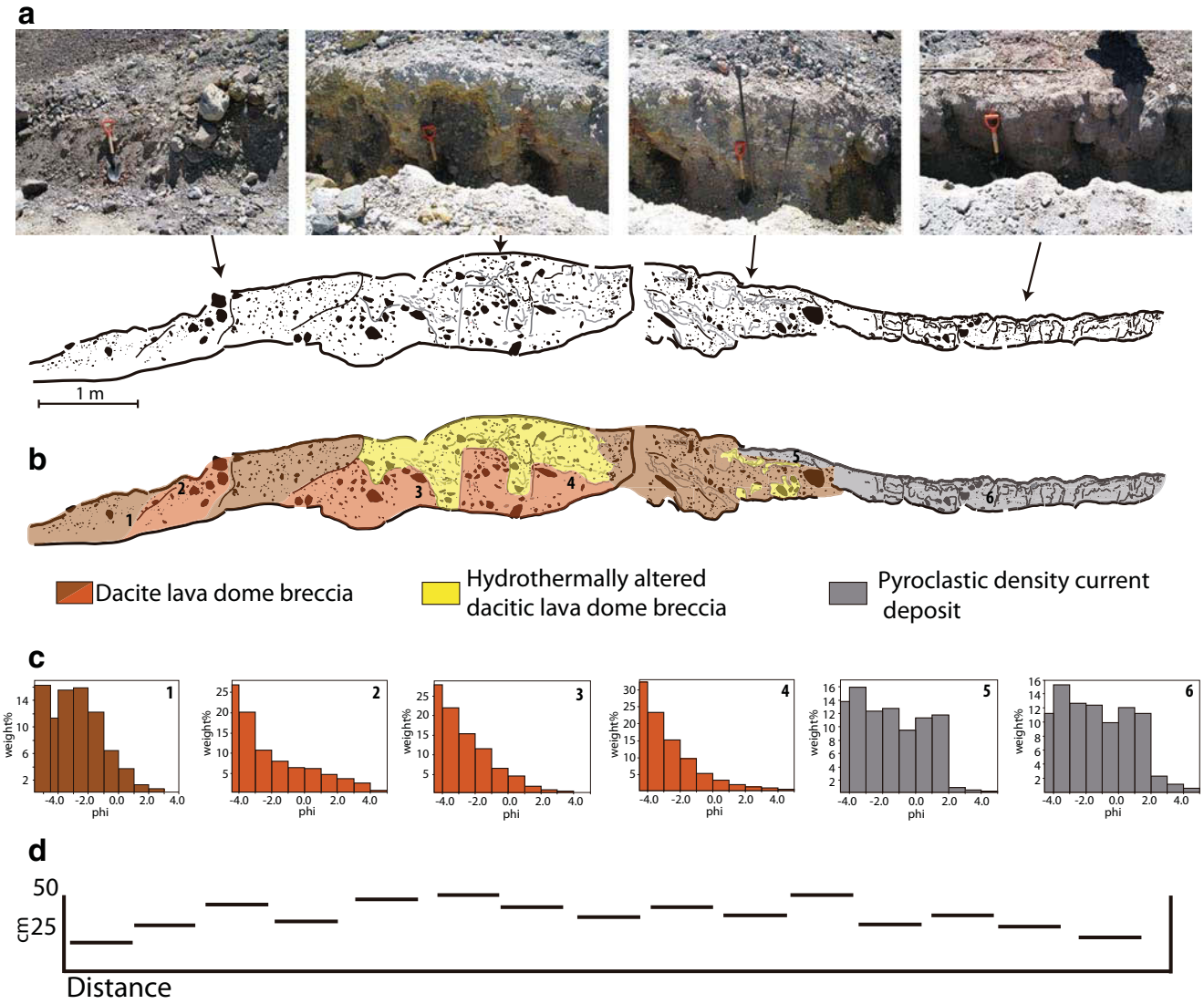

Fig. 7 **a** Sketch depicting the 1–1.5-m-high, 8–10 m-long cross section of a ridge of the unit 2a. A photo of the ridge and its location are shown in Figs. 4d and 5a, respectively. The sketch represents the ridge (facing uphill). *Irregular black dots* symbolize blocks, and *thin grey lines* represent contacts and/or structures. Photographs show the different parts of the ridge. **b** Interpretation of the different sections of the ridge according to distinct facies. Note the contact between the DAD breccia and the PDC deposit. **c** Histograms of matrix granulometry of parts 1–6 of the ridge as shown in b. **d** Maximum block size across the ridge showing the difference between the coarser core and the finer lateral parts of the ridge

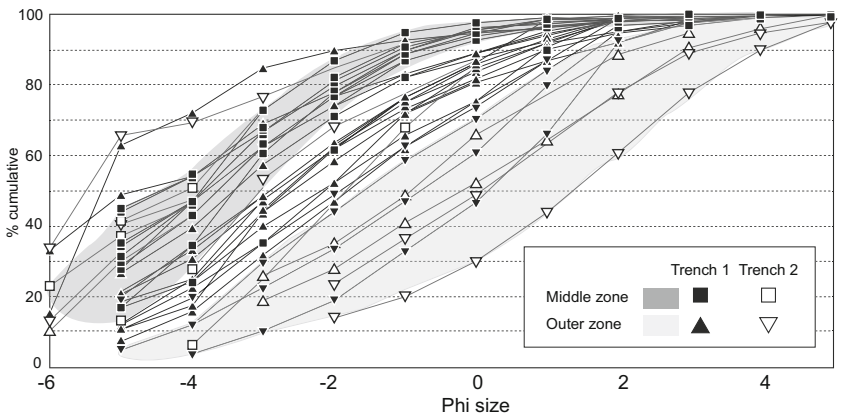

Fig. 8 Cumulative grain size curves for the matrix samples collected in both trenches. Note the enrichment in coarse material in the middle (core) zone compared with the lateral zones

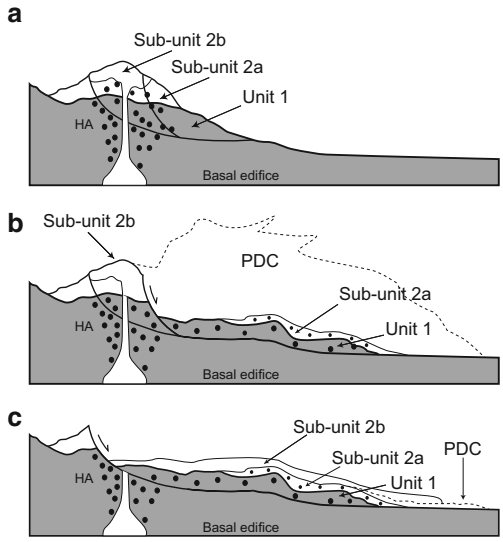

Fig. 9 **a**–**c** Sequential evolution of the Tutupaca sector collapse. Correspondence between debris avalanche units and the rock sequences at the edifice are indicated

there is a gradual change of grain size distributions, with the ridge core coarser and better sorted that the margins (Figs. 7 and 8). Textural evidence suggests that cataclasis could have also contributed to change the grain size distribution along motion. Better sorting in the ridge core may indicate that this part was the most stable (possibly static), and that granular size segregation could be preserved there, whereas the least sorted marginal zones with mixing textures, sharp fault-like boundaries and differential lateral movements suggest a higher degree of cataclasis with much larger shear strain than in the ridge core. These features are consistent with static levées bordering a channel in which the granular material flowed. Once formed, the ridges could evolve by continued differential shear along structures as seen frequently in debris avalanches (Shea and van Wyk de Vries 2008; van Wyk de Vries and Davis 2014; Roverato et al. 2015), and by spreading of the granular mass, which accounts for the increase of separation of the ridge axes with distance.

Many ridges are associated with, or start at, greater than a meter-sized blocks (Figs. 4 and 6), as shown by differential movement of the blocks with respect to the body of the avalanche. This suggests that this differential movement may have contributed also to the initiation or development of some ridges. A block moving faster or slower than the main mass would generate a local forward or backward force. This force could then generate the constriction by impacted and accumulated block lines. The steep contacts seen in the trenches may be strike-slip faults that accommodate differential constriction in the transport direction. The role of both granular fingering and differential block movements are compatible, and could have contributed contemporaneously to ridge formation and evolution.

Dynamic implications of contrasting landslide surface textures

The Tutupaca debris avalanche deposit has two distinct structural units. The first is a ‘classic’ debris avalanche with

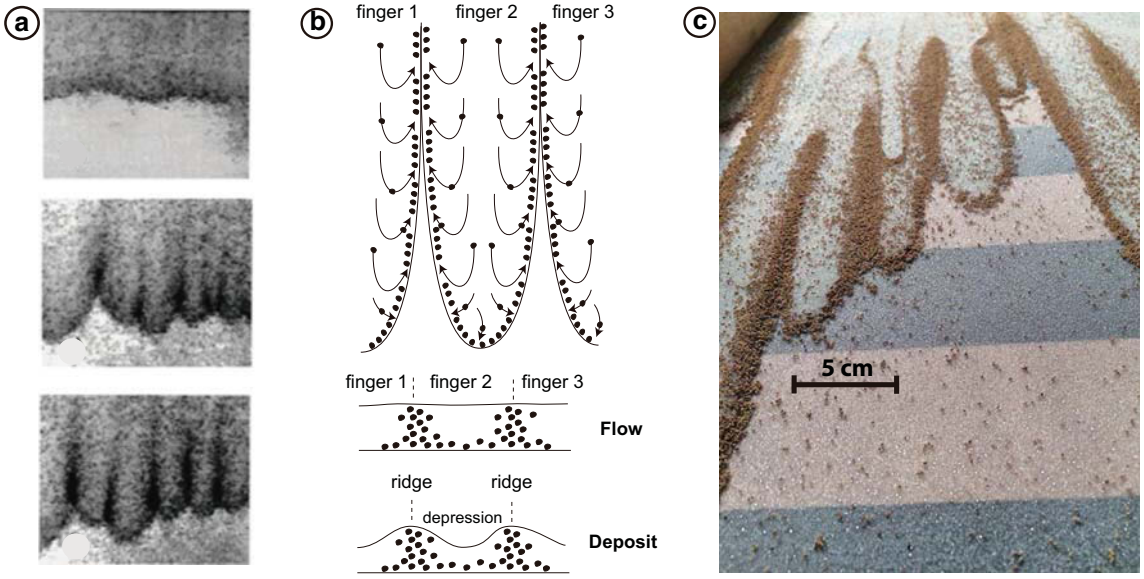

Fig. 10 **a** Temporal evolution of a granular flow in experiments (modified from Pouliquen and Vallance 1999). The camera is moving at the same speed as that of the flow front. Note the formation of digitation (fingers) whose lateral sides (levees) enriched in coarse material merge to form ridges. **b** Schematic representation of the ridges. The merging of lateral levees of two different fingers (*top*) generates ridges between depressions that form once the material is drained (see *bottom*, cross sections in flow and deposit). **c** Photograph of an unpublished experiment showing granular fingering. Larger, segregated brown particles (560–710 μm) form ridges bordering depressions white particles (300–400 μm)

hummocks, showing all the features associated with a translational slide type of emplacement. The second, ridged facies, in contrast, shows evidence of behaviour as a granular flow. The reason for this different mechanical behaviour is probably found in the different source rock, according to the collapse scenario we consider. From the scar shape, its outcrops, and from the distribution of lithology in the avalanche deposit, we propose that the landslide started as a failure in the outer altered basal edifice, which formed the main core avalanche (unit 1) (see Fig. 9). This first slide unit was overrun by a slice from the destabilized dome core and its altered base (unit 2). The ridged deposit sub-unit 2a is composed of this rock from the active dome and the hydrothermal system. This material collapsed and efficiently fragmented while propagating downslope, leading to a granular mass flow that fed the ridged unit. It is possible that the front and lateral parts of the sliding Unit 1 also collapsed and disaggregated during motion to create parts of the frontal more granular flow-ridged deposit. Thus, the mechanical behaviour of the units could have changed during transport.

Ridges at Tutupaca probably formed by a combination of granular fingering and differential movement in the moving mass, and evolved with grain size segregation and granular mass spreading. They evidence a flow behaviour that is not usually associated with debris avalanches (Belousov et al. 1999; Dufresne and Davies 2009) that are generally seen to be emplaced by sliding of a plug on a low friction base (Shea and van Wyk de Vries 2008; Kelfoun et al. 2008). In fact, the Tutupaca debris avalanche deposits show that there can be a dual mechanical behaviour in that both sliding of the relatively undisturbed edifice components and flowing of a little expanded granular mass can coexist in one event. We note that there are ridges on the Socompa debris avalanche (Kelfoun et al. 2008; van Wyk de Vries et al. 2001), and the duality of proximal hummock-dominated Toreva sliding to a more fluid-like granular flow behaviour in distal areas could also have occurred there. Our interpretation on avalanche dynamics should be equally applicable to ridges observed in landslide deposits in extraterrestrial environments (e.g. Luchitta 1978).

Conclusions

The historical (218 ± 14 aBP) debris avalanche deposit of Tutupaca volcano has two distinct units: a hummocky slide deposit and a ridged granular flow deposit. The two different units mostly originate from the different lithologies and varying magmatic and hydrothermal conditions in the initial edifice. The lower slide (unit 1) came from the lower volcano flank, where failure began in altered hydrothermal layers. The granular flow (units 2a and 2b) developed from the back of the landslide incorporating more of the brittle active dome core as well as active hydrothermal material. Unit 1 slid as a translational debris avalanche to maintain original gross stratigraphy and produce a faulted body with hummocks. In contrast, unit 2 was more fragmented and travelled as a granular flow over and between the translational unit 1. The ridged surface of unit 2 may have resulted from a combination of granular flow processes: granular fingering, differential block velocities and spreading.

The bi-modal mechanical behaviour described here in a volcanic debris avalanche has important implications for modelling the hazards of such phenomena. Any predictive modelling should take into account the possibility of mass movements with various mechanical behaviours, and include different material properties in the edifice and take into account the initial landslide structure, all of which influence the complexity of the resulting volcanic debris avalanche deposit.

Acknowledgments This work is part of a Peruvian–French cooperation programme carried out between the Instituto Geológico, Minero y Metalúrgico (INGEMMET) and the French Institut de Recherche pour le Développement (IRD). It was partially founded by the JEAI project financed by the IRD. This research was also supported by the French Government Laboratory of Excellence initiative n°ANR-10-LABX-0006, the Région Auvergne and the European Regional Development Fund. This is Laboratory of Excellence ClerVolc contribution n° 186. We thank the constructive reviews of A. Dufresne, an anonymous reviewer, and the Associate Editor L. Capra.

References

Andrade D, van Wyk de Vries B (2010) Structural analysis of the early stages of catastrophic stratovolcano flank-collapse using analogue models. Bull Volcanol 72:771–789

Belousov A, Belousova M, Voight B (1999) Multiple edifice failures, debris avalanches and associated eruptions in the Holocene history of Shiveluch volcano, Kamchatka, Russia. Bull Volcanol 61:324–342

Blott SJ, Pye K (2001) GRADISTAT: a grain size distribution and statistics package for the analysis of unconsolidated sediments. Earth Surf Process Landf 26:1237–1248

Clavero JE, Sparks RSJ, Huppert HE (2002) Geological constraints on the emplacement mechanism of the Parinacota avalanche, northern Chile. Bull Volcanol 64:40–54. doi:10.1007/s00445-001-0183-0

Dufresne A, Davies TR (2009) Longitudinal ridges in mass movement deposits. Geomorphology 105:171–181

Eppler DB, Fink J, Fletcher R (1987) Rheologic properties and kinematics of emplacement of the Chaos Jumbles rockfall avalanche,Lassen Volcanic National Park, California. J Geophys Res 92:3623–3633

Félix G, Thomas N (2004) Relation between dry granular flow regimes and morphology of deposits: formation of levées in pyroclastic deposits. Earth Planet Sci Lett 221:197–213

Glicken H (1991) Sedimentary architecture of large volcanic-debris avalanches. In: Smith GA, Fisher RV (eds) Sedimentation in volcanic settings 45: 99–106

Glicken H (1998) Rockslide-debris avalanche of May 18, 1980, Mount St. Helens Volcano, Washington. Bull Geol Soc Jpn 49:55–106

Gray JMNT, Kokelaar BP (2010) Large particle segregation, transport and accumulation in granular free-surface flows. J Fluid Mech 652:105–137

Iverson RM (1997) The physics of debris flows. Rev Geophys 35:245–296

Jessop DE, Kelfoun K, Labazuy P, Mangeney A, Roche O, Tilliere J-L, Trouillete M, Thibault G (2012) LiDAR derived morphology of the 1993 Lascar pyroclastic flow deposits, and implication for flow dynamics and rheology. J Volcanol Geotherm Res 245–246:81–97. doi:10.1016/j.jvolgeores.2012.06.030

Johnson CG, Kokelaar BP, Iverson RM, Logan M, LaHusen RG, Gray JMNT (2012) Grain-size segregation and levee formation in geophysical mass flows. J Geophys Res 117:F01032. doi:10.1029/2011JF002185

Kelfoun K, Druitt TH (2005) Numerical modeling of the emplacement of Socompa rock avalanche, Chile. J Geophys Res 110, B12202. doi:10.1029/2005JB003758

Kelfoun K, Druitt TH, van Wyk de Vries B, Guilbaud MN (2008) Topographic reflection of the Socompa debris avalanche, Chile. Bull Volcanol 70:1169–1187. doi:10.1007/s00445-008-0201-6

Legros F (2002) The mobility of long-runout landslides. Eng Geol 63: 301–331

Lipman PW, Mullineaux DR (Eds) (1981) The 1980 eruptions of Mount St. Helens, Washington (No. 1250). US Dept. of the Interior, US Geological Survey

Lube G, Cronin SJ, Platz T, Freundt A, Procter JN, Henderson C, Sheridan MF (2007) Flow and deposition of pyroclastic granular flows: a type example from the 1975 Ngauruhoe eruption, New Zealand. J Volcanol Geotherm Res 161:165–186

Luchitta BKA (1978) Large landslide on mars: geological society of America bulletin 89:1601–1609

Mallogi F, Lanuza J, Andreotti B, Clement E (2006) Erosion waves: transverse instabilities and fingering. Europhys Lett 75:825

Mangeney A, Bouchut F, Thomas N, Vilotte JP, Bristeau MO (2007) Numerical modeling of self-channelling granular flows and of their levée channel deposits. J Geophys Res Solid Earth 112, F02017

McSaveney MJ (1978) Sherman Glacier rock avalanche, Alaska, U.S.A. Rockslides and Avalanches. Elsevier, Amsterdam, pp 197–258

Naranjo JA, Francis P (1987) High velocity debris avalanche at Lastarria Volcano in the North Chilean Andes. Bull Volcanol 49:509–514

Paguican EMR, van Wyk de Vries B, Lagmay AMF (2014) Hummocks: how they from in and how they evolve in rockslide-debris avalanches. Landslides 11:67–80

Pouliquen O, Vallance JW (1999) Segregation induced instabilities of granular fronts. Chaos 9:621–630

Pouliquen O, Delour J, Savage SB (1997) Fingering in granular flows. Nature 386:816–817

Richards JP, Villeneuve M (2001) The Llullaillaco volcano, northwest Argentina: construction by Pleistocene volcanism and destruction by sector collapse. J Volcanol Geotherm Res 105:77–105

Roverato M, Cronin S, Procter J, Capra L (2015) Textural features as indicators of debris avalanche transport and emplacement, Taranaki volcano. Geol Soc Am Bull 127:3–18

Samaniego P, Valderrama P, Mariño J, de Wyk de Vries B, Roche O, Manrique N, Chedeville C, Fidel L, Malnati J (2015) The historical (218 ± 14 aAP) explosive eruption of Tutupaca volcano (Southern Peru). Bull Volcanol 77:51. doi:10.1007/s00445-015-0937-8

Shaller PJ (1991) Analysis of a large moist landslide, Lost River range, Idaho, USA. Can Geotech J 28:584–600

Shea T, van Wyk de Vries B (2008) Structural analysis and analogue modelling of the kinematics and dynamics of large-scale rock avalanches. Geosphere 4:657–686

Siebert L (1984) Large volcanic debris avalanches: characteristics of source areas, deposits, and associated eruptions. J Volcanol Geotherm Res 22:163–197

Siebert L, Glicken H, Ui T (1987) Volcanic hazards from Bezymianny- and Bandaï-type eruptions. Bull Volcanol 49:435–459

van Wyk de Vries B, Davies T (2014) Landslides, debris avalanches and volcanic gravitational deformation. In: Sigurdsson H, Houghton B, McNutt S, Rymer H, Stix J (eds) Encyclopedia of volcanoes, 2nd edition. Elsevier

van Wyk de Vries B, Self S, Francis PW, Keszthelyi L (2001) A gravitational spreading origin for the Socompa debris avalanche. J Volcanol Geotherm Res 105:225–247

Voight B, Komorowski J-C, Norton GR, Belousov AB, Belousova M, Boudon G, Francis PW, Franz W, Heinrich P, Sparks RSJ, Young SR (2002) The 26 December (Boxing Day) 1997 sector collapse and debris avalanche at Soufriere Hills Volcano, Montserrat, W.I. In: Druitt TH, Kokelaar BP (eds) The eruption of Soufriere Hills Volcano, Montserrat, from 1995 to 1999. Mem Geol Soc London 21: 363–407

Chapter 5:

GRANULAR FINGERING AS A MECHANISM FOR RIDGE FORMATION IN VOLCANIC MASS FLOWS: LABORATORY EXPERIMENTS AND IMPLICATION FOR THE TUTUPACA DEBRIS AVALANCHE DEPOSIT, SOUTHERN PERU

1. Introduction

Debris avalanches and landslides occur in many geological contexts at any scale and represent major geological hazards (Dufresne and Davies, 2009). The kinematics and dynamics of these gravitational mass flows can be studied through analysis of the architecture and the surface structures of their deposits. The geological literature reports various surface structures, namely ridges (or elongated/longitudinal ridges, Dufresne and Davies, 2009), flow bands (Belousov et al., 1999) and hummocks (Paguican, et al., 2012). Ridges are common in volcanic environments (Figure 1) such as the debris avalanche deposits of Mount St. Helens (Voight et al., 1980), Socompa (Van Wyk de Vries et al., 2001), Shiveluch (Belousov et al. 1999) and Tutupaca (Valderrama et al., 2016); but also in non-volcanic deposits such as those of Mink Creek (Geertsema et al., 2006) and Acheron (Smith et al. 2006). Samaniego et al., (2015) and Valderrama et al., (2016) have reported very well-preserved ridges in an historic debris avalanche deposit (~200-230 yBP) of Tutupaca volcano in southern Peru. Valderrama et al., (2016) concluded that these ridges give insights into the dynamics of the debris avalanche and may be the consequence of granular segregation and fingering, a physical process observed in experiments on polydisperse granular flows (Pouliquen et al., 1997; Pouliquen and Vallance, 1999; Mallogi et al., 2006; Gray and Kokelaar, 2010; Johnson et al., 2012).

The present work is aimed at further investigating granular fingering in order to discuss the mechanisms of debris avalanches. We performed analogue experiments on granular flows using bidisperse mixtures as in previous similar studies but considering systematically different concentrations of the granular components. We report for the first time the different stages of granular segregation and fingering and discuss how the grain size difference between the granular components influence the shape and the surface structures of the flow deposits. Finally, we show that the structures in experiments share many similarities with those described at the Tutupaca volcano debris avalanche, which permits us to further discuss the emplacement mechanisms of this volcanic mass flow.

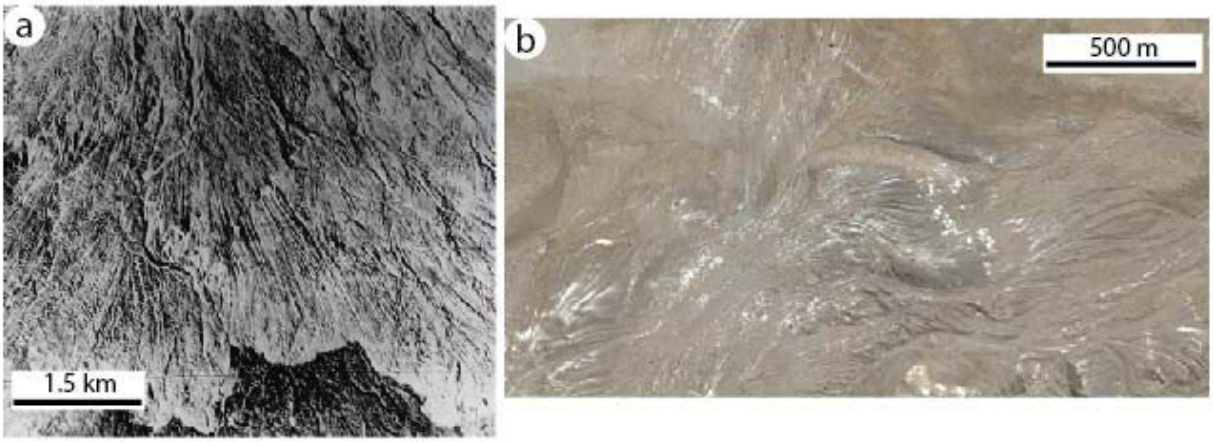

Figure 1. Longitudinal ridges at surface of the debris avalanche deposits of (a) Shiveluch volcano (Belousov et al., 1999) and (b) Tutupaca volcano (Valderrama et al., 2016).

2. Fingering: a fundamental granular flow process

Granular fingering was first reported by Pouliquen et al. (1997) and further investigated by Pouliquen and Vallance (1999), Mallogi et al. (2006) and Woodhouse et al., (2012). Pouliquen et al. (1997) carried out experiments on bidisperse granular flows on rough inclines (Figure 2). They used mixtures of small subspherical glass beads of diameter of 0.5 mm and of large particles made of angular crushed fruit stone of size of 0.5 – 0.63 mm, with volume concentrations of the coarse component of 5 vol.%. Flows were generated in a channel, 2 m-long and 70 cm-wide, whose rigid substrate was made rough by gluing the same particles as the fine granular flow component. The bidisperse mixtures were released from a reservoir with constant gate opening of 6 mm, hence generating flows of nearly constant thickness down the slope. Granular fingering arose as a consequence of particle segregation. The larger particles segregated at the surface of the flows because of the combined effects of percolation of the small beads through the shearing granular network and of squeeze expulsion of the large components. Once at the flow surface, these larger particles travelled faster than the rest of the flowing mass, because the flow velocity across the flow depth increased upwards, and as a consequence they concentrated at the flow front. The large particles were deflected along the steepest surface slope at the flow front and accumulated to form local instabilities characterized by emerging frontal lobes with static lateral levees immediately behind. Large friction associated to the sliding of these

irregular-shapes particles helped amplifying the frontal instabilities, which progressively acquired the shape of granular fingers of nearly constant width and with well-defined coarse-grained levees. Segregation and granular fingering were favoured by recirculation of the coarse grains at the flow front as particles that reached the flow base were reinjected upwards to the free surface where segregation acted again (Figure 2). This recirculation process was investigated in detail in large-scale experiments by Johnson et al. (2012) and theoretically by Gray and Kokelaar (2010). A key result of Pouliquen et al. (1997) in the context of the present study is that the coarse-grained joint margins of the granular fingers resemble the ridges observed at the surface of many debris avalanche deposits.

Granular fingering was further investigated in later experimental studies. Pouliquen and Vallance (1999) used various bidisperse mixtures but only with 5 vol.% of the coarse component and reported results similar to that of Pouliquen et al. (1997). Malloggi et al., (2006) demonstrated that granular fingering occurred as well in subaqueous flows while Woodhouse et al. (2012) showed that separated fingers may form. The formation of granular fingers was also addressed theoretically by Woodhouse et al. (2012) and Gray et al. (2015). The aim of our experimental study is to further investigate granular fingering by taking into account wider ranges in grain size difference and relative proportions of the components of the bidisperse mixtures than in earlier studies, as detailed below.

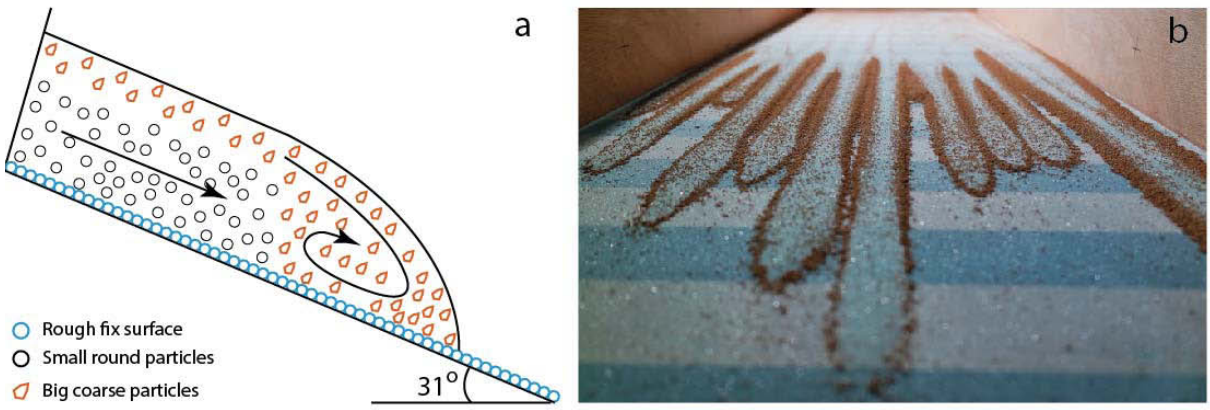

Figure 2. (a) Schematic representation of granular segregation in our experiments (from Pouliquen et al. 1997). Round particles are glass beads of size 300-400 µm while the coarse particles are crushed fruit stones of mean size of 600 to 1000 µm. (b) Photography of an experimental deposit; note how coarse particles accumulate at the edges of granular fingers.

3. Experimental procedure

Experimental device and particles

The experimental device consisted of a 1.45 x 0.45 m channel inclined at 31° and with a rough base (Figure 3). The channel was connected to a reservoir of a volume of 18 000 cm^3 from which the granular mixtures were released to generate the flows. The reservoir was equipped with a double gate system to ensure a constant mixture outflow rate. The aperture of the back door was set to 1.5 cm for all experiments while the front door was entirely removed to release the particles. The roughness of the channel base was obtained by gluing 300-400 µm subspherical glass particles onto an adhesive paper sheet that laid on the channel base. As some substrate particles could be entrained by the flows, the base was replaced every 10 experiments to ensure a nearly constant roughness. The experiments were filmed with a high resolution (1920x1080 pixels) video camera in order to investigate the flow kinematics and the segregation processes. Transversal black marks were placed beneath the non-opaque rough base every 5 cm in order to allow for measurement of the flow front propagation.

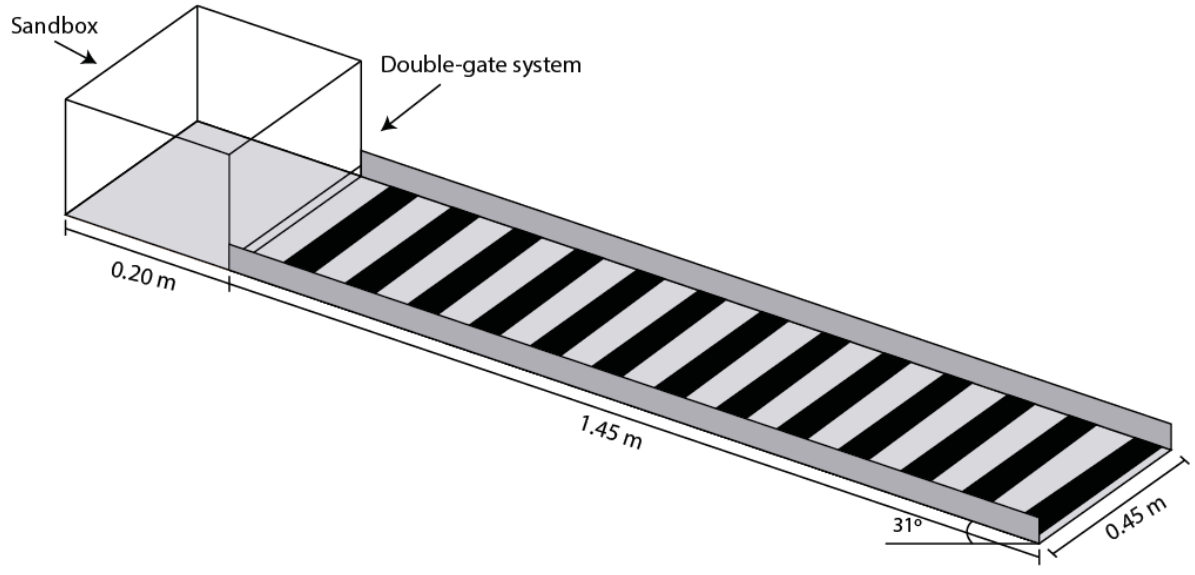

Figure 3. Experimental setup for studying granular fingering.

Experiments were made with four bidisperse mixtures of (1) subspherical glass beads with a grain size of 300-400 µm and (2) coarse angular particles made of crushed fruit stones

(cf. Dufresne and Davies 2009; Pouliquen and Vallance 1999) with grain size ranges from 600-710 µm up to 900-1000 µm (Table 1). The percentage of the coarse component in the mixtures varied from 5 to 50 wt.% (Table 1). All experiments were made with an initial mass of the mixtures of 1 kg. Before each experiment, the bi-disperse material was stirred gently and thoroughly to generate mixtures as homogeneous as possible.

Round particles: Glass beads		Coarse particles: Crushed fruit stones	
Grain size (µm)	Mass fraction (%)	Grain size (µm)	Mass fraction (%)
300-400	50% to 95%	600-710	5%, 10%, 15%, 20%, 30%, 40%, 50%
		710-800	5%, 10%, 15%, 20%
		800-900	5%, 10%, 15%, 20%
		900-1000	5%, 10%, 15%, 20%

Table 1. Particles used in the experiments. The particles were sieved to obtain narrow grain size distributions.

Photogrammetry

After each experiment, at least 14 photographs with a 20-megapixel resolution were taken from different view angles in order to perform photogrammetry and obtain 3D models of flow deposits. A white halogen light was used to stand out the detailed shapes and structures of the deposits. Photogrammetry was done using the software Agisoft Photoscan Professional Edition version 1.1.6 for Mac (see Smith et al., 2015 for details on the method). In order to improve the digital elevation models (DEM) resolution, we made a "georeference process" using the photogrammetry software. To do that, we created our own reference system with a minimum unit size of 0.05 mm and we calibrated it using the coordinates of 7 fixed points previously marked on the experimental device. Data processing permitted us to obtain DEMs of the experimental deposits with a 0.5 mm of resolution (Figure 4). Lastly, the DEMs were used to retrieve cross-sections of the structures (fingers and lobes) and to

compare the values of the thickness of the deposits and of the size of the different structures with those measured in situ with a ruler.

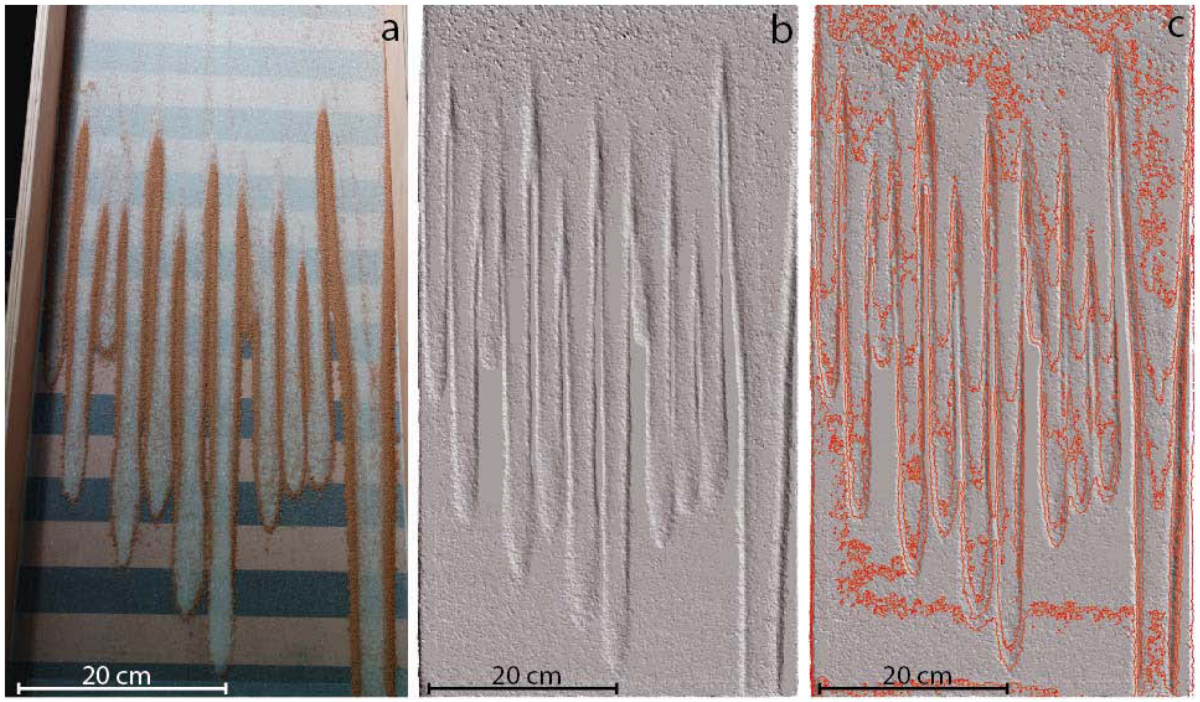

Figure 4. (a) Photograph of a deposit in the experimental device. The mixture is composed of 75 wt.% of glass particles (300 – 400 µm) and 15 wt.% of crushed fruit stones (600-710 µm). (b) Digital elevation model (DEM) obtained from photogrammetry, with a resolution of 0.5 mm/pixel. (c) 1 mm elevation lines generated from the DEM.

4. Results

In this section we first present preliminary experiments that permitted us to define the parameters we chose to investigate granular fingering in detail. Then we report the flow kinematic data as well as the morphological measurements retrieved from the deposits (final length, thickness and width of the fingers, spacing between fingers).

Preliminary tests

We tested different mixtures with various grain sizes and proportions of particles. We first used mixtures of glass beads (300-400 µm) and the smaller coarse particles (600-710 µm) at concentrations of 5 to 50 wt.% (Table 1). On the basis of this first series of experiments, we concluded that the flows experienced well-defined granular segregation

and fingering for coarse particle concentrations between 5 to 20 wt.%. Then, experiments were made with coarse particles of larger grain sizes (Table 1) at concentration of 5 to 20 wt.%.

The inclination of the channel and the mass of material released from the reservoir were chosen according to the experiments that generated deposits with the longest possible length (shorter than the channel length). We concluded that the most appropriate slope angle and material mass were 31 degrees and 1 kg, respectively. At lower angles the flows stopped too close to the gate while at higher angles they propagated out the channel. We carried out 114 experiments with these initial conditions and reconstructed the deposits morphologies from a total of 1596 photographs. High definition videos of the experiments also permitted us to determine the flow kinematics and to identify the occurrence of the three stages of emplacement, as described below (Figures 5 and 6).

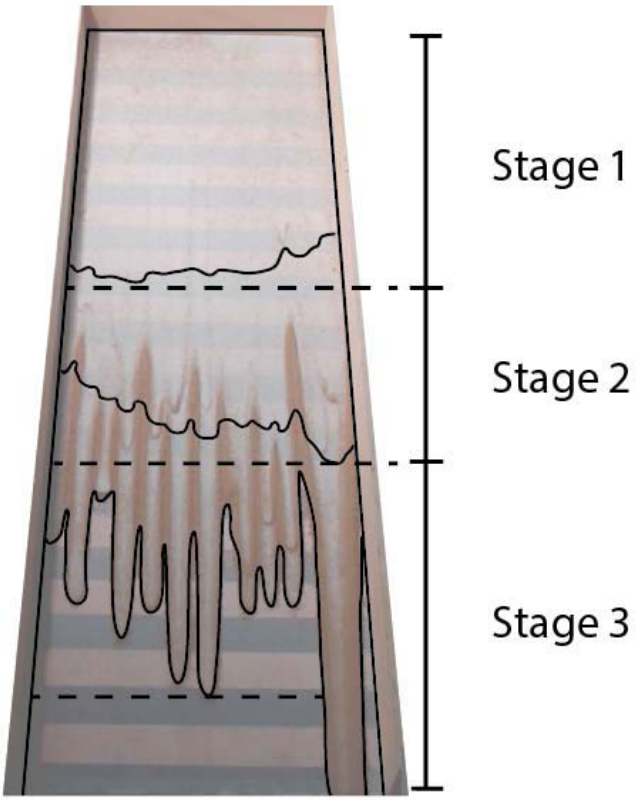

Figure 5. Representation of the 3 stages of emplacement. Stages 1, 2 and 3 correspond respectively to segregation of the particles, accumulation of the coarse particles at flow front, and granular fingering.

Flow kinematics

Stage one (S1): Segregation

Particle segregation occurs as soon as the granular mixture propagates downslope after gate opening. Most of the small particles percolate downwards while the coarse particles move to the top of the flow and concentrate at the front (Figure 6). This stage is characterized by the highest flow front velocity, which is about 40 cm/s and is independent on both the coarse particles size and concentrations (Figure 7).

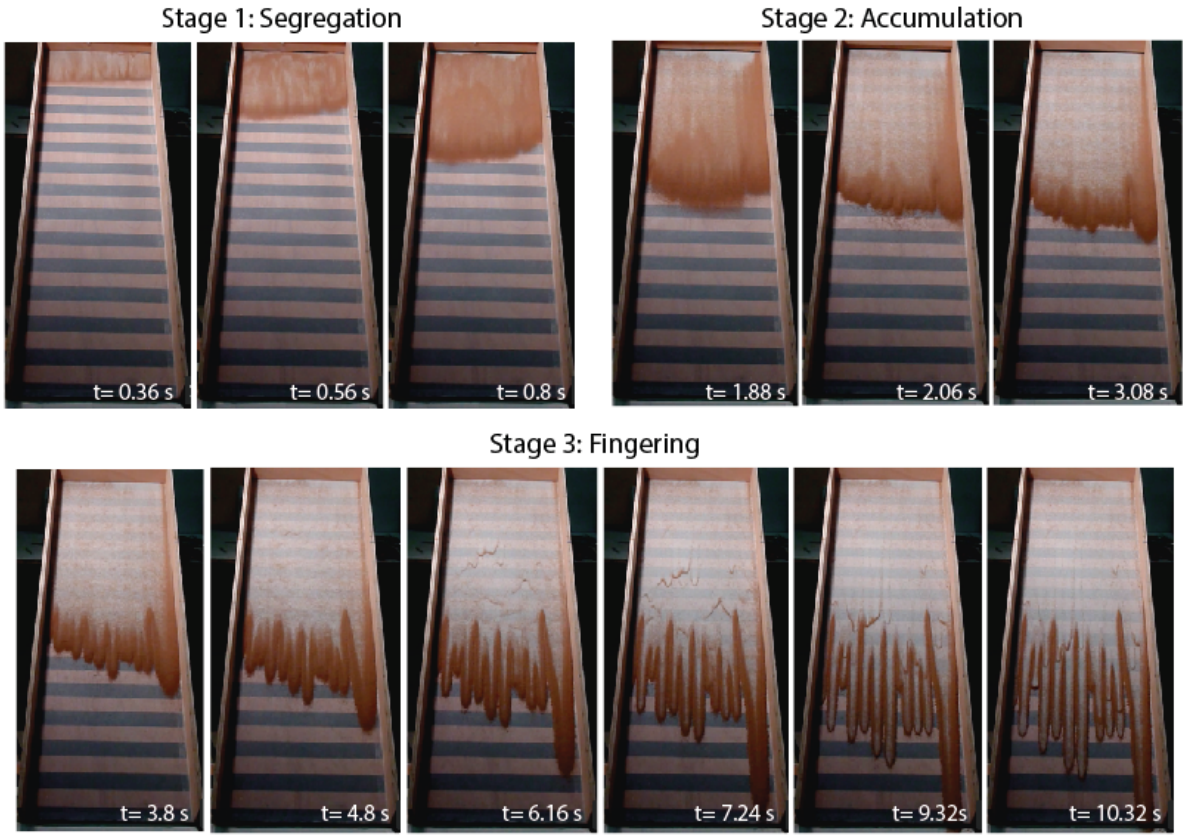

Figure 6. Stages of flow propagation. Snapshots of an experiment with 15 wt.% of 600-710 µm coarse particles. The experimental flow stops at t=10.32 s.

Stage Two (S2): Accumulation of coarse particles at flow front

During this stage most of the coarse particles accumulate at the flow front (Figures 5 and 6). This phenomenon causes instabilities (Woodhouse et al., 2012), and the flow front slows down (or even stops for a short duration in some experiments) while the rest of mass propagates at the initial velocity acquired at Stage 1. In consequence, the front is overtaken by the material behind, which causes a surface wave and causes flow propagation

downslope. Front instabilities then grow to form emerging fingers. After a couple of seconds, about 80 % of the coarse particles have accumulated at the front (Figure 6, t=2.06 s).

Detailed information on the times and distances at which this second stage begins and ends for the different mixtures is presented in Figures 7 and 8. For mixtures with ≤20 wt.% of coarse particles, stage 2 begins at distances of 60-80 cm from the source and at times of 2-3 s after release, except for mixtures with 900-1000 µm coarse particles for which these distances and times are significantly larger, i.e. 75-95 cm and 3-3.5 s, respectively. The distance travelled during stage 2 is fairly short, typically 5-15 cm. The complementary experiments with ≥30 wt.% of 600-710 µm particles, however, reveal that the distance travelled is much larger, up to 68 cm at a concentration of 50 wt.% (Figure 8). The flows propagate at relatively slow velocities of 5-15 cm/s during stage 2 (Figure 7)

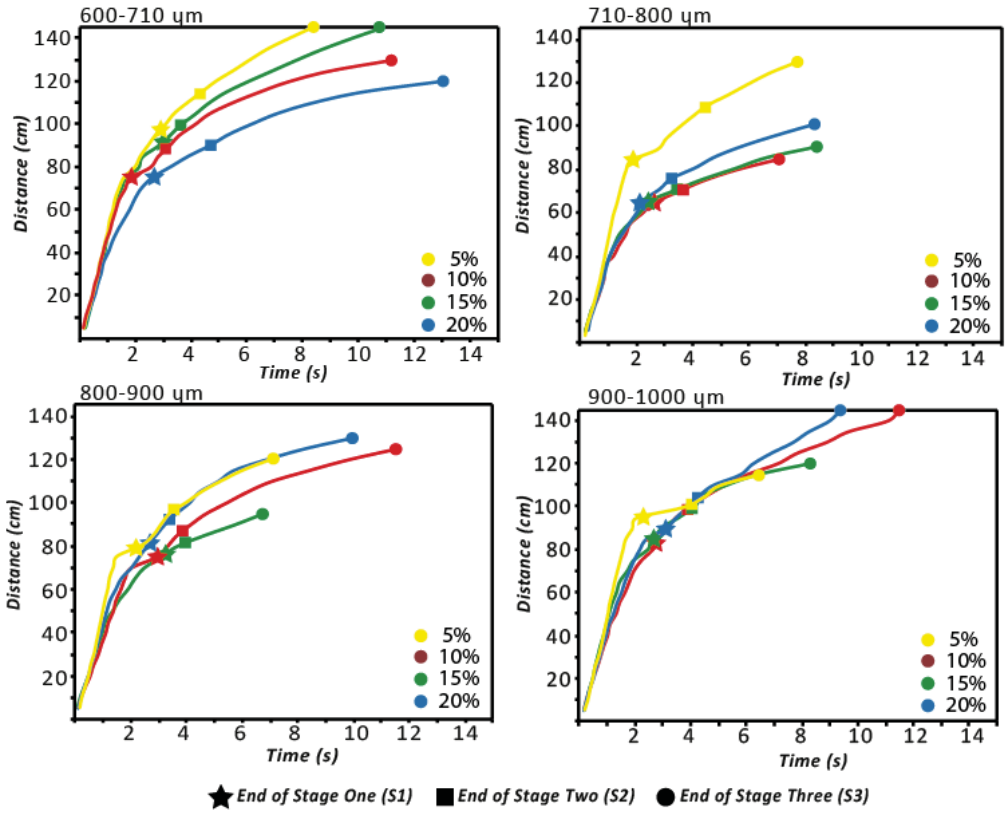

Figure 7. Kinematic data of the flows of different granular mixtures. The stars mark the end of the segregation stage (Stage 1), the squares mark the end of the accumulation stage (Stage 2), and the dots indicate the end of the fingering stage (Stage 3) as well as the end of the experiment. Note that some flow runouts exceed the length of the channel (140 cm).

Stage Three (S3): Fingering

The final stage of propagation is characterized by granular fingering and a significant diminution of the velocity of the moving mass (Figure 6). The fingers form as a consequence of particle size segregation, accumulation of coarse particles at the flow front and formation of local instabilities, which grow to form fingers with coarse-rich static margins bordering a fines-rich central channel (Pouliquen et al., 1997). Accumulation of the coarse particles at the flow front, which began during stage 2 and decreased the velocity of the moving mass, further operates during this last stage and causes even lower propagation velocities of about 2-3 cm/s until the granular mass halts (Figure 7). The fingers delimited by the stable margins have a constant width, and the flowing granular mass mainly composed of small particles in the central channel eventually drains once material supply from the source is no longer available. Notice that during this late stage of emplacement some low amplitude surface waves may form in the proximal area before the fingers emerge (see Figure 6 at t>6.16 s). Detailed data on the distance travelled during the three stages can be found in Figure 8.

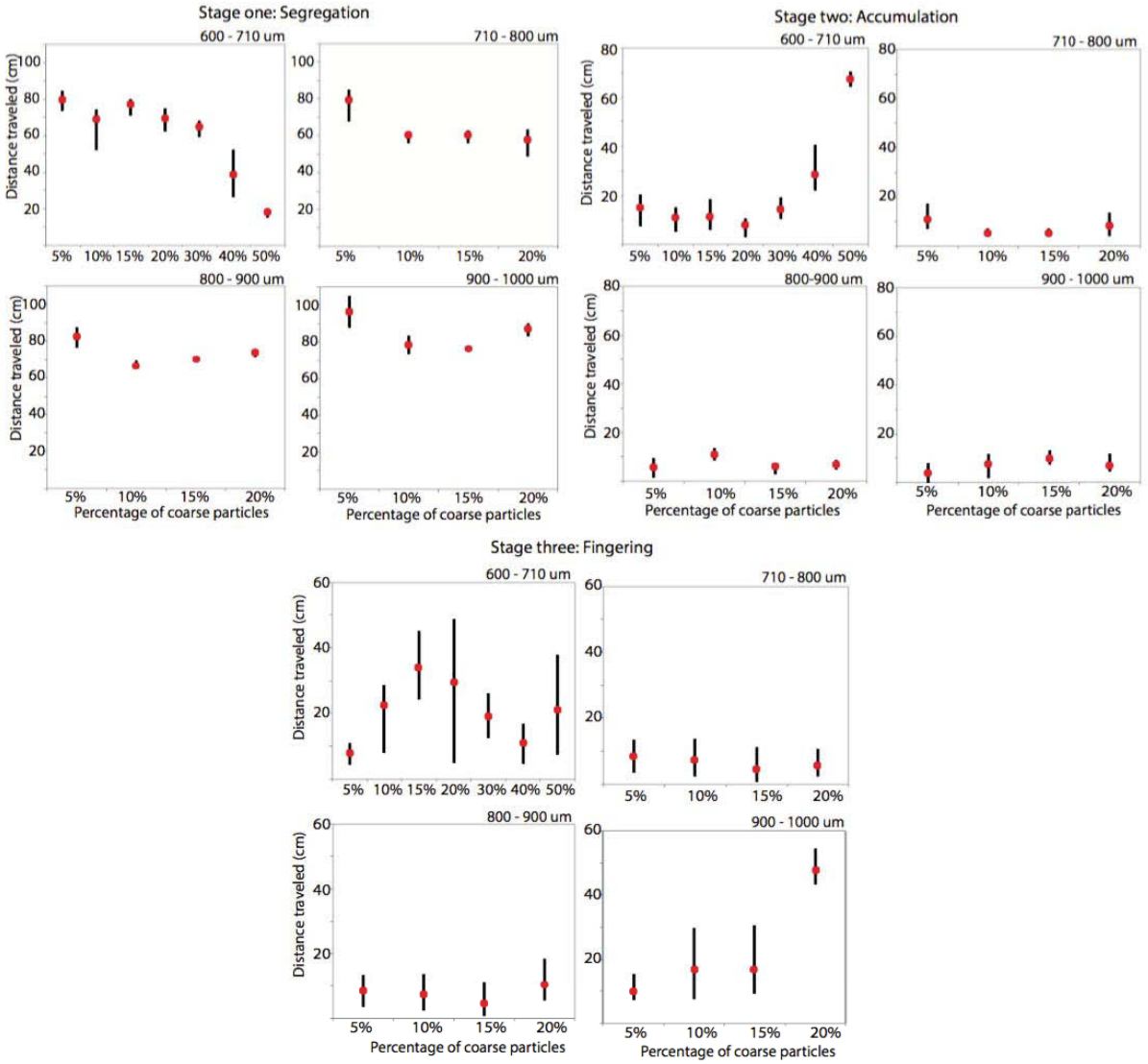

Figure 8. Distance travelled by the granular mass during the three stages. The size and proportion of the coarse particles are indicated. Stage one begins as soon as the reservoir gate is open while stages two and three begin as soon the previous stage ends.

An important result of our experiments is that the fingers are either separated or merged depending on the nature of the granular mixtures (Figure 9). Fingers are clearly merged, and their joint margins form longitudinal ridges, when the grain size difference between the two components is small (i.e. with the 600-710 µm coarse particles) and at coarse concentrations of 10-20 wt.% (lower concentrations of 5 wt.% do not promote enough segregation for allowing emergence of distinct fingering). At these conditions the mean distance travelled by the fingers is 21-30 cm, with fairly large ranges of values of 40-50 cm (Figure 8), and in some cases the fingers propagate out of the device (Figure 6). In contrast, fingers are almost absent or are significantly shorter and/or separated in other

mixtures. In particular, well-defined separated fingers form at the largest grain size difference and coarse concentration (e.g. mixture with 20% of 900-1000 µm coarse particles, see Figure 9).

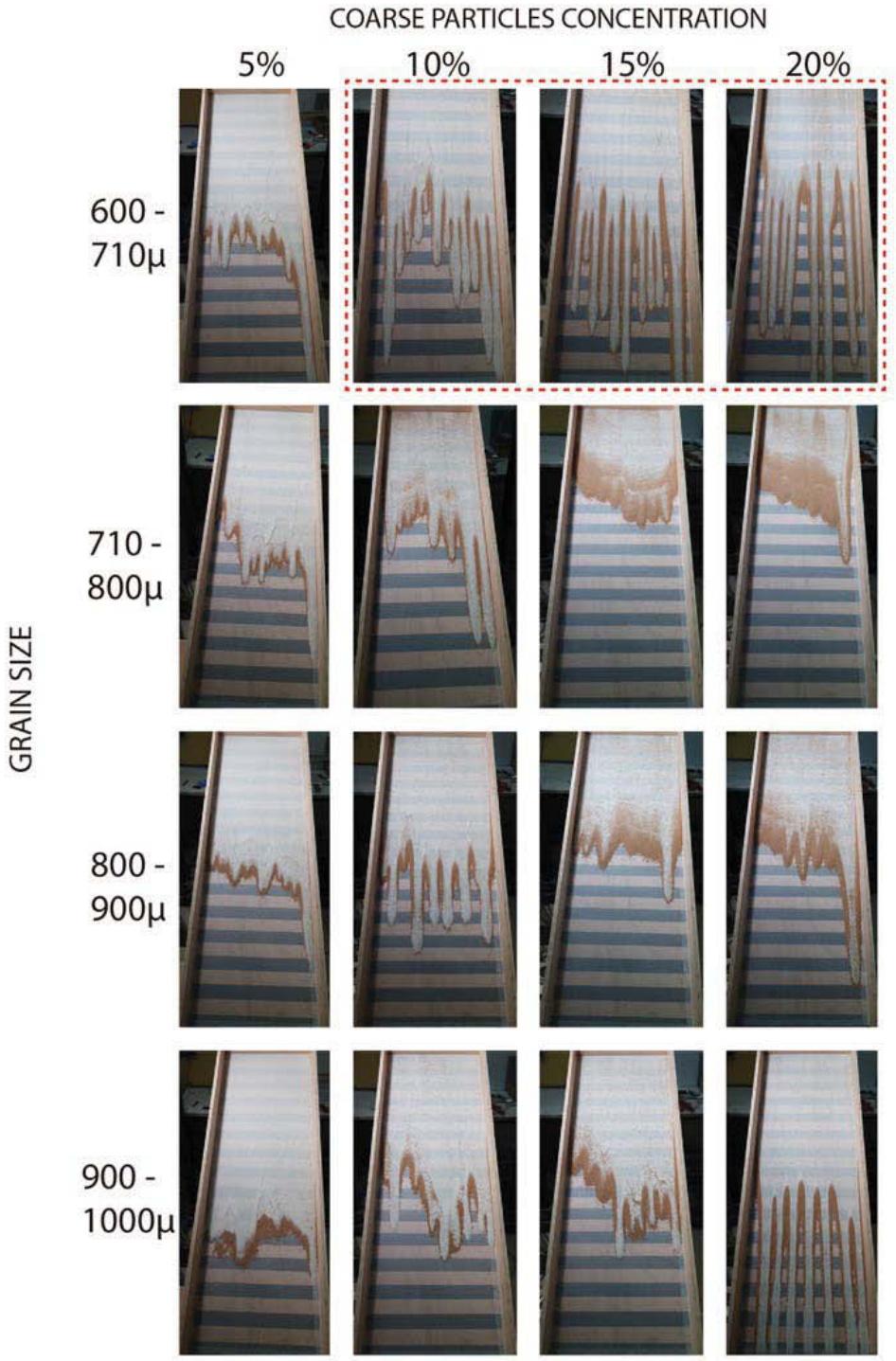

Figure 9. Final deposits in the experiments with different granular mixtures. The dashed red square shows the most favourable conditions for the formation of well-developed merged fingers, which generate longitudinal ridges.

Morphology of the deposits

The morphology of the deposits was measured with a ruler and through photogrammetry, with a precision of 1 mm and 0,5 mm, respectively. We report below the length, the width and the thickness of the fingers as well as the spacing between them.

Length of the fingers

The fingers are the longest for the mixture with the 600-710 µm coarse particles (Figure 10). Their mean length increases from ~35 cm at 5 wt.% concentration up to ~63 cm at 20 wt.% concentration. Notice that the ranges of length is quite large, typically ~30-75 cm. Complementary experiments at higher concentrations reveal that the length of the fingers is ~49-69 cm (Figure 10). Fingers are significantly shorter for the 710-800 µm mixture as their mean length is only ~10-20 cm. At coarse concentrations of 5-10 wt.%, however, some fingers are quite long (up to 50 cm). At higher coarse concentrations of 15% and 20% the fingers are very poorly developed and rather resemble joint lobes (Figure 9). In other cases, with larger coarse particles the fingers have lengths intermediate between those reported above for the other mixtures, with typical values of 17-36 cm except for the 20 wt.%, 900-1000 µm mixture that generated well-defined and long separated fingers.

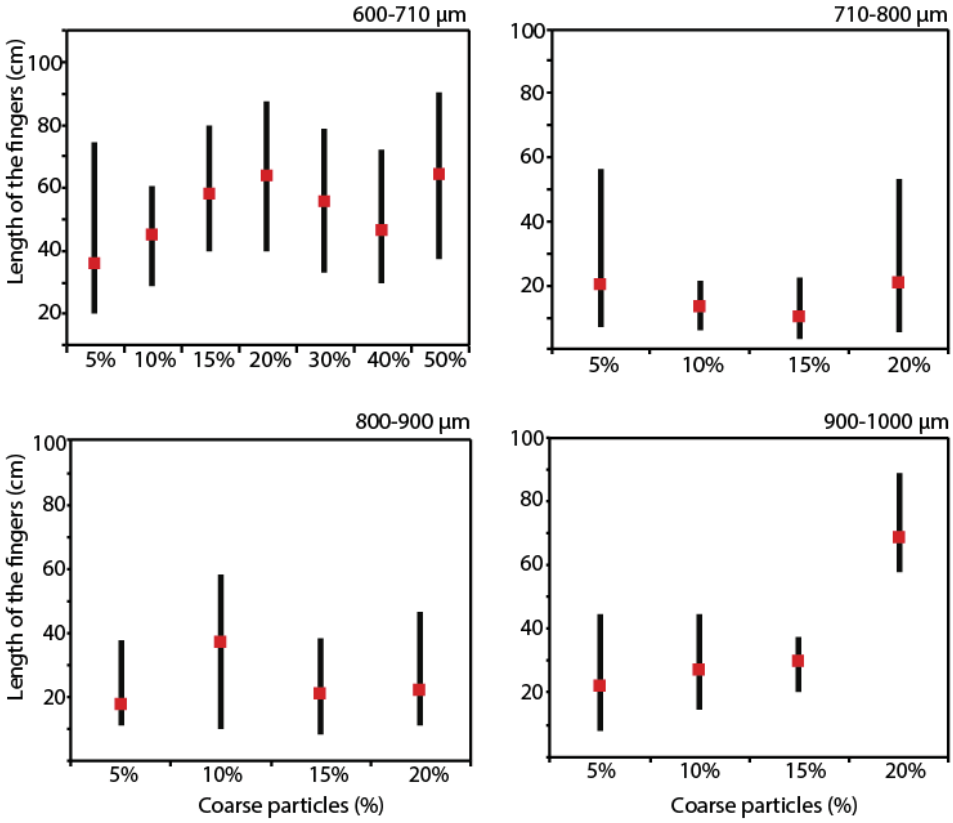

Figure 10. Length of the granular fingers generated by the different mixtures. Black lines correspond to the range of values and the red squares show the average values.

Thickness and width of the fingers

For the mixtures with 5-20 wt.% of coarse particles the typical thickness of the fingers is 2-4 mm (thickness ranges are ~1 mm) and there is no clear trend with the concentration of the coarse components, except for the 710-800 µm mixture for which thicker fingers of 3-6 mm are observed (Figure 11). Complementary experiments at 30-50 wt.% of 600-710 µm coarse particles reveal that the fingers become thicker as the coarse concentration increases. Notice that the well-defined separated fingers in the 20 wt.%, 900-1000 µm mixture are thinner (~1 mm) than in other cases and show negligible variation in thickness.

The mean width of the fingers is of ~4-5 cm for all mixtures (with ranges of values of ~2-3 cm) and it tends to increase with the concentration in coarse particles (Figure 12). This characteristic is less pronounced for the mixture with the 600-710 µm coarse particles, but complementary experiments with 30-50 wt.% of the coarse component show a clear increase of the width of the fingers up to ~10 cm at 50 wt.% concentration.

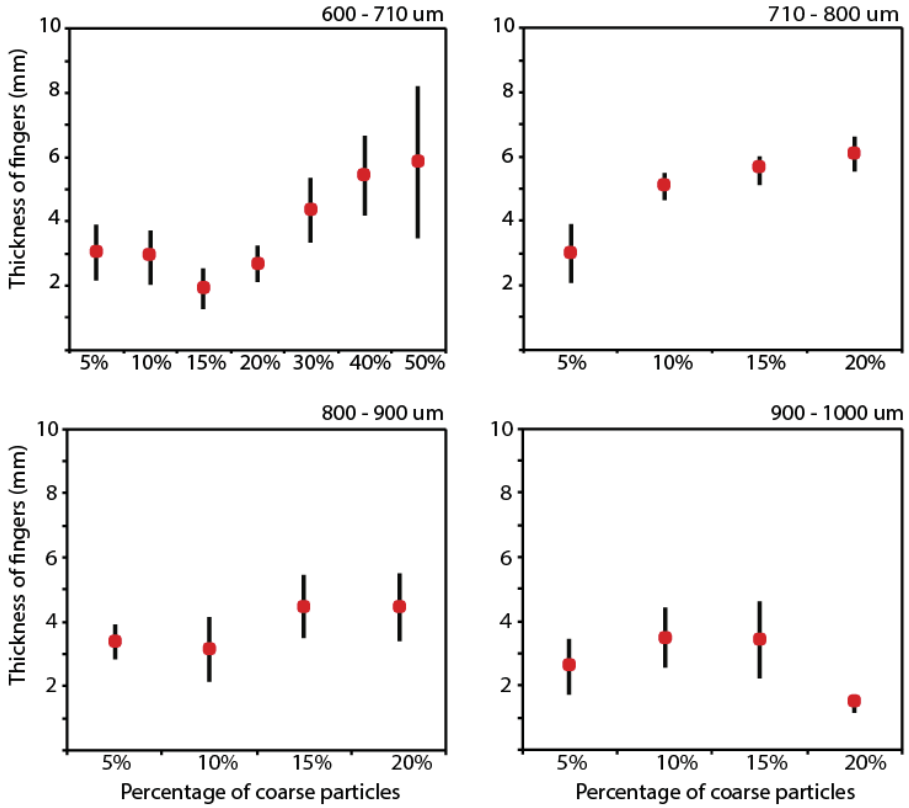

Figure 11. Thickness of the granular fingers generated by the different mixtures. Black lines correspond to the range of values and the red squares show the average values.

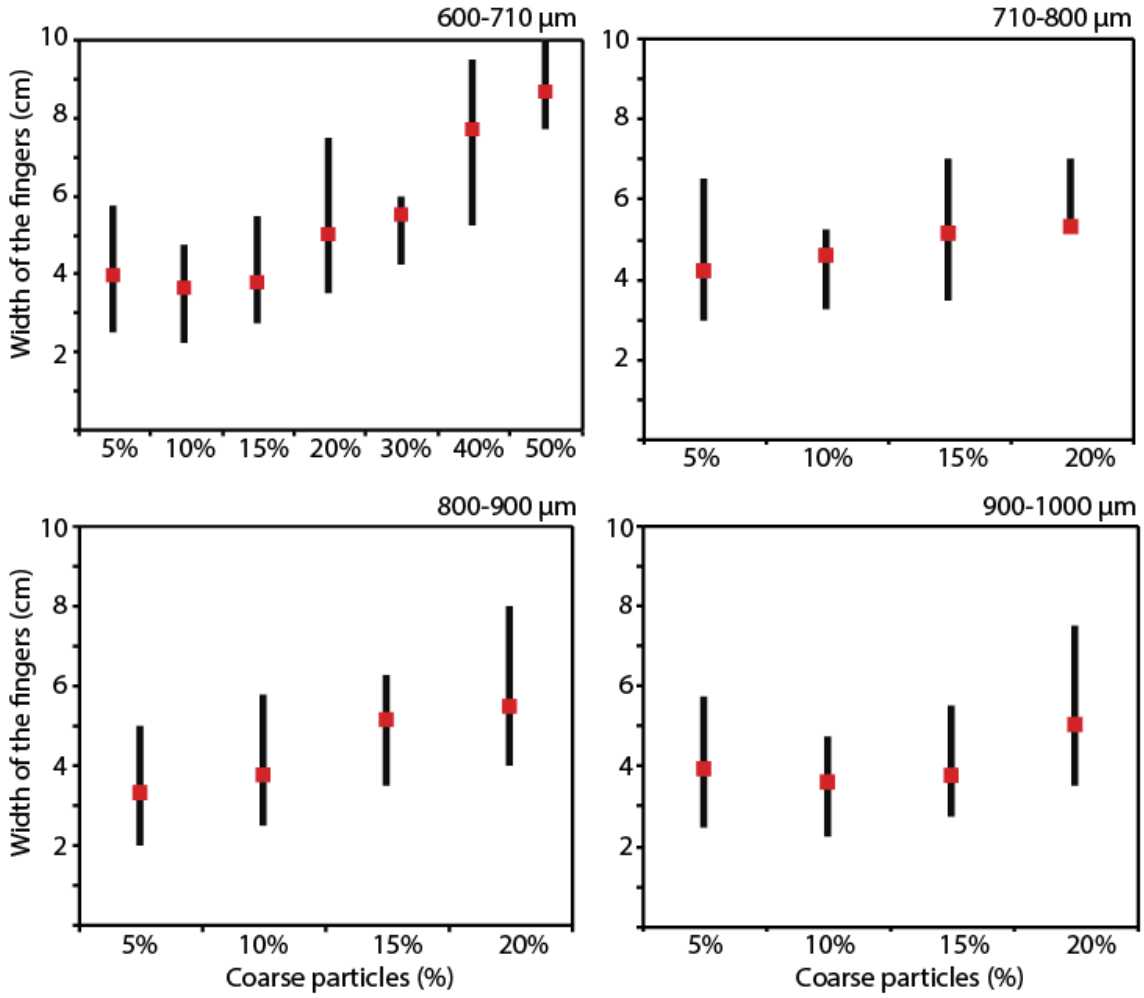

Figure 12. Width of the granular fingers generated by the different mixtures. Black lines correspond to the range of values and the red squares shows the average values.

Distance between axis and margins of the fingers

As discussed by Valderrama et al., (2016), the distance between axis and margins of the fingers is one important factor for the creation of ridges in a granular flow. In this context, we made measurements on the experimental deposits.

For distances between the margins of the fingers, two measurements for each pair of fingers were made: one for the minimum distance between the fingers, commonly where fingers emerge (where Stage 3 starts), and the other measures for the longest distance between the fingers, commonly in the most distal part of the deposit close to the front of the fingers (Figure 13). The data were obtained both by direct measurement on the experimental deposit and by photogrammetry.

the mixtures with 10-20 wt.% of 600-710 µm coarse particles have the greater amount of fingers with small distances less than 5 mm while the longest distance between fingers for this mixture is less than 3 cm. Other mixtures showed that the fingers were either poorly developed or had in most cases larger distance of separation (Figure 14).

The distance between the axis of the fingers was obtained from the digital elevation models, considering the geometric centre of the fingers(Figure 13). The mean distance is approximately constant and in the range 3.5-5 cm, except for the mixture with 600-710 µm coarse particles were the distance clearly increases with the concentration of coarse particles (Figure 15).

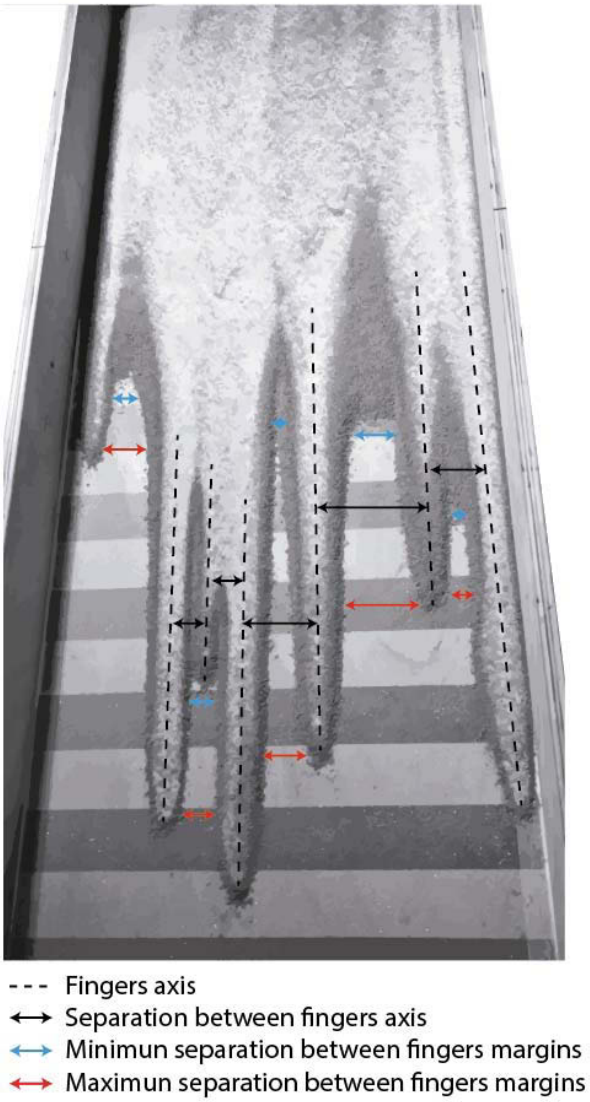

Figure 13. Photography of deposit with the different types of measurement indicated. The blue and red arrows show the minimum and maximum distance between fingers, respectively. Black arrows show the distance between the axes of the fingers, marked by dashed line.

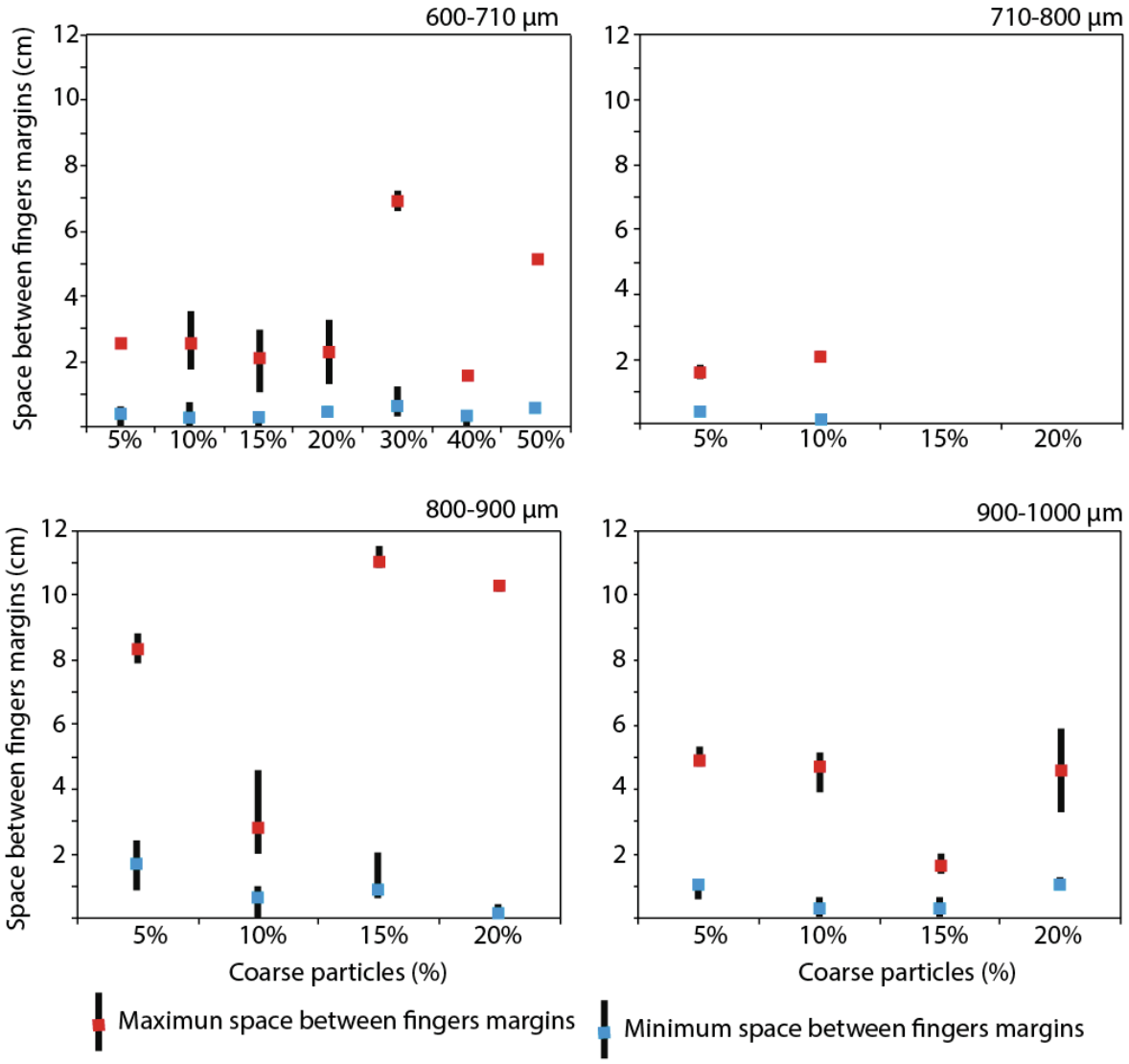

Figure 14. Distance between the fingers for the mixtures at different concentrations of coarse particles. The red and blue squares show the average maximum and minimum distance between fingers, respectively.

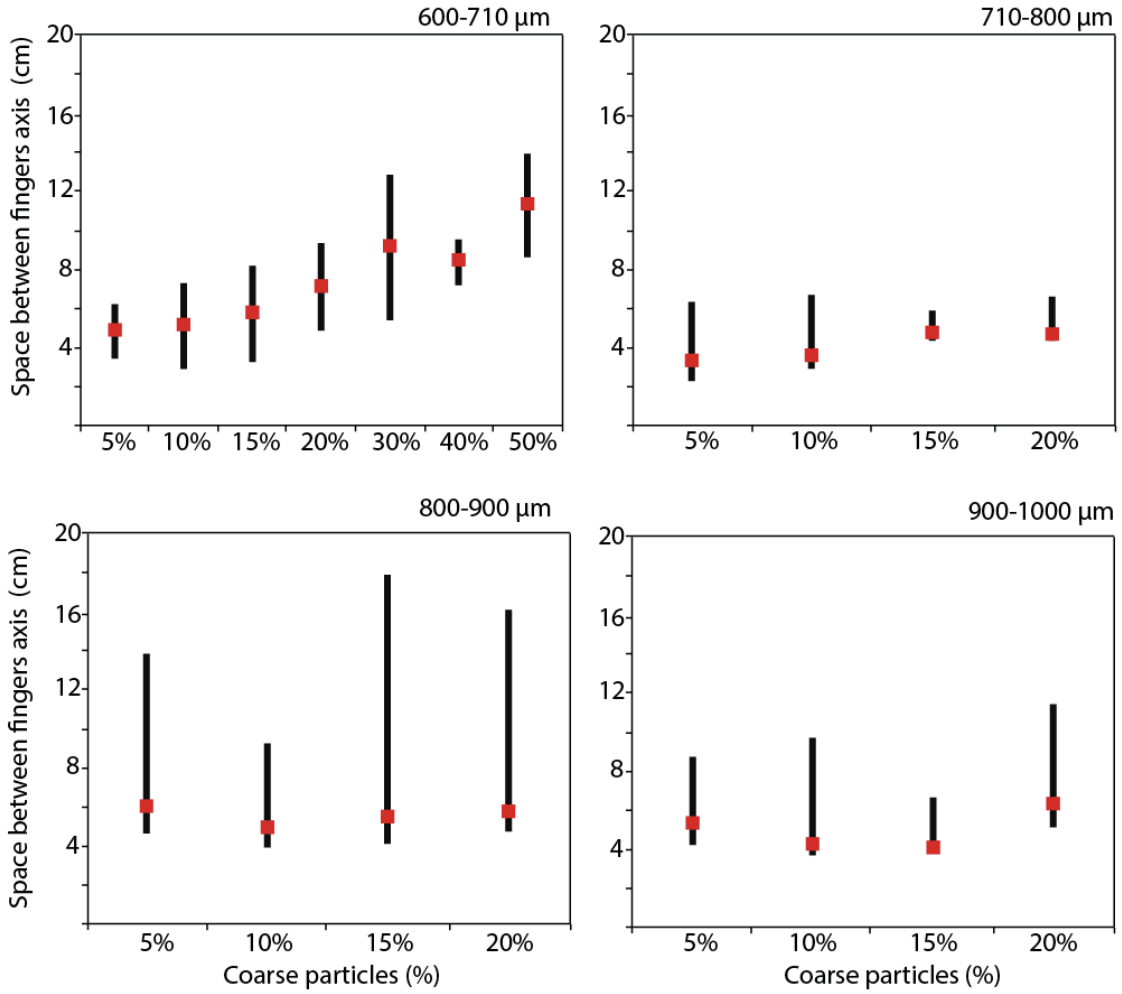

Figure 15. Distance between the axis of the fingers for the mixtures at different concentrations of coarse particles.

5. Discussion

Granular fingers and ridges in experiments

Our experiments show that longitudinal ridges are formed through coalescence of levées of adjacent fingers (Figure 9). Hence, these ridges are well-developed in case the fingers are (i) sufficiently long and (ii) merged (notice that ridges may have a single or two peak heights, see Figure 16). These conditions are met in our study when the grain size difference between the two components of the granular mixture is moderate (that is for 300-400 glass beads mixed with 600-710 µm crushed fruit stones) and the concentration of the coarse particles is low (10-20 wt.%). At lower concentrations there are not enough coarse particles to promote efficient segregation and hence fingering, whereas at higher concentrations the coarse particles accumulate at the flow front, stop motion and inhibit

fingering so that the front of the deposit consists of series of more or less defined rounded lobes, as observed for mixtures with large grain size difference. In some cases, however, wide fingers may emerge from coarse-rich lobes and travel downslope but then they are clearly separated each other. The thickness of the fingers decreases as their length increases, regardless the grain size and concentration of the coarse particles in the mixtures (Figure 16).

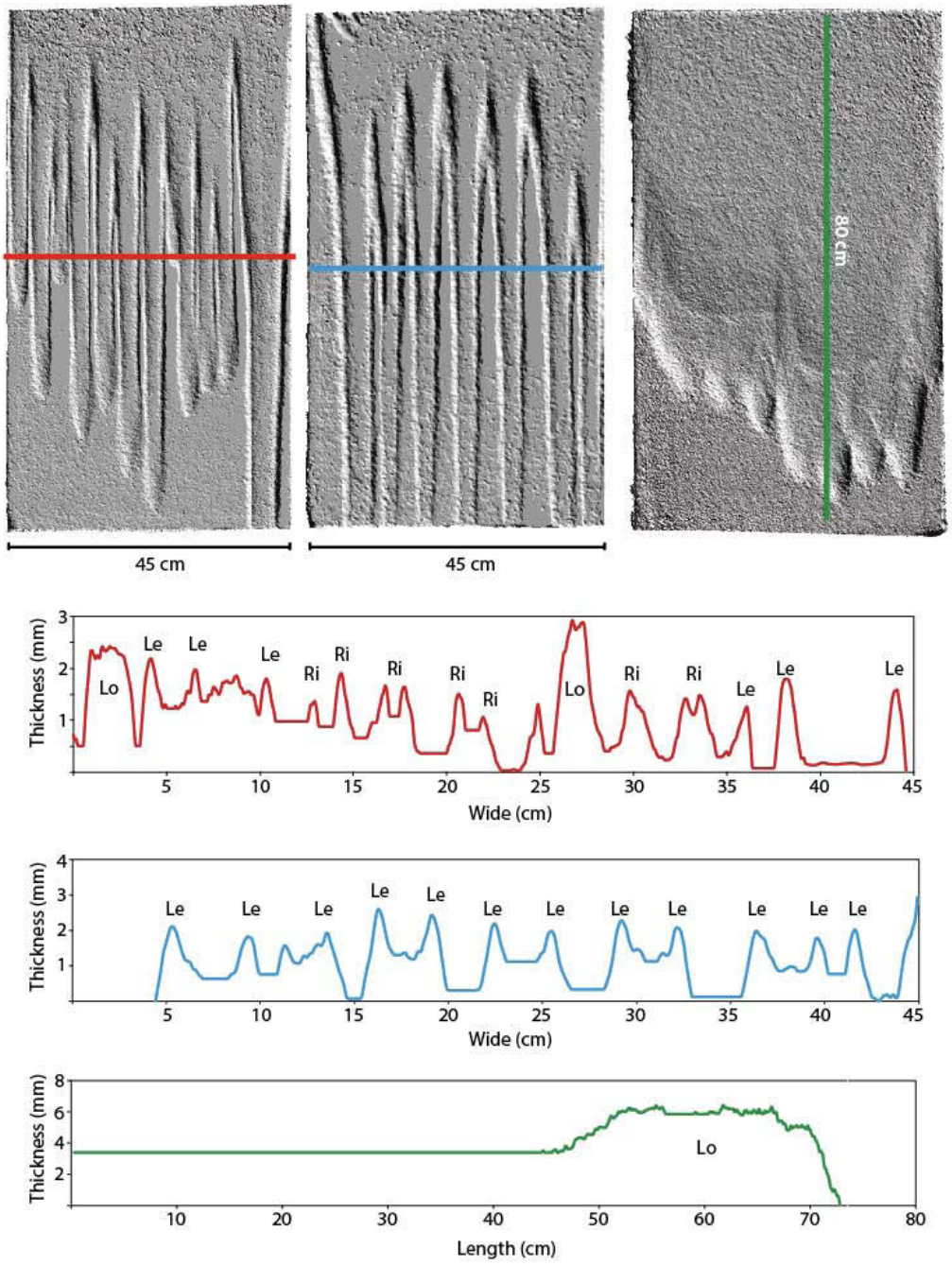

Figure 16. 3D models of the experimental deposits generated by photogrammetry. The three different main types of deposit geometries are shown: merged fingers (600-710 µm at 15 wt.%, red), separated fingers (900-100 µm at 20%, blue), and non-developed fingers (710-800 µm at 15%, green). Notation: lobes (Lo), levees (Le) and ridges (Ri).

Comparison with a natural case: The Tutupaca debris avalanche deposits

We now compare qualitatively our experimental results with observations made at a natural debris avalanche deposit. We consider the Tutupaca volcano located in southern Peru and which was investigated recently by our group (Samaniego et al., 2015, Valderrama et al., 2016). The last historical (218±14 aBP) eruption of Tutupaca generated a large sector collapse that triggered a debris avalanche and an associated pyroclastic eruption (Samaniego et al., 2015). The debris avalanche deposits are characterized by two distinct units: Unit 1 containing a large amount of hydrothermally altered material that belongs to the older basal edifice, and Unit 2 consisting of fresh dacitic rocks from the youngest dome complex. Interestingly, the debris avalanche deposits have different surface morphologies, including longitudinal ridges as well as distal surface and frontal lobes (Figure 17). The analysis made by Valderrama et al., (2016) on more than 300 ridges revealed that these are 200–500 m long, 10–30 m wide, 1–5 m high, regularly spaced (30-50 m), and that they fan slightly outward. Furthermore, the ridges have coarser cores and finer troughs, which suggest grain size segregation during emplacement of the debris avalanche (see Fig. 7 in Valderrama et al., 2016). Considering these structural and granulometric data Valderrama et al., (2016) argued that the ridges were formed through granular fingering and that most of the debris avalanche behaved like a granular flow. Our new experimental data further support this conclusion and also give more insights into the granular behaviour of the Tutupaca debris avalanche.

Figure 17a shows a large area of the Tutupaca debris avalanche deposit with subparallel ridges, at a distance of 4-5 km north of the amphitheatre. In principle, these ridges resemble those formed in experiments for which merged levees of granular fingers formed similar ridges enriched in coarse particles. In nature, the varying underlying topography of the substrate on which the avalanche propagated as well as the possibility of the granular mass to spread radially led to non rectilinear ridges, in contrast to the experiments. Figure 17b shows another area at about 6 km north-west of the amphitheatre, with a series of structures that can be interpreted as superposed frozen flow pulses with several frontal lobes. These structures are very similar to those in our experiments for which granular fingering could not develop because of large grain size difference between the components and/or too large coarse particle concentrations. Direct comparison between the natural case and the experiments is not straightforward because the Tutupaca debris

avalanche material is polydisperse rather than strictly bidisperse. Our experimental results, however, suggest that a relatively high proportion of large blocks, present at the source or acquired progressively during emplacement of the avalanche through size segregation, may be the cause of the lobate surface structures of the area shown in Figure 17b.

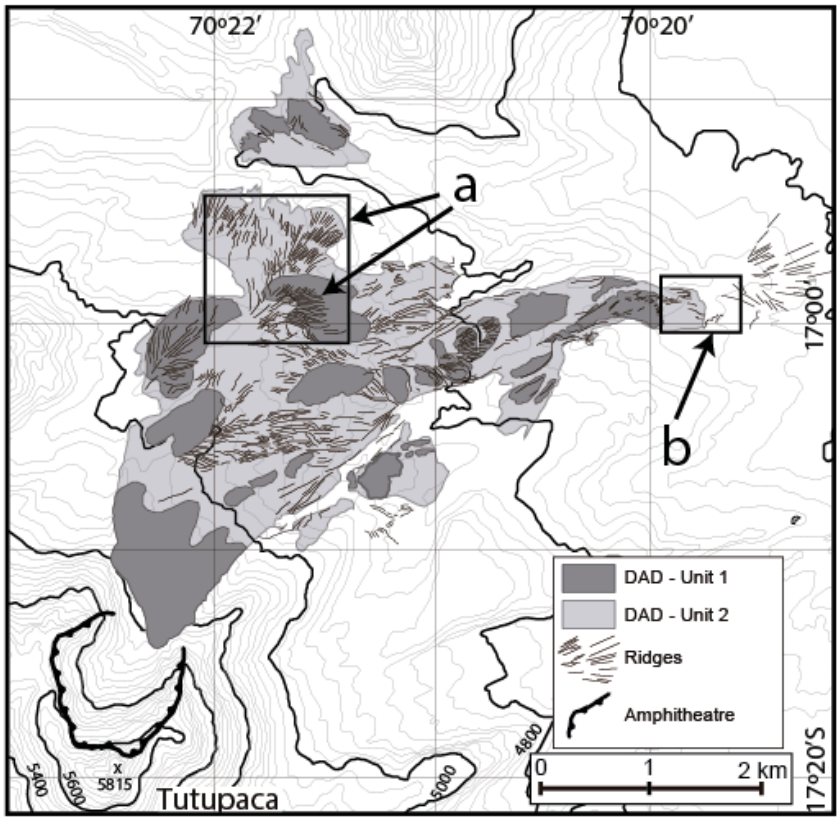

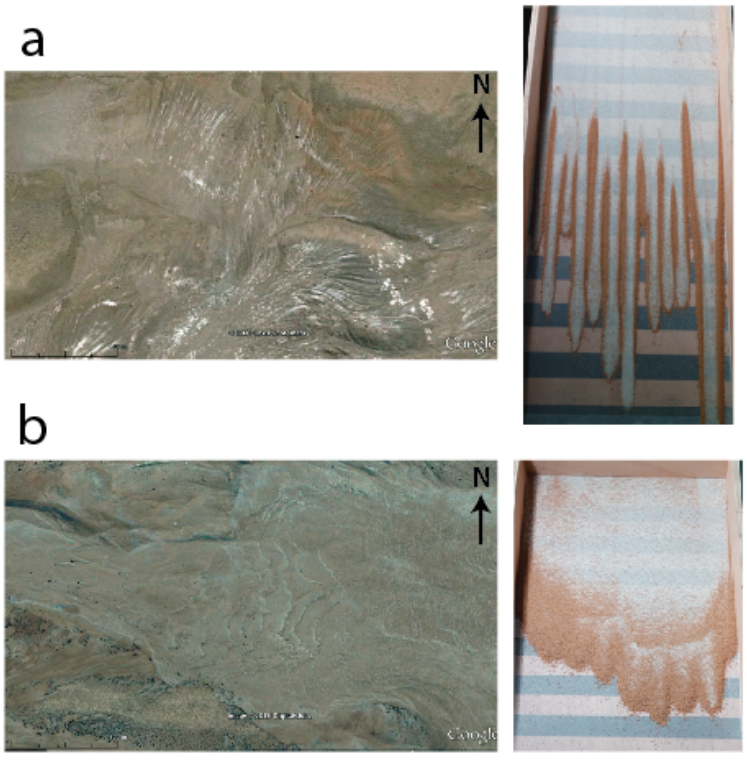

Figure 17. Map of Tutupaca volcano showing the two units of the 218±14 aBP debris avalanche deposit and their longitudibal ridges (from Valderrama et al., 2016) and comparison with experimental results. (a) Subparallel ridges of length of 150-600 m and distance between axis of 5-25 m, and experimental deposit of the mixture with 15 wt.% of 600-710 µm coarse particles showing ridges formed from merged levées of granular fingers. (b) Frontal and distal lobes, and experimental deposit of the mixture with 15 wt.% of 710-800 µm coarse particles showing distal surface and frontal lobes.

6. Conclusion

Our comprehensive set of laboratory experiments permitted us to explore the phenomenon of granular fingering in more detail than in earlier studies. The experiments have shown that longitudinal ridges rich in coarse particles form as a consequence of merging of the longitudinal levees of parallel granular fingers. This was observed when the grain size difference between the components of the granular mixture was small (i.e. 300-400 µm beads mixed with 600-710 µm coarse angular particles) and when the concentration of the coarse particles was higher than 10 wt.%.; fingering did not occur in similar mixtures but at coarse concentrations of 5 wt.% because particle segregation was not efficient enough. Well-defined fingers did not form in other mixtures with larger grain size differences, which rather generated series of frontal lobes of short length. Long fingers did form, however, in mixtures with high fractions of very coarse particles (e.g. 20% of 900-1000 µm particles) but in that case they were clearly separated from each other and hence did not form longitudinal ridges.

Qualitative comparisons of the ridges generated in the laboratory experiments with similar structures observed in some debris avalanches suggest that natural ridges may result from merged levees of joint granular fingers. The Tutupaca recent debris avalanche is an example of ridges possibly due granular segregation and related fingering, which could have been favoured by the presence of two distinct source materials with distinct physical characteristics: the hydrothermally-altered laves from the old Tutupaca edifice and the fresh dome lavas from the younger dome complex. We conclude that the Tutupaca debris avalanche behaved as a granular flow that enable segregation and fingering processes.

Chapter 6:

SUMMARY AND CONCLUSIONS

SUMMARY

This work is part of a wider research project conducted between the Peruvian "Instituto Geológico, Minero y Metalúrgico" (INGEMMET) and the French "Institut de Recherche pour le Développement" (IRD), through the Laboratoire Magmas et Volcans at Blaise Pascal University. The main goal of this project was to do a comprehensive study of the Tutupaca volcanic complex that included the following topics: (1) the reconstruction of the main eruptive stages of this complex, (2) the petrological characterization of its volcanic products, and (3) the in-depth study of two Holocene - recent large debris avalanches, this latter topic is the core of this PhD research project. All the information presented here is intended to help hazards assessment related to this little known albeit active volcano of Southern Peru. The information gained on this single site can then be used to compare with other volcanoes and volcanic lithology – dominated sites in Peru.

The dynamics of debris avalanche deposits and their triggering mechanism have been well studied and debated by the scientific community (see Introduction Chapter). The main contribution of this work is (1) to show two examples of eruption related edifice collapse, where the landslides involved an active dome and where the collapses probably triggered co-eval eruption, at least in one case (Chapters 2 and 3), and (2) a comprehensive study of the surface structures, namely the ridges, that we observe in the two most recent debris avalanches of Tutupaca (Chapters 4 and 5). This work was possible due to the exceptionally dry climate of the Andean highlands, that assure an extremely good state of conservation of the deposits and their surface structures. This preservation allowed us to make very detailed studies of the geological characteristics of the avalanche, and therefore, through these also its dynamic. We can analyze the processes through which one of the most notable features of Tutupaca were formed: the longitudinal ridges. With this work, we want to contribute to understanding the origin and dynamics of the processes that control the generation of ridges, which we have identified as the consequence of granular segregation and fingering.

CONCLUSIONS

Eruptive chronology of Tutupaca volcano

The Tutupaca volcanic complex rises from the basement at 4400–4600 m above sea level and is composed of an old, highly altered and eroded basal edifice and two younger twin peaks (The Western and Eastern Tutupaca). Several active fault systems have been identified in this part of the Andean cordillera, the main one being a series of NNW-trending normal faults with a sinistral component (*cf.* Fidel et al., 2001), which cut the volcanic complex and probably control its structural development.

The ***Basal Tutupaca*** is the oldest part of the complex. This is a highly eroded edifice, consisting of a succession of Pleistocene, andesitic lava flows, and scarce pyroclastic flow deposits. The summit zone has an uneven topography and displays strong hydrothermal alteration. This upper and central part of the edifice has multiple peaks consisting of lava sequences cut by the intense glacial erosion resulting in the eroded morphology and U-shaped, radially oriented valleys. Major moraine deposits are found in the southern part of the complex, which were probably formed during the Last Glacial Maximum (LGM) broadly dated at 17–25 ka in the Western Cordillera of the Peruvian Andes (Bromley et al., 2009).

Western Tutupaca is a younger edifice that overlies the Basal Tutupaca, and consists of dacitic lava sequences, domes and debris avalanche deposits. It is formed by several domes, which have diameters of 1-1.5 km and heights of 400-500 m. Overlying these domes, a lava sequence has been identified showing a meter-thick stratification, reaching more than 200 m thick and forming the upper part of the cone. These sequences are widely affected by glacial erosion, are partly covered by snow and host several small rock glaciers. A debris avalanche deposit is located on the western side of this edifice, which has a minimum thickness of 100 to 150 m and displays a block-rich facies. This deposit is covered by Last Glacial Maximum (LGM) moraine deposits, and it has an undulated and eroded surface. A sequence of Late Pleistiocene to Holocene tephra fallout deposits outcropping in the distal south-western part of the volcano shows that this edifice experienced plinian to subplinian eruptions during its history.

Eastern Tutupaca is the youngest edifice composed of at least 7 coalescing lava domes and theirassociated deposits, among which are block-and-ash pyroclastic flow deposits and debris avalanche deposits. Based on its young morphology and the lack of

glacial erosion, it is considered of Holocene age and from historical accounts, and the current fumaroles, to be still potentially active. This dome complex was cut by a 1-km-wide horseshoe-shaped amphitheater open to the NE. Two debris avalanche deposits associated with this edifice were identified: an older deposit that is channelized in the valleys located to the E and SE of the volcano (the Azufre debris avalanche deposit) and a younger deposit that outcrops immediately to the NE of the amphitheater (the Paipatja debris avalanche deposit).

The Azufre debris avalanche deposit

This debris avalanche deposit is found in the S and SE sectors of the Tutupaca volcanic complex, with important branches to the W and E, the main characteristic of this debris avalanche deposit is that it is channelized into four valleys. This debris avalanche deposit has two different sub-units: the more voluminous is a hydrothermal-rich sub-unit having a maximum thickness of 30-40 m; and the second one being a block-rich sub-unit that displays variable thickness ranging from 5 to 15 m. Both units correspond to two contrasted lithologies in the source area: the hydrothermally-rich subunit corresponding to the Basal edifice, and the block-rich subunit to the dacitic domes. This debris avalanche deposit has abundant hummocks associated with stretching of the avalanche material. Run-up and super-elevation structures were also found and were used to estimate the velocity of the avalanche (from 25 to 69 m/s), these values are in agreement with those reported for other debris avalanches.

On the basis of field observations and stratigraphic information, we associate this debris avalanche to a first phase of dome growth of Eastern Tutupaca edifice. In fact, this edifice was constructed on top of the older highly hydrothermalized edifice and traversed by an active fault system. This situation created the conditions for the destabilization and collapse of the new growing volcanic edifice. Thus, the triggering mechanism for this debris avalanche is the extrusion of the most recent dacitic domes onto an unstable and deformed substratum.

The 200-230 y BP Tutupaca debris avalanche and the dynamic implications of ridges.

The most recent major debris avalanche of Tutupaca volcano occurred only 218 ± 14 years before present (yBP) and is related to one of the largest explosive volcanic events to

have occurred in southern Peru during historical times. The debris avalanche deposit (<1 km^3) is genetically and spatially associated with a sequence of pyroclastic density currents deposits. Both units were emplaced synchronously.

Like the Azufre debris avalanche deposit, this avalanche has two well-defined sub-units: the lower one is a volcanic breccia consisting of highly cataclased, hydrothermal-rich fragments, which is overlain by an upper, block-rich unit composed of fresh dark grey dome rocks. In addition, the deposit has two main types of structures, a lower hummocky debris avalanche deposit and an upper ridged but not hummocked deposit. The latter deposit is characterized by a rough surface morphology consisting of longitudinal, elongated ridges that commonly diverge with distance from the amphitheatre. These ridges are present in both units, and are characterized by 200–700-m-long, 20–40-m-high and 10-30 m wide. There is no relationship between the length of the ridges and their distance from the scarp. In fact, the ridge axis distance varies from ~30 to 35 m in the proximal area to ~60 m at 6 km from the scar. No relationship between the ridge size and lithology is found.

Cross sections exposed within the ridges reveal coarser cores and finer troughs, suggesting a grain-size segregation process during emplacement. We interpret the Tutupaca ridges as joined margins of the lateral levées of granular fingers, where the large blocks were concentrated. In this context, inter-ridge depressions formed as the flowing granular mass drained the central part of the fingers that became progressively less elevated than the ridges, as shown for self-channelling granular flows depicting levée-channel morphology.

The presence of both ridged and hummocky deposits in the same event shows that, as different lithologies combine and collapse sequentially, materials with different mechanical properties can coexist in one landslide, leading to contrasting emplacement dynamics.

Based on characteristics of the deposits, it is observed that hot dome lava was involved in the sector collapse, and that juvenile magma was erupted with or immediately after the collapse. Thus, the ascent of a new batch of dacitic magma, coupled with the fact that the new Tutupaca dome complex was constructed inside of the amphitheatre left by

the Azufre avalanche, on top of an older, altered volcanic sequence, probably induced the destabilisation of the hydrothermally active edifice. It is worth noting that to the Azufre debris avalanche is not covered by any pyroclastic eruptive material, while the more recent deposits are covered by the Paipatja pyroclastic density currents deposits.

Granular fingering as a mechanism for ridge formation

In order to understand the granular fingering processes inferred from field data at Tutupaca, we made a series of analogue experiments on granular flows using bi-disperse mixtures, using systematically different concentrations of the granular components. Experiments were made with four bi-disperse mixtures of sub-spherical glass beads with a grain size of 300-400 µm and coarse angular particles made of crushed fruit stones with grain size ranges from 600-710 µm up to 900-1000 µm. The percentage of the coarse component in the mixtures varied from 5 to 50 wt.%. All experiments were made with an initial mass of the mixtures of 1 kg.

The experiments show that the flow kinematics are divided into 3 stages:

Stage one is characterised by particle segregation and occurs as soon as the granular mixture propagates downslope after release. Most of the small particles percolate downwards while the coarse particles move to the top of the flow and concentrate at the front.

Stage two consists of accumulation of coarse particles at the flow front. This process causes instabilities and the flow front, which slows down while the rest of mass propagates at the initial velocity acquired at Stage one.

Stage three is characterized by granular fingering and a significant diminution of the velocity of the moving mass. The fingers form as a consequence of particle size segregation, accumulation of coarse particles at the flow front and formation of local instabilities, which grow to form fingers with coarse-rich static margins bordering a fines-rich central channel.

The experiments have shown that longitudinal ridges rich in coarse particles form as a consequence of merging of the longitudinal levees of parallel granular fingers. Well-defined fingers did not form in other mixtures with larger grain size differences, which rather generated series of frontal lobes of short length. Long fingers did form, however, in mixtures

with high fractions of very coarse particles but in that case they were clearly separated from each other and hence did not form longitudinal ridges.

Based on extensive fieldwork and experiments conducted during this investigation, we can conclude that the ridges associated with the Tutupaca recent debris avalanche are associated with a process of granular segregation. Part of the Tutupaca debris avalanche behaved as a granular flow that enable segregation and fingering process. This mechanism was enhanced by the two contrasted lithologies at the source: the hydrothermally-altered laves from the old Tutupaca edifice and the fresh dome lavas from the younger dome complex.

Perspectives

This study allows us to make an in-depth analysis of two debris avalanche deposits from their origin to the dynamic emplacement. To go further from the field work, a geophysical survey would help to identify the internal arrangement of the different subunits of the avalanche and could also reveal the ancient relief on which the deposit was emplaced debris avalanche. The methods could be the radar, for the structural detail, and electromagnetism / gravity for the deposit thickness.

Analogue experiments have given robust results in simple configuration. The next step for further experiments could consist in the development of a device that has a more complex channel morphology that would allow experiments involving a sudden change of direction and/or slope angle or a topographic barrier with which the flow would interact. In addition, the use of a larger variety of particles would create a poly-dispersed mixture that would be a closer analogue to the natural material.

This study has identified two regimes of transport for debris avalanches at Tutupaca: (1) a brittle regime for which a faulted material slid over the topography, and (2) a granular flow regime resulting in elongated ridges. It was not possible, however, to determine how and under what conditions a mass will behave in one or the other way. This issue represents a potential new research topic, which could be addressed through experimental studies by considering the following issues. The Tutupaca hummocky deposits are derived from the lower part of the edifice and they preserve the stratigraphy though the material is strongly fractured. In contrast, the ridged deposits originated from higher in the scar and did not

preserve the stratigraphy, which suggests that the material was on motion for long duration and could be fragmented thoroughly, thus creating a granular flow. Another example of such a granular flow regime and associated ridges in the deposits is Socompa (Shea and van Wyk de Vries 2008).

Finally, the results of this study can be applied to other volcanic edifices and volcanic terrains in mountainous areas, in Peru and elsewhere. The events of destabilisation identified at Tutupaca could occur in many other configurations, where volcanic edifices are built up on previously altered, glaciated terrain, which is fairly common in Peru. Also, debris avalanches are not restricted to volcanoes, and the emplacement mechanisms identified at Tutupaca are likely to occur at many sites in Peru (e.g. 1962 and 1970 Nevado Huascaran, Evans et al., 2009).

REFERENCES

A

Adams, N. K., de Silva, S. L., Self, S., Salas, G., Schubring, S., Permenter, J. L., & Arbesman, K. (2001). The physical volcanology of the 1600 eruption of Huaynaputina, southern Peru. *Bulletin of Volcanology*, *62*(8), 493-518.

Allmendinger, R. W., Jordan, T. E., Kay, S. M., & Isacks, B. L. (1997). The evolution of the Altiplano-Puna plateau of the Central Andes. *Annual review of earth and planetary sciences*, *25*(1), 139-174.

Allstadt, K. (2013). Extracting source characteristics and dynamics of the August 2010 Mount Meager landslide from broadband seismograms. *Journal of Geophysical Research: Earth Surface*, *118*(3), 1472-1490.

Andrade, S. D., & van Wyk de Vries, B. (2010). Structural analysis of the early stages of catastrophic stratovolcano flank-collapse using analogue models. *Bulletin of Volcanology*, *72*(7), 771-789.

Apmann, R. P. (1973). Estimating discharge from superelevation in bends.*Journal of the Hydraulics Division*, *99*(hy 1).

B

Bachelery, P., Labazuy, P., & Lénat, J. F. (1996). Avalanches de débris sous-marines et subaériennes à La Réunion. *Comptes rendus de l'Académie des sciences. Série 2. Sciences de la terre et des planètes*, *323*(6), 475-482.

Bagnold, R. A. (1956). The flow of cohesionless grains in fluids. *Philosophical Transactions of the Royal Society of London A: Mathematical, Physical and Engineering Sciences*, *249*(964), 235-297.

Barriga, V. M. (1941). *Memorias para la Historia de Arequipa* (Vol. 2). Editorial La Colmena.
Belousov, A. B. (1996). Pyroclastic deposits of March 30, 1956 directed blast at Bezymianny volcano. *Bull Volcanol*, *57*, 649-662.

Belousov, A., Belousova, M., & Voight, B. (1999). Multiple edifice failures, debris avalanches and associated eruptions in the Holocene history of Shiveluch volcano, Kamchatka, Russia. *Bulletin of Volcanology*, *61*(5), 324-342.

Belousov, A., Voight, B., & Belousova, M. (2007). Directed blasts and blast-generated pyroclastic density currents: a comparison of the Bezymianny 1956, Mount St Helens 1980,

and Soufrière Hills, Montserrat 1997 eruptions and deposits. *Bulletin of Volcanology*, *69*(7), 701-740.

Bernard, B. (2008). *Etude des dépôts d'avalanches de débris volcaniques: analyse sédimentologiques d'exemples naturels et identification des mécanismes de mise en place* (Doctoral dissertation, Université Blaise Pascal-Clermont-Ferrand II).

Bernard, B., de Vries, B. V. W., & Leyrit, H. (2009). Distinguishing volcanic debris avalanche deposits from their reworked products: the Perrier sequence (French Massif Central). *Bulletin of volcanology*, *71*(9), 1041-1056.

Bernard, B., Hidalgo, S., Robin, C., Beate, B., & Quijozaca, J. (2014). The 3640–3510 BC rhyodacite eruption of Chachimbiro compound volcano, Ecuador: a violent directed blast produced by a satellite dome. *Bulletin of Volcanology*, *76*(9), 1-20.

Blott, S. J., & Pye, K. (2001). GRADISTAT: a grain size distribution and statistics package for the analysis of unconsolidated sediments. *Earth surface processes and Landforms*, *26*(11), 1237-1248.

Borgia, A., Ferrarit, L., & Pasquarèf, G. (1992). Importance of gravitational spreading in the tectonic and. *Nature*, *357*, 6375.

Bourdier, J. L., Boudon, G., & Gourgaud, A. (1989). Stratigraphy of the 1902 and 1929 nuée-ardente deposits, Mt. Pelée, Martinique. *Journal of volcanology and geothermal research*, *38*(1), 77-96.

Bromley, G. R., Schaefer, J. M., Winckler, G., Hall, B. L., Todd, C. E., & Rademaker, K. M. (2009). Relative timing of last glacial maximum and late-glacial events in the central tropical Andes. *Quaternary Science Reviews*,*28*(23), 2514-2526.

Byrdina, S., Ramos, D., Vandemeulebrouck, J., Masias, P., Revil, A., Finizola, A., Zuniga, K.G., Cruz, V., Antayhua, Y. and Macedo, O. (2013). Influence of the regional topography on the remote emplacement of hydrothermal systems with examples of Ticsani and Ubinas volcanoes, Southern Peru. *Earth and Planetary Science Letters*, *365*, 152-164.

C

Calvache, M.L., Williams, S. N. (1992). Lithic-dominated pyroclastic flows at Galeras volcano, Colombia—An unrecognized volcanic hazard. *Geology*, *20*(6), 539-542.

Capra, L., Macıas, J. L., Scott, K. M., Abrams, M., & Garduño-Monroy, V. H. (2002). Debris avalanches and debris flows transformed from collapses in the Trans-Mexican Volcanic Belt,

Mexico–behavior, and implications for hazard assessment. *Journal of Volcanology and Geothermal Research*, *113*(1), 81-110.

Capra, L. (2006). Abrupt climatic changes as triggering mechanisms of massive volcanic collapses. *Journal of Volcanology and Geothermal Research*, *155*(3), 329-333.
Carrasco-Núñez, G., Siebert, L., & Capra, L. (2011). Hazards from volcanic avalanches. *Horizons in Earth Science Research*, *3*, 199-227.

Chow, V. T. (1959). Open-channel hydraulics. New York, McGraw-Hill, 680 p

Clavero, J., Sparks, R., Huppert, H., & Dade, W. (2002). Geological constraints on the emplacement mechanism of the Parinacota debris avalanche, northern Chile. *Bulletin of Volcanology*, *64*(1), 40-54.

Clavero, J., Polanco, E., Godoy, E., Aguilar, G., Sparks, R. S. J., van Wyk de Vries, B., ... & Matthews, S. (2004). Substrata influence in the transport and emplacement mechanism of the Ollague debris avalanche (Northern Chile).*Acta Vulcanologica*, *16*(1/2), 59.

Cobeñas, G., Thouret, J. C., Bonadonna, C., & Boivin, P. (2012). The c. 2030yr BP Plinian eruption of El Misti volcano, Peru: Eruption dynamics and hazard implications. *Journal of Volcanology and Geothermal Research*, *241*, 105-120.

Cotten, J., Le Dez, A., Bau, M., Caroff, M., Maury, R. C., Dulski, P., ... & Brousse, R. (1995). Origin of anomalous rare-earth element and yttrium enrichments in subaerially exposed basalts: evidence from French Polynesia.*Chemical Geology*, *119*(1), 115-138.

D

De Silva, S. L., & Francis, P. W. (1990). Potentially active volcanoes of Peru-Observations using Landsat Thematic Mapper and space shuttle imagery. *Bulletin of Volcanology*, *52*(4), 286-301.

de Silva, S. L., Davidson, J. P., Croudace, I. W., & Escobar, A. (1993). Volcanological and petrological evolution of volcan Tata Sabaya, SW Bolivia.*Journal of Volcanology and Geothermal Research*, *55*(3), 305-335.

Deplus, C., Le Friant, A., Boudon, G., Komorowski, J. C., Villemant, B., Harford, C., ... & Cheminée, J. L. (2001). Submarine evidence for large-scale debris avalanches in the Lesser Antilles Arc. *Earth and Planetary Science Letters*, *192*(2), 145-157.

Donnadieu, F., & Merle, O. (1998). Experiments on the indentation process during cryptodome intrusions: new insights into Mount St. Helens deformation. *Geology*, *26*(1), 79-82.

Druitt, T. H. (1992). Emplacement of the 18 May 1980 lateral blast deposit ENE of Mount St. Helens, Washington. *Bulletin of Volcanology*, *54*(7), 554-572.

Druitt, T.H., Calder, E.S., Cole, P.D., Hoblitt, R.P., Loughlin, S.C., Norton, G.E., Ritchie, L.J., Sparks, R.S.J. and Voight, B. (2002). Small-volume, highly mobile pyroclastic flows formed by rapid sedimentation from pyroclastic surges at Soufrière Hills Volcano, Montserrat: an important volcanic hazard. *MEMOIRS-GEOLOGICAL SOCIETY OF LONDON*, *21*, 263-280.

Dufresne, A., & Davies, T. R. (2009). Longitudinal ridges in mass movement deposits. *Geomorphology*, *105*(3), 171-181.

E

Elsworth, D., & Voight, B. (1996). Evaluation of volcano flank instability triggered by dyke intrusion. *Geological Society, London, Special Publications*,*110*(1), 45-53.

Eppler, D. B., Fink, J., & Fletcher, R. (1987). Rheologic properties and kinematics of emplacement of the Chaos Jumbles rockfall avalanche, Lassen Volcanic National Park, California. *Journal of Geophysical Research: Solid Earth*, *92*(B5), 3623-3633.

Evans, S. G., Guthrie, R. H., Roberts, N. J., & Bishop, N. F. (2007). The disastrous 17 February 2006 rockslide-debris avalanche on Leyte Island, Philippines: a catastrophic landslide in tropical mountain terrain. *Natural Hazards and Earth System Science*, *7*(1), 89-101.

Evans, S. G., Bishop, N. F., Smoll, L. F., Valderrama P., Delaney, K. B., & Oliver-Smith, A. (2009). A re-examination of the mechanism and human impact of catastrophic mass flows originating on Nevado Huascarán, Cordillera Blanca, Peru in 1962 and 1970. *Engineering Geology*, *108*(1), 96-118.

Eychenne, J., & Le Pennec, J. L. (2012). Sigmoidal particle density distribution in a subplinian scoria fall deposit. *Bulletin of volcanology*, *74*(10), 2243-2249.

F

Félix, G., & Thomas, N. (2004). Relation between dry granular flow regimes and morphology of deposits: formation of levées in pyroclastic deposits. *Earth and Planetary Science Letters*,*221*(1), 197-213.

Fidel L, Zavala B (2001) Mapa preliminar de amenaza volcánica del volcán Tutupaca. Boletín 24, Serie C: Geodinámica e Ingeniería Geológica, INGEMMET, 109 p

Francis, P. W., Gardeweg, M., Ramirez, C. F., & Rothery, D. A. (1985). Catastrophic debris avalanche deposit of Socompa volcano, northern Chile.*Geology*, *13*(9), 600-603.

Francis, P. W., & Wells, G. L. (1988). Landsat Thematic Mapper observations of debris avalanche deposits in the Central Andes. *Bulletin of Volcanology*,*50*(4), 258-278.

G

Geertsema, M., Clague, J. J., Schwab, J. W., & Evans, S. G. (2006). An overview of recent large catastrophic landslides in northern British Columbia, Canada. *Engineering Geology*, *83*(1), 120-143.

Gerbe, M. C., & Thouret, J. C. (2004). Role of magma mixing in the petrogenesis of tephra erupted during the 1990–98 explosive activity of Nevado Sabancaya, southern Peru. *Bulletin of Volcanology*, *66*(6), 541-561.

Giachetti, T., Paris, R., Kelfoun, K., & Pérez-Torrado, F. J. (2011). Numerical modelling of the tsunami triggered by the Güìmar debris avalanche, Tenerife (Canary Islands): comparison with field-based data. *Marine Geology*, *284*(1), 189-202.

Glicken, H. (1991). Sedimentary architecture of large volcanic-debris avalanches.

Glicken, H. (1998). Rockslide-debris avalanche of May 18, 1980, Mount St. Helens volcano, Washington. *BULLETIN-GEOLOGICAL SURVEY JAPAN*, *49*, 55-106.

Gray, J. M. N. T., & Kokelaar, B. P. (2010). Large particle segregation, transport and accumulation in granular free-surface flows. *Journal of Fluid Mechanics*, *652*, 105-137.

Gray, J. M. N. T., Gajjar, P., & Kokelaar, P. (2015). Particle-size segregation in dense granular avalanches. *Comptes Rendus Physique*, *16*(1), 73-85.

Guthrie, R.H., Friele, P., Allstadt, K., Roberts, N., Evans, S.G., Delaney, K.B., Roche, D., Clague, J.J. and Jakob, M. (2012). The 6 August 2010 Mount Meager rock slide-debris flow, Coast Mountains, British Columbia: characteristics, dynamics, and implications for hazard and risk assessment. *Natural Hazards and Earth System Sciences*, *12*(5), 1277-1294.

H

Hantke, G., & Parodi, I. (1966). Colombia, Ecuador and Peru. *Catalog of Active Volcanoes of the world and solfatara fields, Rome, IAVCEI*, *19*, 1-73.

Hantke G, Parodi A (1966) Catalogue of the active volcanoes of the world, Part XIX, Colombia, Ecuador and Peru, IAVCEI Naples, Italy, 73 pp

Harpel, C. J., de Silva, S., & Salas, G. (2011). The 2 ka Eruption of Misti Volcano, Southern Peru—The Most Recent Plinian Eruption of Arequipa's Iconic Volcano. *Geological Society of America Special Papers*, *484*, 1-72.

Hoblitt, R. P., Miller, C. D., & Vallance, J. W. (1981). Origin and stratigraphy of the deposit produced by the May 18 directed blast. *US Geol. Surv. Prof. Pap*,*1250*, 401-420.

I

Instituto Nacional de Estadística e Informática (Perú). Dirección Técnica de Demografía e Indicadores Sociales. (2008). *Perfil sociodemográfico del Perú: Censos Nacionales 2007: XI de población y VI de vivienda*. INEI.

Iverson, R. M. (1995). Can magma-injection and groundwater forces cause massive landslides on Hawaiian volcanoes?. *Journal of Volcanology and Geothermal Research*, *66*(1), 295-308.

Iverson, R.M. (1997). The physics of debris flows. *Reviews of Geophysics* 35:245– 296

Iverson, R. M., & Denlinger, R. P. (2001). Flow of variably fluidized granular masses across three-dimensional terrain: 1. Coulomb mixture theory. Journal of Geophysical Research: Solid Earth, 106(B1), 537-552.

J

Jessop, D. E., Kelfoun, K., Labazuy, P., Mangeney, A., Roche, O., Tillier, J. L., ... & Thibault, G. (2012). LiDAR derived morphology of the 1993 Lascar pyroclastic flow deposits, and implication for flow dynamics and rheology. *Journal of Volcanology and Geothermal Research*, *245*, 81-97.

Johnson, C. G., Kokelaar, B. P., Iverson, R., Logan, M., LaHusen, R. G., & Gray, J. M. N. T. (2012). Grain-size segregation and levee formation in geophysical mass flows. *Journal of Geophysical Research: Earth Surface*, *117*(F1).

K

Kelfoun, K., & Druitt, T. H. (2005). Numerical modeling of the emplacement of Socompa rock avalanche, Chile. *Journal of Geophysical Research: Solid Earth*, *110*(B12).

Kelfoun, K., Druitt, T., van Wyk de Vries, B., & Guilbaud, M. N. (2008). Topographic reflection of the Socompa debris avalanche, Chile. *Bulletin of Volcanology*, *70*(10), 1169-1187.

Kendrick, E., Bevis, M., Smalley, R., Brooks, B., Vargas, R. B., Laurıa, E., & Fortes, L. P. S. (2003). The Nazca–South America Euler vector and its rate of change. *Journal of South American Earth Sciences*, *16*(2), 125-131.

Kerle, N., & De Vries, B. V. W. (2001). The 1998 debris avalanche at Casita volcano, Nicaragua—investigation of structural deformation as the cause of slope instability using remote sensing. *Journal of Volcanology and Geothermal Research*, *105*(1), 49-63.

Kokelaar, B. P., Graham, R. L., Gray, J. M. N. T., & Vallance, J. W. (2014). Fine-grained linings of leveed channels facilitate runout of granular flows.*Earth and Planetary Science Letters*, *385*, 172-180.

Komorowski, J.C., Jenkins, S., Baxter, P.J., Picquout, A., Lavigne, F., Charbonnier, S., Gertisser, R., Preece, K., Cholik, N. and Budi-Santoso, A. (2013). Paroxysmal dome explosion during the Merapi 2010 eruption: Processes and facies relationships of associated high-energy pyroclastic density currents. *Journal of Volcanology and Geothermal Research*, *261*, 260-294.

L

Lagmay, A. M. F., de Vries, B. V. W., Kerle, N., & Pyle, D. M. (2000). Volcano instability induced by strike-slip faulting. *Bulletin of Volcanology*, *62*(4-5), 331-346.
Lucchitta, B. K. (1979). Landslides in Valles Marineris, Mars. *Journal of Geophysical Research: Solid Earth*, *84*(B14), 8097-8113.

Legros, F., Cantagrel, J. M., & Devouard, B. (2000). Pseudotachylyte (frictionite) at the base of the Arequipa volcanic landslide deposit (Peru): implications for emplacement mechanisms. *The Journal of Geology*, *108*(5), 601-611.

Legros, F. (2002). The mobility of long-runout landslides. *Engineering Geology*, *63*(3), 301-331.

Lipman, P. W., & Mullineaux, D. R. (Eds.). (1981).*The 1980 eruptions of Mount St. Helens, Washington* (No. 1250). US Dept. of the Interior, US Geological Survey.

Lowe, D. R. (1976). Grain flow and grain flow deposits. *Journal of Sedimentary Research*, *46*(1).

Lube, G., Cronin, S. J., Platz, T., Freundt, A., Procter, J. N., Henderson, C., & Sheridan, M. F. (2007). Flow and deposition of pyroclastic granular flows: A type example from the 1975 Ngauruhoe eruption, New Zealand. *Journal of Volcanology and Geothermal Research*, *161*(3), 165-186.

Lucchitta, B. K. (1978). A large landslide on Mars.*Geological Society of America Bulletin*, *89*(11), 1601-1609.

M

Macías, J. L., Arce, J. L., García-Palomo, A., Mora, J. C., Layer, P. W., & Espíndola, J. M. (2010). Late-Pleistocene flank collapse triggered by dome growth at Tacaná volcano, México-Guatemala, and its relationship to the regional stress regime. *Bulletin of volcanology*, *72*(1), 33-53.

Malloggi, F., Lanuza, J., Andreotti, B., & Clément, E. (2006). Erosion waves: Transverse instabilities and fingering. *EPL (Europhysics Letters)*, *75*(5), 825.

Mamani, M., Wörner, G., & Sempere, T. (2010). Geochemical variations in igneous rocks of the Central Andean orocline (13 S to 18 S): Tracing crustal thickening and magma generation through time and space. *Geological Society of America Bulletin*, *122*(1-2), 162-182.

Mangeney, A., Bouchut, F., Thomas, N., Vilotte, J. P., & Bristeau, M. O. (2007). Numerical modeling of self-channeling granular flows and of their levee-channel deposits. *Journal of Geophysical Research: Earth Surface*, *112*(F2).

Manrique N (2013) Evolución Vulcanológica y Magmática del Edificio Reciente del Complejo Volcánico Tutupaca (Tacna). Universidad Nacional San Agustín de Arequipa. Tesis. 90 p

Manrique N (2016) Les processus et conditions pré-éruptifs responsables du déclenchement de l'éruption récente du volcan Tutupaca (Pérou). Université Blaise Pascal. Mémoire de Travail d'Etude et de Recherche. 26p

Mariño, J. (2002). Estudio geológico vulcanológico y evaluación de peligros del volcán Ticsani (sur del Perú). *Universidad Nacional de Ingeniería, Lima*.

Marino, J., Cacya, L., Rivera, M., & Thouret, J. C. (2009). Mapa Geológico del Volcán Ticsani. *INGEMMET Arequipa*.

Masías, P., Antayhua, Y. and Ramos D. (2011). Estudios Geoquímicos Preliminares de las Manifestaciones Geotermales del Volcán Tutupaca (Tacna). Informe Técnico, Dirección de Geología Ambiental. INGEMMET

McCormac, F. G., Hogg, A. G., Blackwell, P. G., Buck, C. E., Higham, T. F., & Reimer, P. J. (2004). SHCal04 Southern Hemisphere calibration, 0–11.0 cal kyr BP.

McSaveney, M. J. (2012). Sherman glacier rock avalanche, Alaska, USA. *Rockslides and avalanches*, *1*, 197-258.

Middleton, G. V. (1993). Sediment deposition from turbidity currents. *Annual Review of Earth and Planetary Sciences*, *21*, 89-114.

Montalto, A., Vinciguerra, S., Menza, S., & Patanè, G. (1996). Recent seismicity of Mount Etna: implications for flank instability. *Geological Society, London, Special Publications*, *110*(1), 169-177.

N

Naranjo, J. A., & Francis, P. (1987). High velocity debris avalanche at Lastarria volcano in the north Chilean Andes. *Bulletin of Volcanology*, *49*(2), 509-514.

Norabuena, E. O., Dixon, T. H., Stein, S., & Harrison, C. G. (1999). Decelerating Nazca-South America and Nazca-Pacific plate motions.*Geophysical Research Letters*, *26*(22), 3405-3408.

P

Paguican, E. M. R., van Wyk de Vries, B., & Lagmay, A. M. F. (2012). Volcano-tectonic controls and emplacement kinematics of the Iriga debris avalanches (Philippines). *Bulletin of volcanology*,*74*(9), 2067-2081.

Paguican, E. M. R., van Wyk de Vries, B., & Lagmay, A. M. F. (2014). Hummocks: how they form and how they evolve in rockslide-debris avalanches. *Landslides*, *11*(1), 67-80.

Palmer, B. A. (1991). Volcanic Debris Avalanche Deposits in New Zealand—Lithofacies Organization in Unconfined, Wet-Avalanche Flows.

Pierson, T. C. (1985). Initiation and flow behavior of the 1980 Pine Creek and Muddy river lahars, Mount St. Helens, Washington. *Geological Society of America Bulletin*, *96*(8), 1056-1069.

Pouliquen, O., Delour, J., Savage, S.B. (1997). Fingering in granular flows. *Nature* 386:816–817

Pouliquen, O. (1999). Scaling laws in granular flows down rough inclined planes. *Physics of Fluids (1994-present)*, *11*(3), 542-548.

Pouliquen, O., & Vallance, J. W. (1999). Segregation induced instabilities of granular fronts. *Chaos: An Interdisciplinary Journal of Nonlinear Science*,*9*(3), 621-630.

Procter, J. N., Cronin, S. J., & Zernack, A. V. (2009). Landscape and sedimentary response to catastrophic debris avalanches, western Taranaki, New Zealand. *Sedimentary Geology*, *220*(3), 271-287.

R

Ramos, V. A., & Aleman, A. (2000). Tectonic evolution of the Andes. *Tectonic Evolution of South America*, *31*, 635-685.

Reid, M. E., Sisson, T. W., & Brien, D. L. (2001). Volcano collapse promoted by hydrothermal alteration and edifice shape, Mount Rainier, Washington.*Geology*, *29*(9), 779-782.

Richards, J. P., & Villeneuve, M. (2001). The Llullaillaco volcano, northwest Argentina: construction by Pleistocene volcanism and destruction by sector collapse. *Journal of Volcanology and Geothermal Research*, *105*(1), 77-105.

Rivera, M., Thouret, J. C., Mariño, J., Berolatti, R., & Fuentes, J. (2010). Characteristics and management of the 2006–2008 volcanic crisis at the Ubinas volcano (Peru). *Journal of Volcanology and Geothermal Research*,*198*(1), 19-34.

Rivera, M., Thouret, J. C., Samaniego, P., & Le Pennec, J. L. (2014). The 2006–2009 activity of the Ubinas volcano (Peru): Petrology of the 2006 eruptive products and insights into genesis of andesite magmas, magma recharge and plumbing system. *Journal of Volcanology and Geothermal Research*, *270*, 122-141.

Roche, O., Niño, Y., Mangeney, A., Brand, B., Pollock, N., & Valentine, G. A. (2013). Dynamic pore-pressure variations induce substrate erosion by pyroclastic flows. *Geology*, *41*(10), 1107-1110.

Roverato, M., Cronin, S., Procter, J., & Capra, L. (2015). Textural features as indicators of debris avalanche transport and emplacement, Taranaki volcano. *Geological Society of America Bulletin*,*127*(1-2), 3-18.

S

Samaniego, P., Valderrama, P., Mariño, J., de Vries, B. V. W., Roche, O., Manrique, N., ... & Malnati, J. (2015). The historical (218±14 aBP) explosive eruption of Tutupaca volcano (Southern Peru). *Bulletin of Volcanology*, *77*(6), 1-18.

Savage, S. B., & Lun, C. K. K. (1988). Particle size segregation in inclined chute flow of dry cohesionless granular solids. *Journal of Fluid Mechanics*,*189*, 311-335.

Shaller, P. J. (1991). Analysis of a large moist landslide, Lost River range, Idaho, USA. *Canadian Geotechnical Journal*, *28*(4), 584-600.

Shea, T., & de Vries, B. V. W. (2008). Structural analysis and analogue modeling of the kinematics and dynamics of rockslide avalanches.*Geosphere*, *4*(4), 657-686.

Siebert, L. (1984). Large volcanic debris avalanches: characteristics of source areas, deposits, and associated eruptions. *Journal of volcanology and geothermal research*, *22*(3-4), 163-197.

Siebert, L., Glicken, H., & Ui, T. (1987). Volcanic hazards from Bezymianny-and Bandai-type eruptions. *Bulletin of Volcanology*, *49*(1), 435-459.

Siebert, L. (1992). Threats from debris avalanches. *Nature*, *356*, 658-659.

Siebert, L. (2002). Landslides resulting from structural failure of volcanoes.*Reviews in Engineering Geology*, *15*, 209-235.

Siebert, L., Simkin, T., & Kimberly, P. (2011). *Volcanoes of the World*. Univ of California Press.

Simkin, T., & Siebert, L. (1994). Volcanoes of the World: A Regional Directory, Gazetteer, and Chronology of Volcanism During the Last 10,000 Years, 349 pp. *Geoscience, Tucson, Ariz*.

Smith, G. M., Davies, T. R., McSaveney, M. J., & Bell, D. H. (2006). The Acheron rock avalanche, Canterbury, New Zealand—morphology and dynamics. *Landslides*, *3*(1), 62-72.

Smith, J. A., Mark, B. G., & Rodbell, D. T. (2008). The timing and magnitude of mountain glaciation in the tropical Andes. *Journal of Quaternary Science*,*23*(6-7), 609-634.

Smith, M. W., Carrivick, J. L., & Quincey, D. J. (2015). Structure from motion photogrammetry in physical geography. *Progress in Physical Geography*, 0309133315615805.

Somoza, R. (1998). Updated Nazca (Farallon)—South America relative motions during the last 40 My: implications for mountain building in the central Andean region. *Journal of South American Earth Sciences*, *11*(3), 211-215.

Sparks, R.S.J., Barclay, J., Calder, E.S., Herd, R.A., Komorowski, J.C., Luckett, R., Norton, G.E., Ritchie, L.J., Voight, B. and Woods, A.W. (2002). Generation of a debris avalanche and violent pyroclastic density current on 26 December (Boxing Day) 1997 at Soufriere Hills Volcano, Montserrat. *Geological Society, London, Memoirs*,*21*(1), 409-434.

Stuiver, M., & Reimer, P. J. (1993). Extended 14C database and revised CALIB radiocarbon calibration program, Radiocarbon, 35, 215â€“230.

Stuiver, M., Reimer, P. J., & Reimer, R. W. (2005). CALIB 5.0 (computer program and documentation).

T

Thouret, J.C., Davila, J., Eissen, J.P. (1999). Largest historic explosive eruption in the Andes at Huaynaputina volcano, south Peru. Geology 27: 435–438

Thouret, J. C., Finizola, A., Fornari, M., Legeley-Padovani, A., Suni, J., & Frechen, M. (2001). Geology of El Misti volcano near the city of Arequipa, Peru. *Geological Society of America Bulletin*, *113*(12), 1593-1610.

Thouret, J. C., Rivera, M., Wörner, G., Gerbe, M. C., Finizola, A., Fornari, M., & Gonzales, K. (2005). Ubinas: the evolution of the historically most active volcano in southern Peru. *Bulletin of Volcanology*,*67*(6), 557-589.

Tibaldi, A. (2001). Multiple sector collapses at Stromboli volcano, Italy: how they work. *Bulletin of Volcanology*, *63*(2-3), 112-125.

U

Ui, T., Takarada, S., & Yoshimoto, M. (2000). Debris avalanches.*Encyclopedia of volcanoes*, 617-626.

V

Valderrama, P., Roche, O., Samaniego, P., de Vries, B. V. W., Bernard, K., & Mariño, J. (2016). Dynamic implications of ridges on a debris avalanche deposit at Tutupaca volcano (southern Peru). *Bulletin of Volcanology*, *78*(2), 1-11.

Valdivia, J.G. (1847). Fragmentos para la historia de Arequipa. Folletín de “El Deber”, Arequipa, 109–111 p

Van Wyk de Vries, B., & Francis, P. W. (1997). Catastrophic collapse at stratovolcanoes induced by gradual volcano spreading. *Nature*, *387*(6631), 387-390.

Van Wyk de Vries, B., Kerle, N., & Petley, D. (2000). Sector collapse forming at Casita volcano, Nicaragua. *Geology*, *28*(2), 167-170.

Van Wyk de Vries, B., Self, S., Francis, P. W., & Keszthelyi, L. (2001). A gravitational spreading origin for the Socompa debris avalanche. *Journal of Volcanology and Geothermal Research*, *105*(3), 225-247.

Van Wyk de Vries, B., & Davies, T. (2015). Landslides, debris avalanches and volcanic gravitational deformation. *The Encyclopedia of Volcanoes, 2nd ed.; Sigurdsson, H., Houghton, B., McNutt, S., Rymer, H., Stix, J., Eds*, 665-685.

Vidal, N., & Merle, O. (2000). Reactivation of basement faults beneath volcanoes: a new model of flank collapse. *Journal of Volcanology and Geothermal Research*, *99*(1), 9-26.

Voight, B. (1981). Time scale for the first moments of the May 18 eruption.*US Geol. Surv. Prof. Pap*, *1250*, 69-86.

Voight, B., Janda, R. J., Glicken, H., & Douglass, P. M. (1983). Nature and mechanics of the Mount St. Helens rockslide-avalanche of 18 May 1980.*Geotechnique*, *33*(3), 243-273.

Voight, B., Komorowski, J.C., Norton, G.E., Belousov, A.B., Belousova, M., Boudon, G., Francis, P.W., Franz, W., Heinrich, P., Sparks, R.S.J. and Young, S.R. (2002). The 26 December (Boxing Day) 1997 sector collapse and debris avalanche at Soufriere Hills volcano, Montserrat. *MEMOIRS-GEOLOGICAL SOCIETY OF LONDON*, *21*, 363-408.

W

Wadge, G., Francis, P. W., & Ramirez, C. F. (1995). The Socompa collapse and avalanche event. Journal of Volcanology and Geothermal Research, 66(1), 309-336.
Walker, G. P. (1983). Ignimbrite types and ignimbrite problems. *Journal of volcanology and geothermal research*, *17*(1), 65-88.

Ward, S. N., & Day, S. (2003). Ritter Island volcano—lateral collapse and the tsunami of 1888. *Geophysical Journal International*, *154*(3), 891-902.

Woodhouse, M. J., Thornton, A. R., Johnson, C. G., Kokelaar, B. P., & Gray, J. M. N. T. (2012). Segregation-induced fingering instabilities in granular free-surface flows. *Journal of fluid mechanics*, *709*, 543-580.

Wörner, G., Moorbath, S., & Harmon, R. S. (1992). Andean Cenozoic volcanic centers reflect basement isotopic domains. *Geology*, *20*(12), 1103-1106.

Y

Yoshida, H., Sugai, T., & Ohmori, H. (2012). Size–distance relationships for hummocks on volcanic rockslide-debris avalanche deposits in Japan.*Geomorphology*, *136*(1), 76-87.

Z

Zamacola y Jaureguı J.D. (1804). Apuntes para la historia de Arequipa. Primer festival del libro arequipeño, Arequipa, Edición 1958, 15 p.

Zbar, B., (1991). Die Genese Mafischer Einschluesse in den Andesiten der Zentralen Vulkanzone (Nordchile), Diploma thesis, Universtiät Bochum.

Zora Carvajal, F. (1954). Tacna, Historia y Folklore. Second edition (1969), Editorial Santa María

APPENDIX:

RESULTS OF THE GRANULAR SEGREGATION LABORATORY EXPERIMENTS

600-700 um

Test	Percentage (wt)		Stages	Finger`s Number (F)	T(s)	F1		F2		F3		F4		F5		F6		F7		F8		F9		F10		F11		F12		F13		verage Values									
	Round %	Coarse %				D1	V1	D2	V2	D3	V3	D4	V4	D5	V5	D6	V6	D7	V7	D8	V8	D9	V9	D10	V10	D11	V11	D12	V12	D13	V13	D (cm)	V (cm)	Length (cm)	Width (cm)	t min (mm)	t max (mm)	FAS max	FAS min	FMS max	FMS min
1	95	5	Stage1	1	2	85	43																									85	43								
			Stage2	11	4	24	5	23	6	21	6	11	3	8	2	7	2	6	2	5	1	0	0	7	2	4	1					7	4	21.1	4.0	2.1	4.0	0.4	2.4	5.4	3.1
			Stage3	8	14	20	2	10	1	5	0	4	0	13	1	12	1	2	0													11	1								
2	95	5	Stage1	2	2	75	42	73	40																							74	41								
			Stage2	11	5	33	7	24	5	21	4	19	4	18	4	13	3	13	3	15	3	15	3	13	3	11	2					18	6	20.5	3.8	3.1	4.2	0.3	2.3	5.4	3.5
			Stage3	9	10	26	2	5	0	1	0	2	0	1	0	2	0	6	1	0	0.0	0	0									4	1								
3	95	5	Stage1	2	2	78	37	80	38																							79	38								
			Stage2	10	5	37	7	26	6	91	20	89	20	90	20	92	20	92	20	94	21	93	20	88	19							16	7	21.8	3.5	2.6	3.7	0.4	2.0	5.0	3.7
			Stage3	9	12	31	3	13	1	1	0	3	0	1	0	2	0	3	0	4	0.3	4	0									6	1								
4	95	5	Stage1	2	2	85	39	75	35																							80	37								
			Stage2	7	5	34	7	29	6	24	5	21	4	14	3	9	2	9	2													21	7	31.3	4.1	1.0	4.1	0.3	2.2	5.6	3.5
			Stage3	7	12	26	2	5	0	7	1	7	1	5	0	1	0	1	0													7	1								
5	95	5	Stage1	3	2	78	36	80	37	80	37																					79	37								
			Stage2	9	4	31	6	18	5	12	3	9	2	8	2	5	1	10	3	8	2	5	1									12	7	24.7	3.8	2.1	3.6	0.3	2.9	6.4	3.8
			Stage3	9	12	37	3	9	1	4	0	4	0	7	1	6	1	12	1	11	1.0	2	0									10	1								
6	90	10	Stage1	11	2	55	28	58	29	58	29	56	28	51	25	50	25	50	25	50	25	50	25	50	25	48	24					52	26								
			Stage2	11	3	14	3	14	4	11	3	11	3	12	4	8	2	4	1	5	2	8	2	6	2	8	2					9	7	26.5	3.6	2.2	3.7	0.3	3.0	5.2	2.7
			Stage3	11	10	11	1	32	3	15	2	7	1	5	1	3	0	4	0	1	0.1	3	0	3	0	5	1					8	1								
7	90	10	Stage1	7	3	79	31	79	31	76	30	74	29	75	30	75	30	65	26													75	30								
			Stage2	11	3	6	1	6	2	4	1	7	2	3	1	6	2	8	2	8	2	5	2	3	1	1	0					5	10	32.5	3.2	2.1	4.1	0.2	2.5	6.3	2.5
			Stage3	11	13	47	4	47	4	10	1	32	2	33	3	33	2	15	1	45	3.4	22	2	13	1	12	1					28	3								
8	90	10	Stage1	10	2	75	32	75	32	73	31	70	30	73	31	75	32	75	32	73	31	69	30	65	28							72	31								
			Stage2	10	3	14	3	14	4	11	3	13	4	10	3	14	4	13	4	14	4	12	3	12	3							12	12	34.4	3.4	2.1	3.4	0.2	3.2	6.9	2.8
			Stage3	10	14	41	3	33	2	17	1	28	2	23	2	29	2	23	2	41	2.9	29	2	24	2							29	3								
9	90	10	Stage1	7	3	79	31	79	31	79	31	80	31	77	30	70	27	68	26	65	25											74	29								
			Stage2	13	4	20	4	17	4	11	3	10	3	15	4	20	5	23	6	24	6	27	7	27	7	28	7	27	7	23	6	15	12	30.5	6.2	1.7	3.4	0.3	2.5	6.5	4.2
			Stage3	11	14	47	4	15	1	17	1	27	2	35	3	33	2	13	1	10	0.7	19	1	20	1	22	2					20	2								
10	90	10	Stage1	9	2	73	34	72	33	73	34	75	35	75	35	70	32	68	31	68	31	68	31									71	33								
			Stage2	9	3	15	3	12	4	9	3	10	3	8	2	10	3	10	3	10	3	10	3									10	11	31.6	3.3	1.5	2.7	0.3	1.9	6.3	3.0
			Stage3	9	12	44	4	34	3	29	2	25	2	8	1	16	1	22	2	38	3.0	14	1									25	3								
11	85	15	Stage1	8	2	83	34	80	33	80	33	79	32	77	31	77	32	75	31	68	28											77	32								
			Stage2	8	3	10	2	10	3	9	3	9	3	7	2	8	2	8	2	8	2											8	11	38.6	4.6	1.6	4.0	1.0	2.0	8.0	4.1
			Stage3	8	12	53	5	36	3	29	2	28	2	22	2	26	2	23	2	18	1.4											29	3								
12	85	15	Stage1	10	3	88	32	88	32	87	32	86	32	82	30	77	28	76	28	75	28	73	27	72	26							80	29								
			Stage2	10	4	12	2	12	3	11	3	9	3	8	2	6	2	4	1	5	1	5	1	5	1							7	9	43.9	4.0	1.4	2.2	1.1	3.6	8.1	4.2
			Stage3	10	13	46	4	46	3	48	4	33	2	23	2	25	2	18	1	19	1.4	6	0	16	1							28	3								
13	85	15	Stage1	11	2	84	34	81	33	81	33	81	32	83	33	83	33	82	33	78	31	76	31	75	30	73	29					80	32								
			Stage2	12	3	12	2	8	2	9	3	8	2	6	2	12	4	10	3	12	4	12	4	10	3	10	3	8	2			9	11	46.5	3.5	1.3	2.2	0.3	1.7	5.6	2.3
			Stage3	11	16	50	4	32	2	32	2	37	2	52	3	42	3	34	2	40	2.6	18	1	38	2	28	2					37	3								
14	85	15	Stage1	8	2	93	37	88	35	85	34	78	31	74	30	74	30	76	30	75	30											71	32								
			Stage2	9	3	10	2	12	4	14	4	14	5	12	4	7	2	7	2	9	3	8	2									18	31	53.3	4.1	1.0	2.4	0.5	1.5	6.0	2.5
			Stage3	8	12	43	4	45	4	34	3	31	3	28	2	39	3	36	3	46	3.8											38	4								
15	85	15	Stage1	8	3	93	33	90	32	88	31	88	31	87	31	85	30	94	33	79	28											78	31								
			Stage2	8	4	10	2	10	3	8	2	10	3	9	2	8	2	-2	0	4	1											17	23	57.8	3.6	1.1	2.0	0.4	1.6	5.7	2.6
			Stage3	8	4	43	4	45	11	50	13	48	12	43	11	47	12	43	11	44	10.9											45	4								
16	85	15	Stage1	9	3	79	31	78	31	76	30	76	30	75	30	75	30	74	29	75	30	70	28									75	30								
			Stage2	13	3	11	2	10	3	8	2	7	2	8	2	5	2	2	1	1	0	3	1	4	1	11	4	13	4	6	2	6	9	58.0	3.8	1.2	2.1	0.8	1.2	6.5	2.5
			Stage3	13	13	49	4	38	3	21	2	25	2	27	2	16	1	30	2	9	0.7	17	1	14	1	18	1	41	3	12	1	24	2								
17	80	20	Stage1	8	3	66	24	65	24	68	25	69	25	68	25	69	25	68	25	58	21											66	24								
			Stage2	8	5	16	3	11	2	10	2	15	3	9	2	9	2	12	2	5	1											11	5	0.0	0.0	0.0	0.0	0.7	3.0	6.0	3.0
			Stage3	8	12	25	2	13	1	11	1	24	2	18	2	13	1	19	2	3	0.2											15	2								

Where: T(s) Time in seconds; F: Number of fingers; D(cm): Distance; V (cm/s): Velocity; T(mm): Thickness; FAS(cm): Finger axis separation; FMT(cm): Finger margins separation, maximun and minimum

600-700 um

Test	Percentage (wt.%)		Stages	Finger`s Number (F)	T(s)	F1		F2		F3		F4		F5		F6		F7		F8		F9		F10		F11		F12		F13		Average Values									
	Coarse (%)	Round (%)				D1	V1	D2	V2	D3	V3	D4	V4	D5	V5	D6	V6	D7	V7	D8	V8	D9	V9	D10	V10	D11	V11	D12	V12	D13	V13	D (cm)	V (cm)	Length (cm)	Width (cm)	t min (mm)	t max (mm)	FAS max	FAS min	FMS max	FMS min
18	80	20	Stage1	8	0	68	27	69	27	68	27	72	29	71	28	73	29	70	28	64	25											69	28								
			Stage2	8	4	13	3	11	3	11	3	12	3	8	2	11	3	13	3	8	2											11	3	44.4	4.0	2.3	3.7	0.9	3.5	9.2	5.6
			Stage3	9	15	34	3	15	1	29	2	28	2	40	3	24	2	30	2	34	2.2	16	1									28	2								
19	80	20	Stage1	10	2	58	32	59	33	59	33	61	34	63	35	65	36	66	36	68	38	66	37	61	34							6.5	35								
			Stage2	10	3	3	1	5	2	7	2	9	3	1	0	3	1	6	2	10	3	9	3	3	1							5	3	56.8	11.8	1.9	3.0	0.1	3.2	8.0	5.2
			Stage3	10	36	85	7	79	2	79	2	56	2	23	1	32	1	25	1	40	1.1	20	1	2	0							44	1								
20	80	20	Stage1	8	3	76	28	78	29	78	29	76	28	76	28	75	28	74	28	69	26											75	28								
			Stage2	8	4	6	1	5	1	8	2	7	2	7	2	8	2	7	2	8	2											7	7	60.0	4.0	1.3	2.1	0.0	2.8	7.2	4.0
			Stage3	8	29	40	3	47	2	60	2	63	2	48	2	38	1	46	2	53	1.8											49	2								
21	80	20	Stage1	7	3	68	24	73	26	70	25	73	26	76	27	73	26	65	23													71	25								
			Stage2	7	4	9	2	14	3	4	1	13	3	14	3	12	3	9	2													10	6	52.4	5.4	2.3	3.9	0.4	2.5	8.5	4.5
			Stage3	7	14	14	1	33	2	17	1	30	2	31	2	28	2	19	1													24	3								
22	80	20	Stage1	7	3	80	31	75	29	72	28	68	27	65	25	65	25	58	22													69	27								
			Stage2	7	3	11	2	6	2	6	2	5	1	5	1	5	1	3	1													6	6	49.3	4.6	2.6	2.9	0.2	2.8	7.6	4.2
			Stage3	7	14	54	5	38	3	36	3	36	3	28	2	35	3	12	1													34	3								
23	80	20	Stage1	9	2	65	27	73	30	75	31	76	31	76	31	73	30	73	30	68	28	58	24									70	29								
			Stage2	10	4	11	2	8	2	8	2	13	4	12	3	1	0	9	2	9	2	8	2	1	0							8	7	48.4	4.2	2.4	4.0	0.3	3.0	7.5	5.0
			Stage3	10	17	44	4	25	1	33	2	57	3	55	3	12	1	43	3	33	1.9	34	2	7	1							33	2								
24	80	20	Stage1	7	2	60	27	60	27	59	26	68	30	68	30	68	30	55	25													62	28								
			Stage2	7	4	18	4	13	3	17	4	15	4	12	3	12	3	5	1													13	8	47.9	4.5	2.3	0.4	3.5	9.5	5.2	4.0
			Stage3	7	10	17	1	10	1	21	2	25	2	11	1	23	2	8	1													16	3								
25	70	30	Stage1	4	3	68	26	70	27	68	26	61	23																			66	25								
			Stage2	4	4	13	3	15	4	9	2	6	1																			10	6	43.3	6.4	3.0	6.3	0.8	2.0	8.0	5.3
			Stage3	4	9	23	2	15	2	9	1	3	0																			13	2								
26	70	30	Stage1	6	2	72	29	67	27	58	24	53	22	59	24	64	26															62	25								
			Stage2	6	4	21	4	17	4	10	2	4	1	9	2	12	3															12	8	44.3	5.8	4.2	5.8	0.3	1.8	8.1	5.1
			Stage3	6	14	50	4	19	1	10	1	1	0	9	1	35	2															20	2								
27	70	30	Stage1	5	3	68	25	68	25	70	26	68	25	61	23																	67	25								
			Stage2	5	5	19	4	17	3	14	2	15	3	17	3																	16	6	46.4	5.1	3.2	5.0	1.0	12.1	16.9	5.6
			Stage3	5	11	14	1	14	1	10	1	17	2	14	1																	14	2								
28	70	30	Stage1	5	3	71	25	73	26	71	25	70	25	58	21																	69	24								
			Stage2	5	5	17	3	16	3	8	2	9	2	6	1																	11	5	48.6	5.8	3.2	5.4	0.2	3.0	8.5	5.4
			Stage3	5	13	34	3	27	2	17	1	19	1	9	1																	21	3								
29	70	30	Stage1	6	2	60	29	52	25	62	30	65	31	63	30	55	26															59	29								
			Stage2	6	4	30	6	21	5	22	5	20	5	13	3	10	2															19	9	51.7	5.8	3.2	4.3	0.5	2.5	9.0	5.3
			Stage3	6	15	55	5	3	0	33	2	30	2	23	1	15	1															26	2								
30	80	20	Stage1	7	3	54	19	58	21	63	22	78	28	78	28	83	29	79	28													70	25								
			Stage2	7	4	2	0	7	2	3	1	5	1	8	2	3	1	1	0													3	2	48.0	4.3	2.5	3.8	0.5	2.9	8.0	4.0
			Stage3	7	9	1	0	0	0	1	0	10	1	13	1	13	1	13	1													5	1								
31	60	40	Stage1	4	2	45	23	39	20	40	20	47	24																			34	21								
			Stage2	4	4	21	4	20	4	19	4	16	3																			27	11	22.0	8.4	4.8	6.8	0.3	1.2	9.5	8.0
			Stage3	4	7	8	1	4	0	4	1	3	0																			5	2								
32	60	40	Stage1	5	2	35	21	36	21	41	24	48	28	49	29																	42	25								
			Stage2	5	4	16	3	24	6	31	8	21	6	19	5																	22	10	32.4	8.2	3.8	7.6	0.6	1.9	9.5	8.9
			Stage3	5	10	2	0	5	0	20	2	10	1	12	1																	10	1								
33	60	40	Stage1	6	1	25	30	24	29	25	30	29	35	29	35	27	32															26	27								
			Stage2	6	4	52	11	41	9	38	8	40	9	39	9	36	8															41	11	40.3	7.2	4.5	5.8	0.0	1.3	9.4	5.5
			Stage3	6	12	29	2	8	1	3	0	10	1	5	0	6	0															10	1								

Where: T(s) Time in seconds; F: Number of fingers; D(cm): Distance; V (cm/s): Velocity; T(mm): Thickness; FAS(cm): Finger axis separation; FMT(cm): Finger margins separation, maximun and minimum

600-700 um

Test	Percentage (wt.%)		Stages	Finger`s Number (F)	T(s)	F1		F2		F3		F4		F5		F6		F7		F8		F9		F10		F11		F12		F13		Average Values									
	Coarse (%)	Round (%)				D1	V1	D2	V2	D3	V3	D4	V4	D5	V5	D6	V6	D7	V7	D8	V8	D9	V9	D10	V10	D11	V11	D12	V12	D13	V13	D (cm)	V (cm)	Length (cm)	Width (cm)	t min (mm)	t max (mm)	FAS max	FAS min	FMS max	FMS min
34	60	40	Stage1	5	2	50	24	48	22	53	25	50	24	60	28																	52	25	51.0	7.0	3.6	6.2	0.2	1.2	9.0	6.5
			Stage2	5	5	33	7	24	5	17	3	24	5	20	4																	23	8								
			Stage3	5	12	29	2	16	1	9	1	9	1	22	2																	17	3								
35	60	40	Stage1	6	1	33	27	35	29	39	32	38	31	42	35	40	33															38	31	35.2	7.1	4.2	6.8	0.2	1.0	9.2	6.0
			Stage2	6	3	35	7	30	10	39	13	29	10	26	9	20	7															30	18								
			Stage3	6	10	23	2	1	0	27	3	1	0	14	1	5	1															12	2								
36	50	50	Stage1	1	0	15	31																									15	31	41.7	6.9	2.7	7.3	1.0	1.3	12.0	8.4
			Stage2	6	4	49	10	49	13	44	11	50	13	60	15	55	14															66	19								
			Stage3	6	12	25	2	11	1	3	0	6	0	19	2	17	1															13	2								
37	50	50	Stage1	1	1	15	23																									15	23	62.0	9.0	3.0	9.0	1.1	7.5	17.0	9.1
			Stage2	3	3	55	11	54	17	39	12																					64	25								
			Stage3	3	12	50	4	43	3	22	2																					38	4								
38	50	50	Stage1	3	1	25	37	17	25	17	25																					20	29	46.3	8.3	3.7	7.7	0.0	2.9	10.9	8.3
			Stage2	3	3	56	11	56	16	42	12																					71	25								
			Stage3	3	12	45	4	23	2	3	0																					24	3								
39	50	50	Stage1	1	1	20	33																									20	33	25.8	7.3	4.5	9.0	0.0	4.0	10.0	8.5
			Stage2	4	5	45	9	79	17	67	14	64	14																			68	17								
			Stage3	4	11	1	0	27	2	1	0	2	0																			7	1								
40	50	50	Stage1	1	1	18	35																									18	25	41.3	7.8	3.7	8.0	0.8	5.0	11.0	8.0
			Stage2	3	4	50	10	42	11	55	15																					67	21								

Where: T(s) Time in seconds; F: Number of fingers; D(cm): Distance; V (cm/s): Velocity; T(mm): Thickness; FAS(cm): Finger axis separation; FMT(cm): Finger margins separation, maximun and minimum

710 - 800 um

Test	Percentage (wt.%)		Stages	Finger`s Number (F)	T(s)	F1		F2		F3		F4		F5		F6		F7		F8		F9		F10		F11		F12		F13		Average Values									
	Coarse (%)	Round (%)				D1	V1	D2	V2	D3	V3	D4	V4	D5	V5	D6	V6	D7	V7	D8	V8	D9	V9	D10	V10	D11	V11	D12	V12	D13	V13	D (cm)	V (cm)	Length (cm)	Width (cm)	t min (mm)	t max (mm)	FAS max	FAS min	FMS max	FMS min
1	95	5	Stage1	2	2	65	34	70	36																							68	35	17.2	3.1	2.9	4.1	0.3	1.1	3.0	5.0
			Stage2	10	4	23	5	21	5	18	4	18	4	15	4	11	3	14	3	18	4	17	4	21	5							17	8								
			Stage3	10	8	9	1	10	1	3	0	4	0	1	0	2	0	1	0	4	0.5	1	0	13	2							5	1								
2	95	5	Stage1	2	2	73	36	85	43																							79	39	22.7	3.5	2.0	3.9	0.4	2.0	3.5	6.4
			Stage2	9	4	31	6	18	4	15	4	18	4	8	2	6	1	6	1	5	1	4	1									9	4								
			Stage3	9	9	26	2	5	1	5	0	2	0	6	1	4	0	7	1	2	0.2											6	1								
3	95	5	Stage1	2	2	73	36	83	41																							78	39	29.8	3.5	1.9	3.5	0.4	1.8	3.5	6.2
			Stage2	12	4	25	5	12	3	11	3	13	3	14	3	18	4	10	2	11	3	11	3	10	2	6	1	7	2			12	6								
			Stage3	10	9	18	1	1	0	1	0	4	0	3	0	1	0	1	0	2	0.2	3	0	10	1							4	1								
4	95	5	Stage1	1	2	85	41																									85	41	21.6	3.5	2.1	3.9	0.4	1.5	2.8	5.8
			Stage2	11	4	15	3	12	3	10	3	7	2	6	2	6	2	7	2	5	1	8	2	3	1	3	1					7	4								
			Stage3	7	10	28	2	11	1	8	1	6	1	9	1	10	1	2	0													12	2								
5	95	5	Stage1	1	2	85	38																									85	38	26.9	3.7	1.4	4.1	0.4	2.0	3.0	6.0
			Stage2	11	4	21	4	15	4	13	3	9	2	8	2	6	2	6	2	6	2	6	2	0	0	8	2					7	5								
			Stage3	9	11	40	3	13	1	10	1	3	0	6	1	5	0	13	1	11	0.9	12	1									14	2								
6	90	10	Stage1	8	3	58	21	60	22	61	22	61	22	59	21	60	22	60	22	55	20											59	21	8.8	5.3	5.0	5.7	0.2	2.5	3.5	6.8
			Stage2	7	4	7	1	5	1	4	1	4	1	4	1	3	1	1	0													4	5								
			Stage3	7	6	6	1	4	1	1	0	2	0	0	0	2	0	1	0													2	1								
7	90	10	Stage1	7	3	58	21	60	22	61	22	64	23	64	23	63	23	56	21													61	22	12.7	4.3	4.7	5.7	0.2	2.3	3.6	7.4
			Stage2	7	4	5	1	6	2	5	1	4	1	1	0	5	1	4	1													4	5								
			Stage3	6	8	5	0	17	2	3	0	5	1	6	1	4	0															6	1								
8	90	10	Stage1	9	3	59	23	59	23	62	24	63	25	63	25	64	25	63	24	58	22	55	21									61	24	14.8	3.9	4.9	5.7	0.2	2.6	3.7	7.6
			Stage2	9	3	7	1	6	2	6	2	6	2	4	1	5	1	5	2	3	1	3	1									5	6								
			Stage3	9	8	15	1	13	2	17	2	11	1	3	0	6	1	4	0	1	0.1	1	0									8	2								
9	90	10	Stage1	8	2	58	25	59	26	58	25	56	25	53	23	54	24	55	24	55	24											56	24	21.4	4.6	4.1	5.1	0.2	2.0	3.2	6.9
			Stage2	8	3	13	3	11	4	9	3	6	2	4	1	5	2	6	2	4	1											7	9								
			Stage3	8	11	35	3	35	3	10	1	8	1	1	0	4	0	5	0	15	1.4											14	2								
10	90	10	Stage1	9	3	56	19	59	20	63	21	67	23	67	23	66	23	64	22	63	21	59	20									63	22	9.5	3.8	4.7	5.1	0.2	1.6	3.4	5.6
			Stage2	9	4	4	1	4	1	9	2	4	1	3	1	5	1	4	1	3	1	4	1									4	5								
			Stage3	9	6	8	1	0	0	8	1	5	1	2	0	3	0	6	1	7	1.1	5	1									5	2								
11	85	15	Stage1	7	2	55	26	59	28	58	27	55	26	54	25	55	26	53	25													56	26	19.7	5.1	4.5	5.8	0.0	1.4	4.5	6.1
			Stage2	7	3	14	3	11	4	8	3	5	2	4	1	4	1	6	2													7	9								
			Stage3	7	11	44	4	20	2	3	0	5	0	2	0	0	0	6	1													11	1								
12	85	15	Stage1	5	3	63	22	66	23	63	22	59	21	60	21																	63	22	9.5	4.3	5.5	6.8	0.0	0.0	4.6	6.1
			Stage2	4	4	6	1	7	2	4	1	4	1																			5	4								
			Stage3	4	6	2	0	5	1	0	0	0	0																			2	1								
13	85	15	Stage1	8	3	63	24	65	25	64	25	59	23	54	21	58	22	58	22	55	21											59	23	12.3	5.1	4.8	5.5	0.0	1.0	4.6	6.0
			Stage2	8	4	8	2	5	1	5	1	6	2	1	0	4	1	3	1	3	1											4	4								
			Stage3	8	9	20	2	3	0	4	0	9	1	0	0	0	0	1	0	0	0.0											3	1								
14	80	20	Stage1	6	2	53	23	59	26	61	27	59	26	56	25	51	23															56	25	16.4	6.2	5.6	6.6	0.0	0.0	4.2	5.8
			Stage2	5	3	13	3	11	3	5	2	4	1	3	1																	8	7								
			Stage3	5	10	24	2	1	0	0	0	2	0	0	0																	5	1								

Where: T(s) Time in seconds; F: Number of fingers; D(cm): Distance; V (cm/s): Velocity; T(mm): Thickness; FAS(cm): Finger axis separation; FMT(cm): Finger margins separation, maximun and minimum

710 - 800 um

Test	Percentage (wt.%)		Stages	Finger`s Number (F)	T(s)	F1		F2		F3		F4		F5		F6		F7		F8		F9		F10		F11		F12		F13		Average Values									
	Coarse (%)	Round (%)				D1	V1	D2	V2	D3	V3	D4	V4	D5	V5	D6	V6	D7	V7	D8	V8	D9	V9	D10	V10	D11	V11	D12	V12	D13	V13	D (cm)	V (cm)	Length (cm)	Width (cm)	t min (mm)	t max (mm)	FAS max	FAS min	FMS max	FMS min
15	80	20	Stage1	6	2	65	28	64	27	59	25	56	24	56	24	51	22															59	25	18.6	5.1	6.2	6.6	0.0	0.0	4.3	5.8
			Stage2	5	3	11	2	5	1	3	1	3	1	4	1																	6	6								
			Stage3	5	10	27	2	0	0	1	0	0	0	0	0																	3	1								
16	80	20	Stage1	6	3	65	24	65	24	68	24	64	23	61	22	59	21															64	23	14.3	5.3	6.0	6.5	0.0	0.0	4.0	6.5
			Stage2	4	3	3	1	1	0	3	1	3	1																			4	12								
			Stage3	4	7	12	1	1	0	6	1	1	0																			5	1								
17	80	20	Stage1	6	2	59	26	60	26	58	25	59	26	60	26	60	26															59	26	11.8	5.2	5.0	6.8	0.0	0.0	4.5	6.0
			Stage2	6	4	10	2	8	2	6	2	4	1	5	1	8	2															7	5								
			Stage3	6	8	12	1	0	0	0	0	0	0	0	0	2	0															2	0								
18	80	20	Stage1	6	2	45	26	48	28	48	28	49	28	54	31	48	28															48	28	22.6	5.8	4.8	6.5	0.0	0.0	4.9	7.3
			Stage2	6	3	16	3	14	5	10	4	6	2	15	5	20	7															14	13								
			Stage3	6	10	15	1	7	1	0	0	0	0	8	1	35	3															11	1								

Where: T(s) Time in seconds; F: Number of fingers; D(cm): Distance; V (cm/s): Velocity; T(mm): Thickness; FAS(cm): Finger axis separation; FMT(cm): Finger margins separation, maximun and minimum

800 - 900 um

Test	Percentage (wt)		Stages	Finger`s Number (F)	T(s)	F1		F2		F3		F4		F5		F6		F7		F8		F9		F10		F11		F12		F13		Average Values									
	Round %	Coarse %				D1	V1	D2	V2	D3	V3	D4	V4	D5	V5	D6	V6	D7	V7	D8	V8	D9	V9	D10	V10	D11	V11	D12	V12	D13	V13	D (cm)	V (cm)	Length (cm)	Width (cm)	t min (mm)	t max (mm)	FAS max	FAS min	FMS max	FMS min
1	95	5	Stage1	3	2	75	37	78	38	78	38																					77	38								
			Stage2	10	4	20	4	11	3	10	3	86	24	87	24	84	24	87	24	84	24	83	23	81	23							10	6	14.3	3.7	3.0	4.0	0.6	3.3	3.9	8.2
			Stage3	8	9	30	3	7	1	7	1	2	0	8	1	4	0	8	1	9	1.0											9	2								
2	95	5	Stage1	1	2	85	42																									85	42								
			Stage2	6	3	3	1	0	0	2	1	4	1	3	1	3	1															1	1	18.4	5.0	2.6	4.0	2.8	13.4	8.0	18.4
			Stage3	5	7	15	1	11	2	11	2	6	1	5	1																	9	3								
3	95	5	Stage1	2	2	75	33	78	35																							76	34								
			Stage2	10	3	14	3	11	3	6	2	5	2	4	1	8	2	8	2	5	2	4	1	2	0							6	6	18.6	3.6	2.8	3.9	2.0	10.5	4.6	9.5
			Stage3	8	9	30	3	19	2	10	1	10	1	14	2	9	1	0	0	5	0.5											13	2								
4	95	5	Stage1	1	2	85	41																									85	41								
			Stage2	8	4	8	2	89	24	90	24	90	24	91	25	91	25	88	24	88	24											5	3	14.0	3.3	3.0	3.5	0.8	4.5	7.0	8.5
			Stage3	4	7	13	1	6	1	6	1	2	0																			7	2								
5	95	5	Stage1	1	1	88	61																									88	61								
			Stage2	9	3	12	2	95	31	91	30	91	30	90	30	89	29	88	29	88	29	88	29									3	2	14.3	4.2	2.9	4.1	0.9	3.9	7.9	18.2
			Stage3	8	6	16	1	5	1	4	1	5	1	5	1	1	0	1	0	5	0.7	5	1									5	2								
6	90	10	Stage1	6	2	63	27	63	27	62	27	65	29	69	30	69	30															65	28								
			Stage2	7	3	10	2	5	2	3	1	2	1	2	1	11	4	10	3													7	9	21.4	4.9	3.1	4.4	0.5	3.2	4.8	11.0
			Stage3	7	9	30	3	8	1	1	0	3	0	11	1	23	3	18	2													13	2								
7	90	10	Stage1	8	2	75	32	73	31	70	30	68	29	65	28	63	26	56	24	54	23											65	28								
			Stage2	8	4	18	4	15	4	14	4	13	4	10	3	8	2	6	2	7	2											11	10	24.8	4.7	3.0	4.0	0.9	2.6	4.5	10.5
			Stage3	7	14	53	4	6	0	15	1	19	1	5	0	1	0	3	0													17	2								
8	90	10	Stage1	8	2	72	33	72	33	68	31	66	30	66	30	63	28	63	29	62	28											66	30								
			Stage2	7	3	13	3	6	2	8	3	9	3	5	2	8	3	6	2													8	13	36.0	5.2	1.7	4.3	0.6	3.1	4.3	10.0
			Stage3	7	15	60	5	29	2	25	2	30	2	9	1	8	0	17	1													25	2								
9	90	10	Stage1	7	2	75	31	74	30	73	30	73	30	71	29	63	26	58	24													69	28								
			Stage2	7	3	14	3	14	4	12	4	11	3	12	3	18	5	16	5													14	14	39.6	4.5	1.3	3.7	1.0	3.4	5.0	11.1
			Stage3	7	12	39	3	10	1	13	1	32	3	25	2	28	2	18	2													23	3								
10	90	10	Stage1	8	2	65	30	66	30	69	31	69	31	71	32	74	34	70	32	65	30											69	31								
			Stage2	8	3	15	3	15	5	14	4	12	4	14	4	5	2	10	3	11	4											13	13	33.4	5.0	1.5	4.3	0.4	2.3	4.7	6.8
			Stage3	8	10	34	3	24	2	26	3	26	3	33	3	3	0	26	3	11	1.2											22	3								
11	85	15	Stage1	8	3	71	28	71	28	74	29	75	29	71	28	71	28	70	27	66	26											71	28								
			Stage2	5	3	6	1	6	2	4	1	3	1	7	2																	6	13	27.4	4.8	2.2	5.8	1.5	19.3	6.0	23.0
			Stage3	5	9	29	2	24	3	7	1	10	1	13	1																	13	2								
12	85	15	Stage1	5	3	73	26	70	25	71	25	67	24	66	24																	69	25								
			Stage2	5	4	11	2	6	2	5	1	1	0	3	1																	5	6	20.8	6.3	4.3	5.5	1.3	18.0	6.5	24.0
			Stage3	4	8	21	2	1	0	5	1	3	0																			7	2								
13	85	15	Stage1	7	3	68	22	75	24	73	24	70	23	75	24	69	22	69	22													71	23								
			Stage2	4	3	10	2	1	0	3	1	1	0																			3	10	20.3	5.6	4.0	5.3	1.5	19.2	7.7	25.9
			Stage3	4	8	20	2	6	1	4	0	6	1																			9	2								
14	85	15	Stage1	4	3	68	26	69	26	69	26	75	28																			70	27								
			Stage2	7	4	6	1	6	2	7	2	10	3	8	2	3	1	1	0													6	7	21.0	4.5	3.6	5.4	0.3	3.0	3.1	8.0
			Stage3	7	8	16	1	1	0	4	0	15	2	9	1	2	0	3	0													7	2								
15	85	15	Stage1	7	3	66	24	65	24	68	24	73	26	75	27	73	26	75	27													71	26								
			Stage2	5	4	3	1	12	3	13	3	5	1	10	3																	7	7	16.3	7.7	3.3	5.3	0.5	4.0	3.0	8.0
			Stage3	3	7	6	1	5	1	13	2																					6	2								
16	80	20	Stage1	7	3	73	22	79	24	75	23	73	22	69	21	75	23	68	21													73	22								
			Stage2	5	4	5	1	6	2	10	3	5	1																			6	8	16.6	5.5	3.8	6.2	0.3	19.0	6.3	16.5
			Stage3	5	8	4	0	14	2	8	1	1	0																			5	1								

Where: T(s) Time in seconds; F: Number of fingers; D(cm): Distance; V (cm/s): Velocity; T(mm): Thickness; FAS(cm): Finger axis separation; FMT(cm): Finger margins separation, maximun and minimum

800 - 900 um

Test	Percentage (wt.%)		Stages	Finger`s Number (F)	T(s)	F1		F2		F3		F4		F5		F6		F7		F8		F9		F10		F11		F12		F13		Average Values									
	Coarse (%)	Round (%)				D1	V1	D2	V2	D3	V3	D4	V4	D5	V5	D6	V6	D7	V7	D8	V8	D9	V9	D10	V10	D11	V11	D12	V12	D13	V13	D (cm)	V (cm)	Length (cm)	Width (cm)	t min (mm)	t max (mm)	FAS max	FAS min	FMS max	FMS min
17	80	20	Stage1	7	3	78	27	76	26	75	26	73	25	68	24	68	23	61	21													71	25								
			Stage2	3	4	13	3	9	2	8	2																					5	6	15.3	6.2	3.3	5.7	0.2	15.0	5.0	15.0
			Stage3	3	9	29	2	8	1	10	1																					10	2								
18	80	20	Stage1	6	3	85	26	75	23	75	23	72	22	75	23	71	22															76	23								
			Stage2	5	4	10	2	3	1	4	1	6	1	0	0																	5	5	14.2	5.4	3.4	5.2	0.3	1.2	5.3	12.0
			Stage3	5	10	27	2	0	0	0	0	1	0	3	0																	6	1								
19	80	20	Stage1	8	3	78	31	75	30	73	29	73	29	70	28	68	27	65	26													72	28								
			Stage2	8	3	15	3	6	2	6	2	8	2	8	2	7	2	4	1													8	9	27.2	5.0	4.5	5.8	0.0	1.6	5.0	7.0
			Stage3	6	11	39	3	0	0	3	0	8	1	3	0																	10	1								
20	80	20	Stage1	6	3	85	29	80	27	75	26	70	24	69	24	71	24															75	26								
			Stage2	3	4	8	2	6	2	3	1																					9	13	38.3	6.0	2.0	4.7	0.0	1.3	4.9	9.0
			Stage3	3	12	38	3	13	1	5	0																					19	2								

Where: T(s) Time in seconds; F: Number of fingers; D(cm): Distance; V (cm/s): Velocity; T(mm): Thickness; FAS(cm): Finger axis separation; FMT(cm): Finger margins separation, maximun and minimum

900 - 1000 um

Test	Percentage (wt)		Stages	Finger`s Number (F)	T(s)	F1		F2		F3		F4		F5		F6		F7		F8		F9		F10		F11		F12		F13		Average Values									
	Round %	Coarse %				D1	V1	D2	V2	D3	V3	D4	V4	D5	V5	D6	V6	D7	V7	D8	V8	D9	V9	D10	V10	D11	V11	D12	V12	D13	V13	D (cm)	V (cm)	Length (cm)	Width (cm)	t min (mm)	t max (mm)	FAS max	FAS min	FMS max	FMS min
1	95	5	Stage1	2	2	105	43	105	43																							105	43								
			Stage2	7	4	6	1	5	1	3	1	2	1	4	1	3	1	2	1													3	1	16.4	4.3	2.0	3.6	0.9	5.5	4.5	6.0
			Stage3	8	10	10	1	6	1	5	0	4	0	15	1	8	1	7	1	0	0.0											9	1								
2	95	5	Stage1	8	2	90	41	93	42	93	42	88	40	90	41	95	43	90	41	88	40											91	41								
			Stage2	5	4	20	4	6	1	3	1	8	2	5	1																	8	4	17.6	6.5	2.0	3.8	1.2	4.0	4.5	8.5
			Stage3	5	10	24	2	4	0	3	0	4	0	1	0																	7	1								
3	95	5	Stage1	5	2	83	36	82	35	88	38	93	40	92	40																	87	38								
			Stage2	10	4	16	3	13	3	2	0	2	0	4	1	4	1	8	2	5	1	4	1	8	2							7	5	16.8	3.0	2.2	3.4	0.9	2.2	3.5	5.4
			Stage3	10	8	19	2	3	0	5	1	7	1	7	1	7	1	10	1	8	0.9	7	1	15	2							9	2								
4	95	5	Stage1	5	2	100	43	95	41	95	41	95	41	95	41																	96	41								
			Stage2	4	4	4	1	0	0	1	0	0	0																			1	0	15.7	5.5	1.3	3.0	1.2	7.7	6.9	11.7
			Stage3	4	10	38	3	10	1	9	1	6	1																			16	2								
5	95	5	Stage1	5	2	95	38	100	40	106	43	105	42	103	41																	102	41								
			Stage2	4	5	5	1	0	0	1	0	2	0																			3	1	27.9	6.4	1.0	3.5	1.5	6.0	6.5	10.0
			Stage3	4	9	9	1	3	0	9	1	8	1																			7	2								
6	90	10	Stage1	9	3	85	27	81	25	79	25	78	24	76	24	74	23	71	22	68	21	62	19									75	23								
			Stage2	7	3	4	1	1	0	1	0	0	0	1	0	5	1	3	1													2	9	15.9	4.3	3.0	5.1	0.5	4.8	3.5	9.0
			Stage3	7	10	14	1	24	2	10	1	12	1	6	1	4	0	4	0													11	2								
7	90	10	Stage1	9	4	81	23	83	23	86	25	89	25	90	26	89	25	76	22	76	22	73	21									83	23								
			Stage2	8	4	6	1	4	1	5	1	6	2	6	2	4	1	4	1	5	1											6	10					0.3	4.9	4.6	9.7
			Stage3	9	14	19	2	14	1	11	1	13	1	15	1	19	1	3	0	18	1.3	10	1									11	1								
8	90	10	Stage1	6	3	78	30	79	30	76	29	69	27	68	26	69	27															73	28								
			Stage2	8	4	18	4	16	4	14	4	16	4	11	3	8	2	79	21	78	21											12	11	29.9	4.1	2.1	3.9	0.6	5.0	3.6	9.7
			Stage3	8	16	11	1	50	3	46	3	6	0	5	0	16	1	14	1	20	1.3											21	2								
9	90	10	Stage1	6	3	84	28	83	28	79	26	73	24	73	24	84	28															79	26								
			Stage2	6	3	8	2	8	2	4	1	4	1	5	1	5	1															5	13	38.1	3.9	2.3	3.8	0.5	5.0	4.5	9.6
			Stage3	6	17	54	5	30	2	31	2	2	0	6	0	56	3															30	2								
10	90	10	Stage1	8	3	90	27	89	26	85	25	83	25	78	23	76	23	83	25	86	26											84	25								
			Stage2	7	4	13	3	9	2	7	2	3	1	4	1	14	3	10	2													8	7	24.2	4.6	2.8	4.7	0.0	4.4	4.8	9.7
			Stage3	6	12	28	2	-6	0	-6	0	-3	0	13	1	19	2															7	1								
11	90	10	Stage1	7	3	78	26	75	25	76	25	79	26	81	27	74	25	63	21													75	25								
			Stage2	6	4	8	2	6	2	10	3	9	2	8	2	4	1															9	17	31.0	4.1	2.2	4.7	0.0	3.0	3.5	905.0
			Stage3	6	11	23	2	6	1	24	2	13	1	29	3	19	2															19	3								
12	85	15	Stage1	6	3	86	28	79	25	81	26	75	24	69	22	73	23															77	25								
			Stage2	5	4	9	2	5	1	7	2	2	1	9	2																	7	10	38.0	5.8	1.3	4.0	0.2	1.6	4.0	5.8
			Stage3	3	22	50	4	30	1	2	0																					31	2								
13	85	15	Stage1	10	3	75	25	75	25	78	26	79	26	79	26	79	26	78	26	79	26	75	25	73	24							77	26								
			Stage2	9	4	7	1	8	2	9	2	7	2	7	2	10	3	8	2	9	2	8	2									8	10	24.9	4.5	3.0	4.8	0.1	1.3	3.6	5.6
			Stage3	9	9	12	1	7	1	9	1	9	1	9	1	18	2	5	1	9	1.0	5	1									9	2								
14	85	15	Stage1	9	3	75	27	76	27	76	28	78	28	80	29	78	28	75	27	71	26	68	25									75	27								
			Stage2	9	4	10	2	11	3	13	3	12	3	9	2	13	3	8	2	6	2	5	1									9	9	24.6	4.2	3.3	5.8	0.1	1.2	3.5	5.5
			Stage3	9	11	24	2	10	1	10	1	14	1	16	1	21	2	5	0	2	0.1	3	0									12	2								
15	85	15	Stage1	7	3	88	32	78	28	75	28	71	26	73	27	73	27	71	26													75	28								
			Stage2	6	4	18	4	15	4	11	3	10	2	13	3	9	2															13	10	33.0	4.5	1.8	4.0	0.4	1.5	4.2	5.0
			Stage3	6	15	40	3	8	1	0	0	2	0	6	0	21	1															13	1								
16	85	15	Stage1	7	3	80	30	79	30	78	29	79	30	76	29	76	29	75	28													77	29								
			Stage2	7	3	10	2	9	3	8	2	9	3	9	3	9	3	7	2													9	11	35.0	4.5	1.7	4.6	0.5	1.7	4.3	6.7
			Stage3	7	12	29	2	17	1	13	1	18	1	13	1	23	2	20	2													19	2								

Where: T(s) Time in seconds; F: Number of fingers; D(cm): Distance; V (cm/s): Velocity; T(mm): Thickness; FAS(cm): Finger axis separation; FMT(cm): Finger margins separation, maximun and minimum

900 - 1000 um

Test	Percentage (wt.%)		Stages	Finger`s Number (F)	T(s)	F1		F2		F3		F4		F5		F6		F7		F8		F9		F10		F11		F12		F13		Average Values									
	Coarse (%)	Round (%)				D1	V1	D2	V2	D3	V3	D4	V4	D5	V5	D6	V6	D7	V7	D8	V8	D9	V9	D10	V10	D11	V11	D12	V12	D13	V13	D (cm)	V (cm)	Length (cm)	Width (cm)	t min (mm)	t max (mm)	FAS max	FAS min	FMS max	FMS min
17	80	20	Stage1	6	3	90	32	85	30	85	30	79	28	79	28	79	28															83	30								
			Stage2	6	3	8	2	5	2	3	1	4	1	6	2	6	2															5	10	36.5	5.3	1.7	2.2	1.0	4.5	6.0	8.0
			Stage3	6	23	48	4	55	2	58	2	9	0	34	1	60	3															44	2								
18	80	20	Stage1	7	3	86	30	88	30	88	30	81	28	86	29	85	29	86	29													86	29								
			Stage2	7	3	5	1	5	1	3	1	9	3	5	2	4	1	5	1													5	14	73.4	4.3	1.0	1.0	1.0	3.7	5.5	7.8
			Stage3	7	26	54	5	53	2	55	2	55	2	55	2	56	2	55	2													54	2								
19	80	20	Stage1	6	3	93	32	85	29	88	30	91	31	90	31	89	30															89	30								
			Stage2	6	3	6	1	3	1	3	1	5	1	3	1	6	2															4	13	67.0	5.0	1.0	1.7	1.1	4.0	6.2	12.0
			Stage3	6	25	46	4	41	2	55	2	50	2	53	2	50	2															48	2								
20	80	20	Stage1	6	3	94	32	88	30	88	30	87	29	91	31	92	31															90	26								
			Stage2	6	4	14	3	10	3	11	3	12	3	12	3	13	3															12	13	63.2	5.5	1.0	1.0	1.1	5.5	7.0	14.2
			Stage3	6	25	38	3	48	2	46	2	46	2	42	2	40	2															43	2								

Where: T(s) Time in seconds; F: Number of fingers; D(cm): Distance; V (cm/s): Velocity; T(mm): Thickness; FAS(cm): Finger axis separation; FMT(cm): Finger margins separation, maximun and minimum